Design of Synchronous Reluctance Machines for Automotive Applications

Seyedmorteza Taghavi

A Thesis

In the Department

of

Electrical and Computer Engineering

Presented in Partial Fulfillment of the Requirements

For the Degree of

Doctor of Philosophy (Electrical and Computer Engineering) at

Concordia University

Montreal, Quebec, Canada

March 2015

CONCORDIA UNIVERSITY

SCHOOL OF GRADUATE STUDIES

This is to certify that the thesis prepared

By: Seyedmorteza Taghavi

Entitled: Design of Synchronous Reluctance Machines for Automotive Applications

and submitted in partial fulfillment of the requirements for the degree of

Doctor of Philosophy (Electrical and Computer Engineering)

complies with the regulations of the University and meets the accepted standards with respect to originality and quality.

Signed by the final examining committee:

_____Chair
Dr. G. Gouw

_____External Examiner
Dr. A. M. Omekanda

_____External to Program
Dr. S. Rakheja

_____Examiner
Dr. S. Hashtrudi Zad

_____Examiner
Dr. L.A.C. Lopes

_____Thesis Supervisor
Dr. P. Pillay

Approved by: _____
Dr. A.R. Sebak, Graduate Program Director

March 24, 2015 _____
Dr. A. Asif, Dean
Faculty of Engineering & Computer Science

ABSTRACT

Design of Synchronous Reluctance Machines for Automotive Applications

Seyedmorteza Taghavi, Ph.D.
Concordia University, 2015

This dissertation reports an appropriate design methodology for synchronous reluctance machines, their important technical issues, and possible solutions for traction applications. The synchronous reluctance machines are used in industries owing to their unique merits such as high efficiency, fast dynamic response, and lower cost. Considering these superior properties, recently, this smart synchronous topology became more attractive for electrified powertrain applications in automotive industries. However, compared to the major requirements of the traction motors such as high torque and power density, low torque ripple, wide speed range, and proper size, this machine is still under investigations.

The goals of this research work are first; to identify electrical, magnetic, and geometrical parameters which are dominant in the machine's performance, and second; to verify appropriate design methodology for achieving a higher performance for automotive applications. Hence, analytical and computer aided analysis followed by experimental examinations on prototypes are carried out to support proposed methods and address possible solutions to the machine's technical issues for these particular applications.

Accordingly, the synchronous reluctance machine's fundamental operations, electrical, magnetic, and geometrical parameters are investigated. Analytical approach and a sizing methodology corresponding to the desired specifications are presented through the machine's

mathematical model. Design of transversal laminated anisotropic rotor structure with different geometries is studied to identify the geometrical parameters effects on the machine's performance in particular the output torque and torque ripple. An appropriate geometrical method along with an innovative rotor lamination assembly are proposed for improving the machine's output functions such as torque, power, and saliency ratio. Finally, the future perspective of the research work is discussed for further investigations.

ACKNOWLEDGEMENTS

My deep appreciation is first given to almighty God for blessing me with success in my efforts and blessing me with the erudition of several people whose advice, assistance and encouragement helped me throughout the completion of this thesis.

I would like to express my heartfelt appreciation to my advisor, Professor Pragasen Pillay, for his support and continuous help. His knowledge, invaluable guidance, understanding and patience inspired the completion of this thesis. I am very grateful to work with such an insightful and caring professor.

My sincere gratitude also goes to the members of my graduate study committee; Prof. Luiz Lopes, Prof. Shahin Hashtrudi Zad, and Prof. Subhash Rakheja for their valuable advice and help through my study.

I would like to acknowledge the Department of Electrical and Computer Engineering at Concordia University for providing an excellent academic environment.

Grateful acknowledgment is extended to the Natural Sciences & Engineering Research Council of Canada (NSERC), Hydro-Québec, Connect Canada, Auto21, and TM4 for their support for this research work.

I would like to extend my sincere appreciation to my fellow colleagues and friends at Power Electronics and Energy Research (PEER) Group in P. D. Ziogas Machine and Power Electronics Laboratory, past and present, I honor their friendship and so many good memories.

I dedicate this work to the memory of my parents. I am very grateful and deeply indebted to them for their support and prayers that inspired me to be strong and succeeded.

Last but certainly not the least; I do not have the words to express my gratitude to my beloved family, my wife Parisa and my daughter Taraneh for their patience, care and endless devotion. Paisa's emotional support and priceless love during these years motivated me whenever I was exhausted, hopeless and tired of struggling with the obstacles in my study. No words can express my heartfelt gratitude to them for their endless love, care and sacrifices.

TABLE OF CONTENTS

LIST OF FIGURES

LIST OF TABLES

NOMENCLATURE

EV	Electric vehicle	**RESS**	Rechargeable energy storage system
HEV	Hybrid electric vehicle	**TLA**	Transversal laminated anisotropic
ICE	Internal combustion engine	**ALA**	Axial laminated anisotropic
RESS	Rechargeable energy storage system	**MMF**	Magnetic motive force
IM	Induction motor	**2D**	Two dimension
PMSM	Permanent magnet synchronous motor	**FEA**	Finite element analysis
IPMSM	Interior permanent magnet synchronous motor	**BEW**	Barrier end width
BLDC	Brush-less DC motor	**PWM**	Pulse width modulation
SRM	Switch reluctance motor	**SVPWM**	Space vector Pulse width modulation
SynRM	Synchronous reluctance motor	**CRGO**	Cold rolled grain oriented
BLDC	Brush-less DC	**CRNGO**	Cold rolled non-grain oriented
VAT-SynRM	Variable ampere-turns SynRM	**EMF**	Electromotive force
MTPA	Maximum torque per ampere	**MMF**	Magnetic motive force
FWC	Flux weakening control	**sec.**	Second

LIST OF SYMBOLS

T_e	Electromagnetic torque	η	Efficiency
ω_b	Base speed	R_s	Stator phase resistance
P_o	Number of pole pairs	ρ	Copper resistivity
V_o	DC-bus voltage	ρ_{co}	Copper weight density
ω_r	Maximum speed	ρ_{ir}	Iron weight density
T_{ep}	Peak torque in continuous mode	l_f	Winding end connection length
T_{eb}	Continuous torque at base speed	l_c	Coil length
T_{em}	Maximum torque	λ_s	Slot's permeance
Con	Stator connection (Δ , Y)	K_{fill}	Fill factor
N_s	Number of stator slots	**J**	Current density
n_s	Number of conductor turns per slot	A_{co}	Copper conductor cross section area
q	Number of slots per pole per phase	P_{co}	Copper loss
V_{ph}	Phase voltage	W_{co}	Copper weight
K_{vo}	Converter factor	W_{ir}	Iron weight
B_{1gm}	Maximum air gap flux density, fundamental	P_{ir}	Iron losses
B_{1dm}	Air gap flux density in d-axis, fundamental	P_{mec}	Mechanical losses
B_{1qm}	Air gap flux density in q-axis, fundamental	E_m	Electromagnetic motive force (emf)
μ_o	Air permeability	λ_{dm}	Magnetizing flux in d-axis
ξ	Saliency ratio	λ_{qm}	Magnetizing flux in q-axis

$\mathbf{D_{ro}}$	Rotor outer diameter
$\mathbf{D_{ri}}$	Rotor inner diameter
$\mathbf{D_{so}}$	Stator outer diameter
$\mathbf{D_{si}}$	Stator inner diameter
L	Stake length
$\boldsymbol{\tau}$	Motor pole pitch
$\boldsymbol{\tau_s}$	Stator slot Pitch
$\mathbf{A_s}$	Useful area of slot
$\boldsymbol{\tau_y}$	Chorded coil pitch
g	Air gap length
$\boldsymbol{\lambda}$	Stack aspect ratio (L/τ)
$\boldsymbol{\gamma}$	Pole pitch to air gap ratio (τ/g)
$\mathbf{K_c}$	Carter factor
$\mathbf{K_s}$	Saturation factor
$\mathbf{K_{dm1}}$	D-axis magnetic coefficient, fundamental
$\mathbf{K_{qm1}}$	Q-axis magnetic coefficient, fundamental
$\mathbf{K_{w1}}$	Winding factor
$\mathbf{K_y}$	Chording factor
$\mathbf{L_q}$	Q-axis inductance
$\mathbf{L_{dm}}$	Magnetizing inductance in d-axis
$\mathbf{L_{qm}}$	Magnetizing inductance in q-axis
$\boldsymbol{\lambda_d}$	Flux in d-axis
$\boldsymbol{\lambda_q}$	Flux in q-axis
t	Time
$\mathbf{i_s}$	Stator phase current
$\mathbf{P_{mo}}$	Continuous output power
$\mathbf{I_{dm}}$	Magnetizing current in d-axis
$\mathbf{I_{qm}}$	Magnetizing current in q-axis
P	Number of poles
$\boldsymbol{\omega}$	Shaft speed
$\boldsymbol{\omega_e}$	Electrical speed
$\mathbf{P_{tot}}$	Total iron losses
$\mathbf{B_{om}}$	Maximum hysteresis flux density at f_o
$\mathbf{B^h_m}$	The h-th harmonic at frequency h_{f1}
$\boldsymbol{\sigma}$	Conductivity
d	Lamination thickness
$\mathbf{K_h}$	Coefficient of hysteresis losses
$\mathbf{K_e}$	Coefficient of excess losses
$\mathbf{R_{cs}}$	Equivalent resistance of stator core losses
$\mathbf{R_{cr}}$	Equivalent resistance of the rotor core losses
$\mathbf{L_{dq}}$	d-q mutual inductance
$\mathbf{V_d}$	D- axis voltage component

$\mathbf{L_m}$	Magnetizing inductance	$\mathbf{V_q}$	Q- axis voltage component
$\mathbf{L_{\sigma s}}$	Leakage inductance	$\mathbf{I_d}$	D- axis current component
$\mathbf{L_d}$	D-axis inductance	$\mathbf{I_q}$	Q- axis current component
$\mathbf{W_{ef}}$	Calculated speed by FEA	$\mathbf{y}$	Stator yoke width
$\mathbf{\sigma_y}$	Yield stress	$\mathbf{T_w}$	Stator tooth width
$\mathbf{\sigma_{FE}}$	Maximum stress calculated by FEA	$\mathbf{T_h}$	Stator tooth height
$\mathbf{\omega_{op}}$	Operating speed	$\mathbf{R_g}$	Reluctance of the air gap
$\mathbf{R_t}$	Reluctance of the stator teeth	$\mathbf{R_y}$	Reluctance of the stator yoke
$\mathbf{R_{sk}}$	Reluctance of the K_{th} Segment	$\mathbf{R_{gk}}$	Reluctance of the K_{th} flux barrier

Chapter 1 Introduction

1.1 Research Background

Worldwide interest in clean energy suggests reducing fossil fuel consumption in different industrial sectors such as transportation. The electric vehicle technology roadmap for Canada reported; by 2018, there will be at least 500,000 highway-capable plug-in electric vehicles on Canadian roads, as well as a larger number of hybrid-electric vehicles. Recent advantages of high quality magnetic materials and power electronics have contributed to new energy efficient and high performance electric drives that use new electric motor technologies. Different powertrain topologies equipped with various types of electrical machines have been used in electric (EV) and hybrid electric (HEV) vehicles i.e., induction machines (IM), permanent magnet machines (PMSM), switched reluctance machines (SRM), and DC machines [1, 3, 4]. Amongst them PMSM and IM are the most demanded in auto industries [5] owing to higher efficiency of PMSM and lower cost of IM [6].

The price of permanent magnets is fluctuating. China produces 97% of the rare earth permanent magnet used in vehicle applications and requires an increasing share of the production for their own needs [7]. The ability to maximize the utilization of magnets is paramount as is the investigation and design to reduce the need of or even eliminate permanent magnets. This will reduce the dependence on a sole supplier and provide avenues for reducing costs. The ability to use existing manufacturing facilities as opposed to developing a completely new manufacturing operation is also of considerable importance in order to remain competitive for new technology.

Successful penetration of EVs into the electrified transportation market requires consumer acceptance, infrastructure change, and achieving competitive cost. Important insight into consumer acceptance will come from the market reaction. Consumer reaction to cost, charging time, and driving range will help point the way forward for manufacturers. Advanced electric motors with high efficiency and reasonable cost in EV's powertrain systems have magnificent impact on the vehicle's drive range, battery life time, inverter rating, cooling system capacity, total weight, and cost.

Consequently, the choice of motor for traction is generally determined by manufacturers with respect to three dominant factors: cost, weight, and size. Therefore, proper design of traction motor is crucial in EV and HEV in which compactness and reasonable price are the major requirements in auto industries. In the design procedure, machine's proper size estimation is an important step before attempting to the rotor and stator cores geometrical design. This is more crucial in passenger vehicles in which compactness, size, and weight are indeed the design limitations. Recently, a cost reduction is the main objective in the most worldwide electric vehicle manufacturer's design strategy. Hence, new traction motor topologies such as synchronous reluctance machine in which the rotor anisotropic geometry can eliminate expensive magnet and aluminum or copper bar from rotor structure, became more attractive for automotive applications.

1.2 Literature Survey on Electric Powertrains

Electric vehicles (EV) are propelled by an electric powertrain that is composed of an electric motor powered by rechargeable battery packs. EVs have several advantages over vehicles with internal combustion engines [1, 8]:

- Energy efficient: electric vehicles convert about 60% of the electrical energy from the grid to power at the wheels. Whereas, conventional gasoline vehicles only convert about 20% of the energy stored in gasoline to power at the wheels.
- Environmentally friendly: EVs emit no tailpipe pollutants, although the power plants producing the electricity may produce pollutions.
- Performance benefits: electric motors provide quiet and smooth operation, stronger acceleration, and require less maintenance than the internal combustion engines (ICEs).
- Cost benefit: lower operating and maintenance costs than the ICEs.
- Convenience: home charging for all-electric vehicles.
- Reduce energy dependency: electricity is a domestic energy source; less susceptibility to fuel prices and reduced oil dependency.
- Opportunity to make a "green" choice.

Figure 1.1 shows a modern electric drivetrain. The drivetrain consists of three major subsystems: AC drive, energy storage unit, and low voltage auxiliary equipment. The AC drive, as a subsystem, is composed of an electric motor, a power electronics converter and a controller.

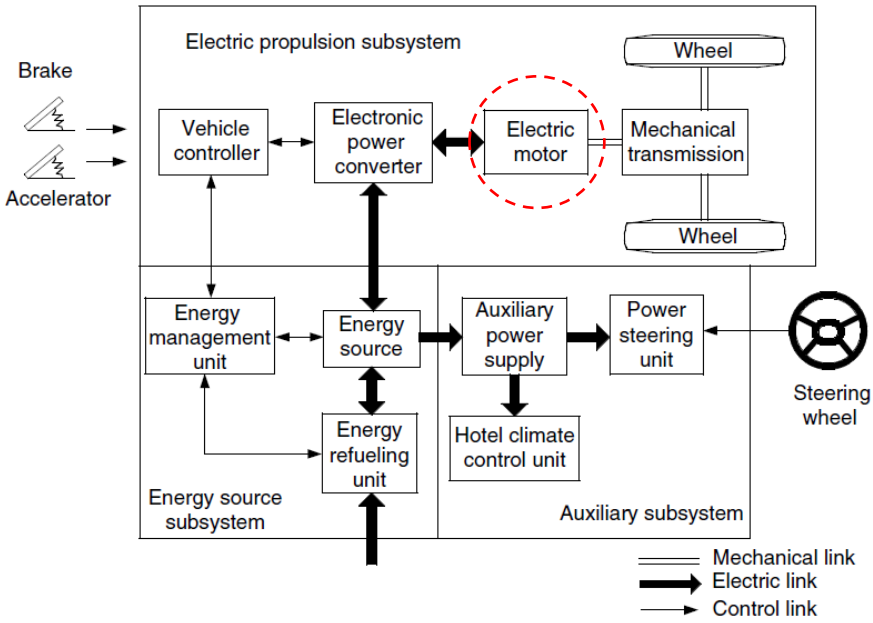

Figure 1.1. General configuration of the modern EV system [1].

Today's EVs typically have a shorter drive range than conventional vehicles. The most light and heavy duty EVs are targeting a range of about 200-300 miles on a fully charged battery. In general, the distance that an electric vehicle can travel on a fully charged battery or drive range is a function of vehicle technology (electric motor performance and control strategy), battery size and its advancement, weight carried, and an individual's driving style. Among them the electric motor, as the only propulsion source, has dominant impact on drive range. Hence, achieving an advanced electric motor for a high performance vehicle which is compact, light, and efficient is a valuable target. However, the electric motor price is still a concern.

1.2.1 Hybrid Electric Powertrain (HEV)

The hybrid electric vehicle in simple terms is the combination of an ICE with one or more electric motor, generator, and a battery pack. It combines the propulsion mechanism with a

rechargeable energy storage system (RESS) composed of a battery pack and an ultra-capacitor, consequently, resulting in better fuel economy.

Two main powertrain architectures in HEV are "Parallel" and "Series" hybrid systems:

- In parallel hybrids, the ICE and the electric motor are both connected to the mechanical transmission and can simultaneously transmit power to the wheels, usually through a conventional transmission. Currently, commercialized parallel hybrids use a single, small (<20 kW) electric motor and a small battery pack. In this architecture, the electric motor is not designed to be the whole source of motive power from launch. Parallel hybrids are also capable of regenerative braking. Additionally, the internal combustion engine may supply a generator for supplemental recharging. Figure 1.2 shows the general configuration of the parallel HEV.

- In series hybrids, only the electric motor drives the drive train and the ICE works as a prime mover of the generator to power the electric motor or to recharge the batteries. The battery pack can be recharged from regenerative braking or from the generator. Series hybrids usually have a smaller combustion engine but a larger battery pack compared to parallel hybrids that implies higher cost and weight compared to parallel. However, this configuration allows operating with higher efficiency in city driving. Figure 1.3 shows the schematic of series HEV.

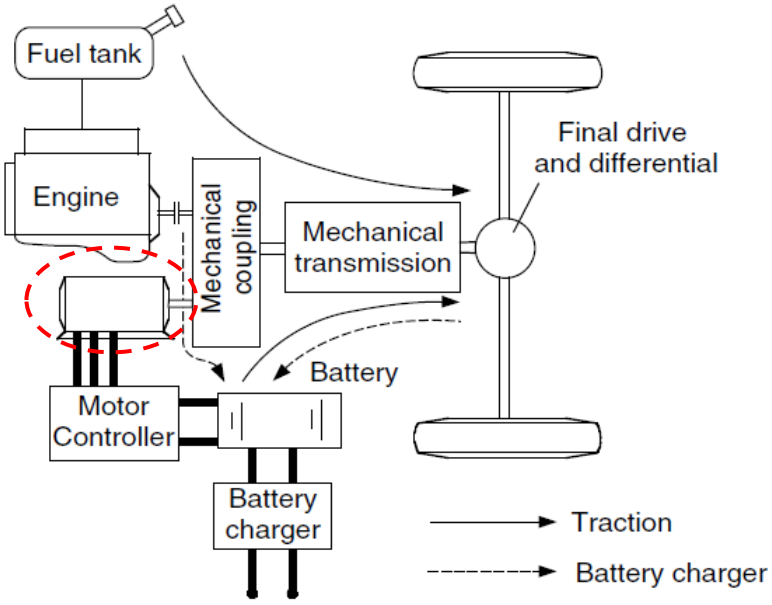

Figure 1.2. General configuration of the parallel HEV system [1].

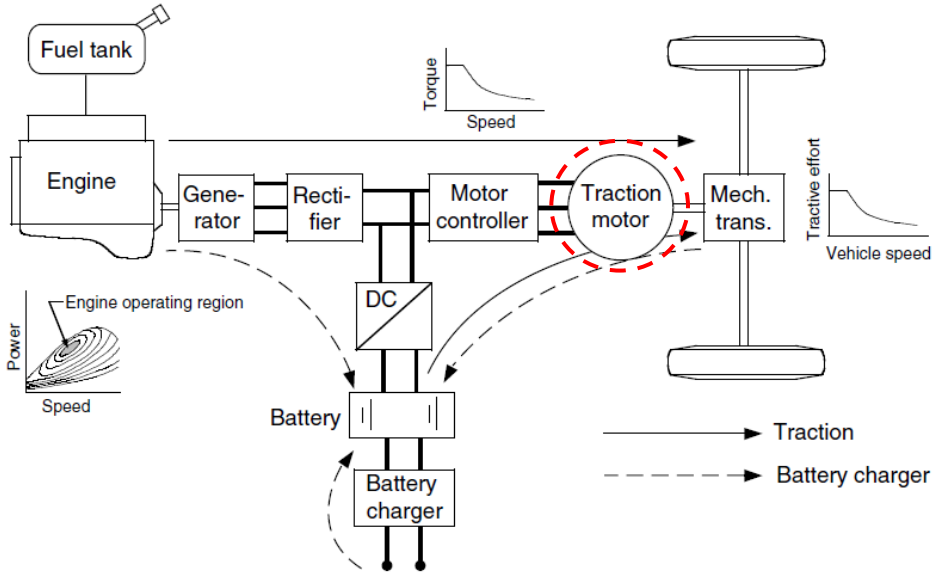

Figure 1.3. General configuration of the series HEV system [1].

1.2.2 Electric Motor Drive Requirements for Traction System

The worldwide trend in efficient energy conservation causes the need to increase the applications of the electric drive trains in the automotive industries, particularly AC drives as traction (EV) or subtraction systems (HEV). Recent advantages of high quality magnetic materials, solid state devices, and microcontrollers have contributed to new, energy efficient and high performance electric drives that use modern electric motors. The motor drive is the heart of the electric powertrain. It consists of the electric motor, the power converter, and the electronic controller, in which the electric motor is the dominant part of the system. In general, electric motors in powertrain applications need to meet major requirements that we can summarize as follows [1, 8, 9]:

- High instant power and high power density
- High torque at low speed and high power at high speed
- Low torque ripple
- Wide speed range
- Fast dynamic response
- High efficiency over full speed range
- High efficiency at regenerative breaking mode
- Reliability and robustness on different operating modes
- Reasonable cost

On the other hand, the choice of electric motor drives for traction systems is generally determined based on three dominant factors by manufacturers: cost, weight, and size. Therefore, an efficient and power dense electric machine with reasonable cost can be considered as a strong alternative for traction applications.

1.2.3 Possible Alternatives of the Electric Motor Drive for Traction

The developments of electric propulsion systems has been affected by the growth of various technologies, especially electric motors [8]. The applications of electric motor drives in EVs and HEVs are considerably different from the industrial types. The differences are due to the vehicle constraints, driver expectations, and energy sources that may be defined as driving cycle schemes. The motor drives that are used in EVs and HEVs usually require frequent starts and stops, high rates of acceleration and deceleration, high torque at low speed for taking-off or hill climbing, low torque at high speed for cruising, and wide speed range of operation. The commutator and commutator-less motors are two main categories of electric motor drives that may be utilized for powertrain.

Figure 1.4 shows the general overview of the electric motor drive alternatives for automotive applications [1]:

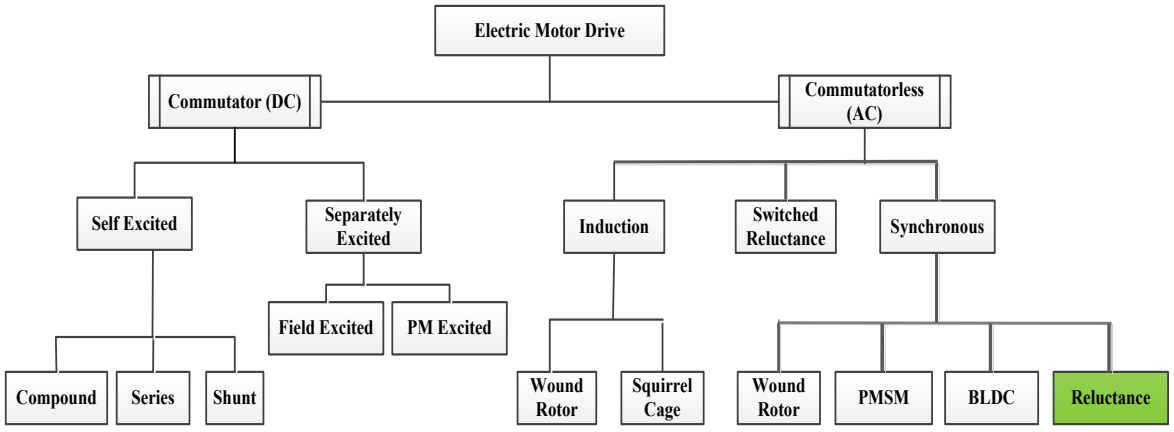

Figure 1.4. Motor drives general overview for automotive applications.

There are a number of competing and complementary electric motor drive technologies which are potentially utilized in commercial HEV and EV propulsion systems. However, among them, the cost and efficiency are the two dominant properties that can influence the selection of the electric motors by manufacturers. Recently, there is a widespread interest in utilizing new alternatives in automotive industries to overcome both the price and efficiency challenges of motor drives and some of these alternatives are currently under investigation for commercial use. In general, the most interesting electric motor architectures in today's automotive industries can be categorized as follows:

- DC machine
- Induction machine (IM)
- Permanent magnet synchronous machine (PMSM, BLDC)
- Switch reluctance machine (SRM)
- Synchronous reluctance machine (SynRM, the strong alternative under investigation)

Moreover, among the previously-mentioned motor drive requirements (1.2.2), the extended drive range ability and energy efficiency are the two fundamental characteristics which are influenced by vehicle dynamics and architecture. Hence, selection of electrical machine for vehicle application needs special attention to the traction motor's speed range and energy efficiency [4]. Table 1.1 reviews a summary of different electric motor drives adopted in today's automotive industries [8, 9];

Table 1.1 Electric Motor Drives Adoption in Automotive Industries

EV & HEV Model	Motor drive system	EV & HEV Model	Motor drive system
 Peugeot-Citroen (France)	DC	 BMW/ X5 (Germany)	IM
 Kia/ Soul (S. Koria)	PMSM	 BMW/ I3 (Germany)	PMSM/IM
 Daimler-Chrisler/Durango (Germany, USA)	IM	 Chevrolet/ Silverado (USA)	IM
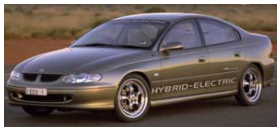 Holden/ ECO (Australia)	SRM	 Tesla/S (USA)	IM
 Toyoa/ Prius (Japan)	PMSM	 Honda/ Insite (Japan)	PMSM
 Chevrolet/ Spark (USA)	PMSM	 Nissan/ Leaf (Japan)	PMSM
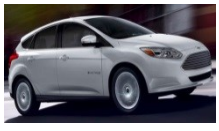 Ford/ Focus (USA)	PMSM	 Toyota/ RAV4 (Japan)	PMSM/IM

1.2.3.1 DC Machine

Since EV was invented in 1834, conventional DC machines have been widely used in electric vehicles as traction motor. This is due to their maturity and well suited torque-speed characteristic to electric powertrain requirements. Due to the limitations associated with the power electronics as well as AC motor drives before1970s, this machine was the most attractive alternative for the electric vehicle applications in which the adjustable speed was a requirement. Today, this machine is still an alternative for different electric traction applications owing to its mature properties which are summarized below [1]:

- Control simplicity
- Good speed regulation
- Frequent starting ability
- Simple braking and reversing
- Proper torque speed characteristic

The operation principal of the DC machine is straight forward and relies on the impact of the armature flux that is characterized by the input voltage and back electromotive force (EMF) in one hand, and the field flux that is created by field current or magnetic material on the other hand. Typically, depending on the mutual interconnection between the field and armature windings, there are four types of the wound-field DC motors. They are separately excited, shunt excited, series excited, and compound excited. Figure 1.5 shows general configuration of a DC motor.

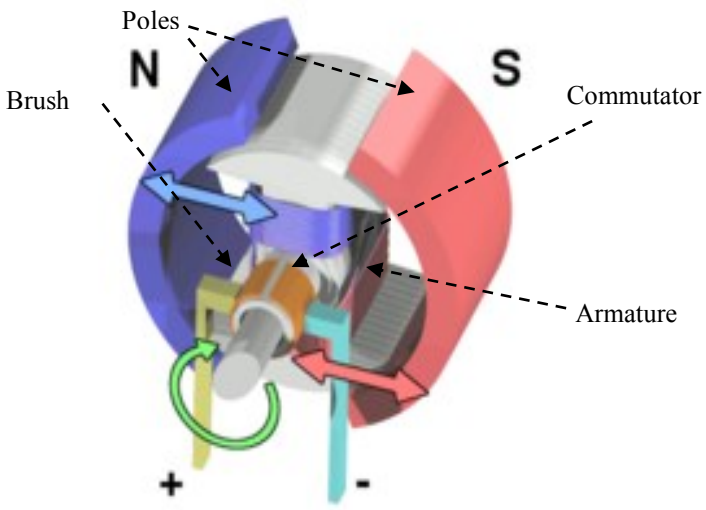

Figure 1.5. General configuration of a DC machine.

Currently, the separately excited DC machine controlled by a DC-DC chopper is mostly used in traction applications that offer several advantages such as control flexibility of the armature and field voltage, higher efficiency, fast dynamic response, and small size. However, the commutator in the structure of the armature is a dominant drawback that increases the operating cost due to regular maintenance and reduces the machine reliability.

1.2.3.2 Induction Machine (IM)

Since, high reliability and maintenance-free operation of the electric motor drives are the prime considerations of the electric powertrain system in EV and HEV technologies, commutator-less motor drive becomes the most attractive alternative for traction in automotive industries. Among them, the IM motor drive is one of the most mature technologies due to its number of advantages over conventional DC commutator drive. These advantages that are also important for automotive applications can be summarized as follows [1, 8-11];

- High efficiency
- Low cost
- High power density
- Robustness
- Ruggedness
- Ability to operate in hostile environments

However, as an AC drive, this machine is not preferred to DC at low power applications due to the cost of the inverter.

The induction machine is an AC machine with asynchronous topology in which the stator and rotor field are rotating at different speeds. The slip is usually small and affects the output power and the torque developed by the machine. IMs can be categorized in squirrel cage and wound rotor types. The most common used type for traction applications is the squirrel cage rotor whereas the wound rotor type is less attractive due to its higher cost and maintenance requirements.

Figure 1.6 and Figure 1.7 show a general configuration and a typical torque speed characteristic of the IM respectively. Torque profile of the IM presents an extended speed range operation over base and maximum speed boundary with constant power that can be obtained by flux weakening control method. This property is one of the major requirements of the powertrain systems. However, at the critical speed, the machine's torque meets the breakdown value which can limit the constant power operation.

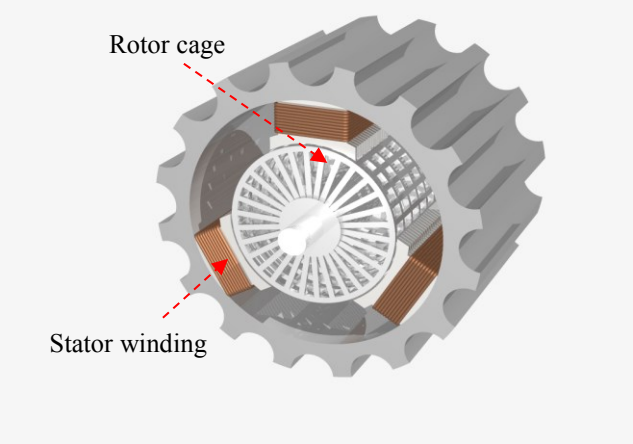

Figure 1.6. General configuration of IM.

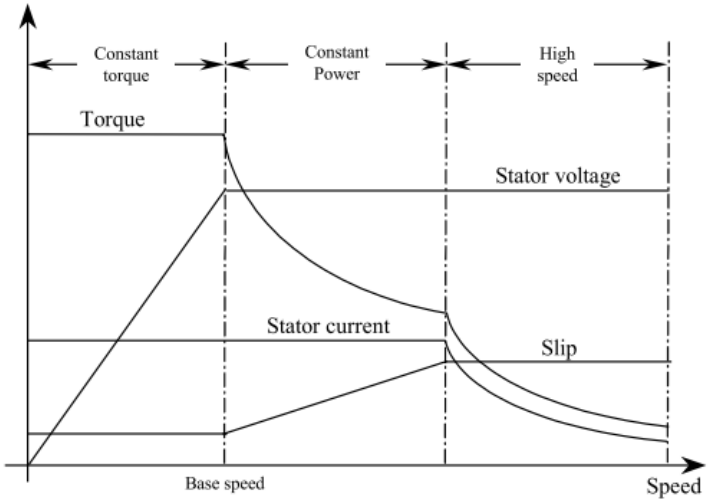

Figure 1.7. Typical torque profile of IM.

1.2.3.3 Permanent Magnet Synchronous Machine (PMSM)

Permanent magnet synchronous machines, particularly interior type (IPM), have been widely used for electric powertrain in EVs and HEVs owing to their unique merits such as high

efficiency and high power density. In this topology, compared to IM, the rotor cage or winding in field excitation mechanism is replaced by high energy rare earth permanent magnet. The resultant machine would be an efficient and power dense motor drive. Considering the location of magnet material in the rotor structure, the PMSM can be divided into two categories which are surface mounted permanent magnet machines (SPM) and interior permanent magnet machines (IPM). The IPMs with extra features such as mechanical robustness and capability of flux weakening at constant power and high speed operation are well suited as vehicles electric powertrain.

With regards to the shape of produced electromotive force (back-emf), permanent magnet machines are divided into two main groups:

- Sinusoidal permanent magnet synchronous machine (PMSM, IPMSM)
- Brush-less DC machine (BLDC)

The PMSM can be fed by sinusoidal voltage wave-forms with sinusoidal back-emf and draws the same sinusoidal current wave-forms through three phases. The BLDC produces a trapezoidal back-emf and draws rectangular pulses of current through only two phases at any instant of time which makes its control technique easier. The IPMSM is the most promising candidate for EV and HEV applications. The major properties of PM motors that are also dominant for traction applications are summarized below [1, 8-10, 12]:

- High efficiency
- Wide speed range (by controlling the conduction angle of power converter)

- High speed operation
- Compactness
- Ease of control
- Fast dynamic response
- Low maintenance
- Ease of cooling
- Low noise

Figure 1.8 and Figure 1.9 show a general configuration and a typical torque speed characteristic of the IMPSM respectively in which ω_b and ω_r are the machine's base and maximum speed.

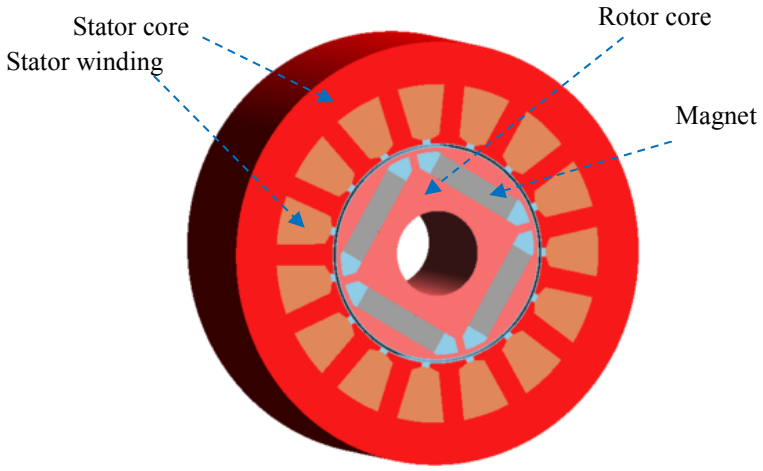

Figure 1.8. General configuration of the IPMSM.

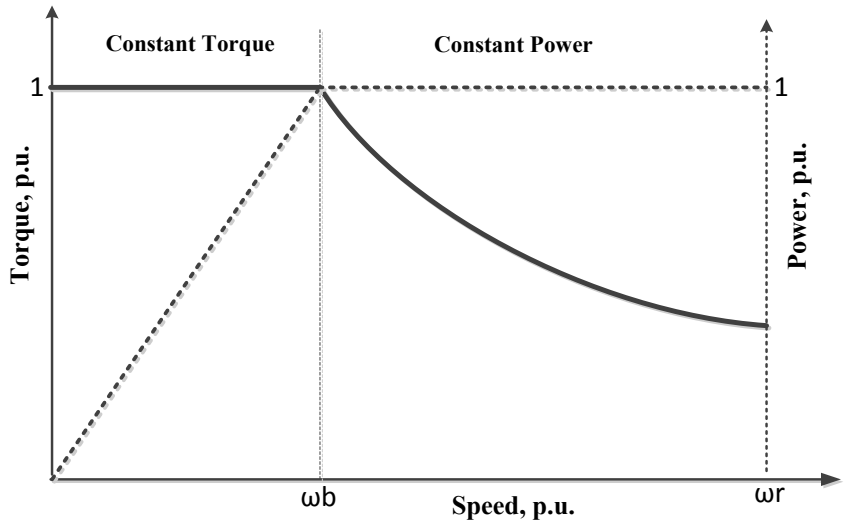

Figure 1.9. Typical torque profile of the IPMSM.

Due to the fixed PM excitation and current control constraint with regards to demagnetization problem, this machine inherently does not have very wide constant power region (flux weakening range). This reduces the machine efficiency at high speed operations, but by controlling the conduction angle of switching devices in power converter, the speed range at constant power region may be extended more than three times. However, at a very high speed the efficiency may drop again [9]. Besides having unique advantages, the BLDC has some drawbacks that can be summarized as follows:

- High cost
- Magnet demagnetization (it may happen in flux weakening)
- Sensitivity to temperature (robustness issue)
- Safety issue (stator may be reenergized by a large number of magnets when the wheel is spinning freely and may produce a high voltage at motor terminals)
- Blocked rotor risk regarding to inverter short circuit failure

1.2.3.4 Switched Reluctance Machine (SRM)

The switched reluctance machine is a double salient single excited motor. The stator consists of simple concentric windings and the rotor has simple structure without any windings, magnets, commutators, and brushes. The SRM rotor's low moment of inertia causes fast dynamic response which leads to fast acceleration. They have high starting torque and high torque to inertia ratio. SRM motor is recognized for having strong potential for traction applications owing to its numerous merits that are summarized below [1, 8, 9, 13, 14]:

- Low cost
- Very wide speed range
- High efficiency
- Simple and rugged structure
- Simplicity in control
- High speed operation capability
- Reliability
- Fault tolerant operation and reliable converter topology
- Easy to cool and insensitive to high temperature

The SRM can inherently operate with a long speed range. Owing to its outstanding torque-speed characteristic (higher maximum speed, $\omega_{r\text{-}srm} >> \omega_{r\text{-}pmsm}$), this machine is capable of operating in variable speed application such as EV's and HEV's electrified propulsion system which offers variable speed powertrains without variable speed gearbox.

Due to its double saliency structure (rotor, stator), the reluctance of the flux path for each phase winding varies with the rotor position. Moreover, since the SRM is commonly designed for high degree of saturation at high phase current, the reluctance of the flux path varies with the

phase current as well. Consequently, the stator flux linkage, phase bulk inductance, and phase incremental inductance are a function of the rotor position and phase current. Figure 1.10 and Figure 1.11 show a general configuration and a typical torque speed characteristic of the SRM. It should be noted that ω_r in Figure 1.11 is much higher than that of the PMSM in Figure 1.9.

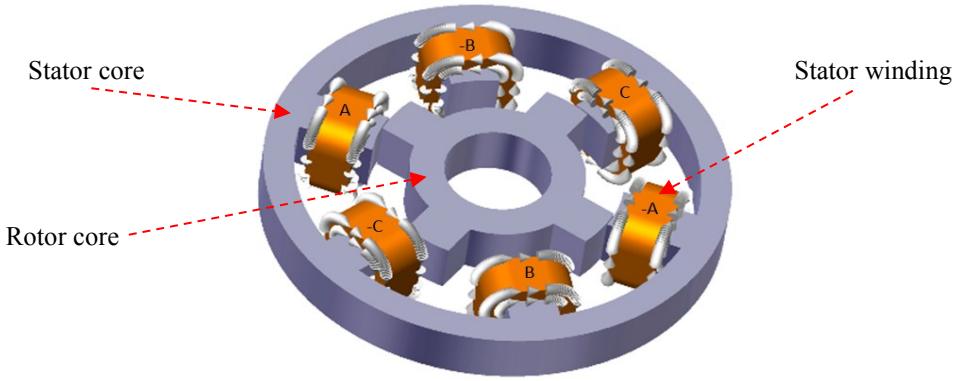

Figure 1.10. General configuration of the SRM.

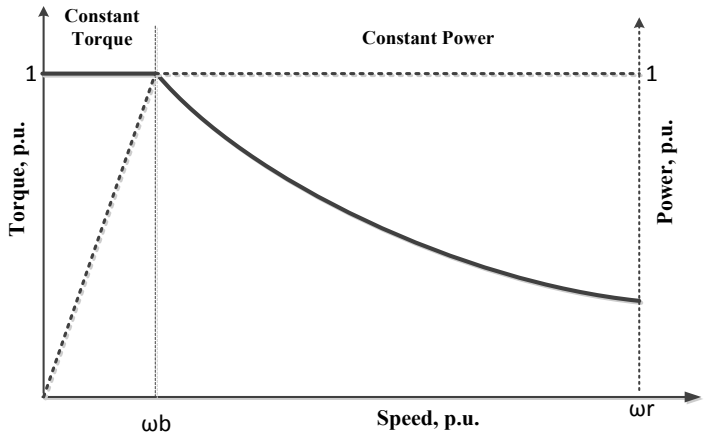

Figure 1.11. Typical torque profile of the SRM.

Despite the excellent properties, the SRM suffers from different drawbacks which outweigh their advantages for automotive applications. These technical issues can be summarized as follows:

- High torque ripple
- Acoustic noise generation
- Considerable DC bus current ripple
- Electromagnetic interference (EMI) noise generation
- Special converter topology
- Complexity in design

1.2.3.5 Synchronous Reluctance Machine (SynRM)

The synchronous reluctance machine (SynRM) is not a new concept. The first theoretical and technical introduction of this motor with reluctance torque production and sinusoidal magnetic motive force (MMF) using the conventional IM stator was made by Kostko in 1923 [15]. However, the machine had suffered from stability and lack of start-up torque during the direct lineup start. Later on, it was shown by Vagati in 1990s that the SynRM can be controlled easily using a closed-loop control technique and the above-mention drawbacks can be overcome with both field oriented and direct torque control methods. Furthermore, the machine would be capable of operating with considerable power and torque density [16-18].

In principle, the SynRM is similar to the conventional salient pole synchronous motor, but does not have an excitation winding in the rotor. In this machine only the rotor is constructed by

barriers (air) and segments (steel) layers. Based on the anisotropic structure of the rotor geometry, the SynRM's rotor can be put in three different categories:

a) Traditional simple rotor

b) Axially laminated anisotropic rotor (ALA)

c) Transversally laminated anisotropic rotor (TLA)

Figure 1.12 shows different anisotropic structures of the SynRM's rotor.

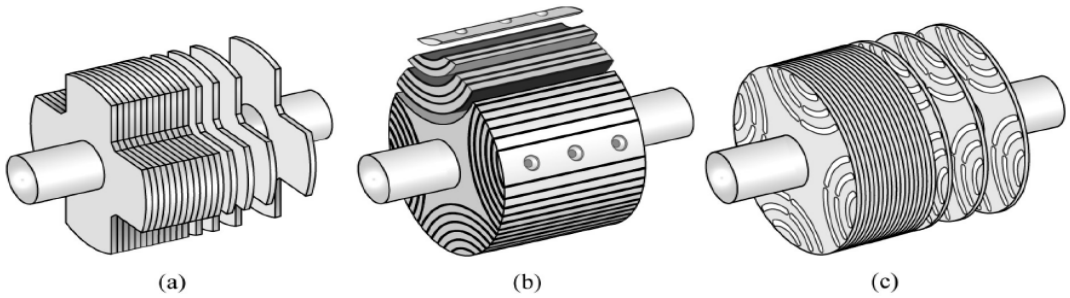

Figure 1.12. Different anisotropic structures of the SynRM's Rotor, (a) traditional simple rotor, (b) axially laminated anisotropic rotor (ALA), (c) transversally laminated anisotropic rotor (TLA).

The main advantages of the SynRM relies on elimination of the rotor copper losses that permits higher continuous torque than an IM of the same size in one hand, and the simple structure of the rotor that leads to lower cost compared to IM and BLDC on the other hand. The synchronous reluctance solution represents a possible alternative to AC drives for traction

applications. In general, the important features of the SynRM can be summarized as follows [18-23]:

- Low cost
- High efficiency
- High torque per ampere capability
- Insensitive to operating temperature
- Simplicity in control and easy field weakening capability
- Identical topology for stator and inverter power circuits to IM
- Short time over load capability
- Simple and rugged structure
- Reliability

The SynRM is a motor for generating torque by variation of the machine's reluctance caused by rotor position. Hence, the reluctance torque produced by the SynRM depends on the saliency effect and is proportional to the difference of the magnetizing inductances (L_d-L_q) of the d-q axis in rotor frame coordinate system. In order to maximize the output torque developed by motor, it is required to increase the ratio of L_d over L_q called "saliency ratio". This parameter is the key in machine design and its optimization process.

The interest in using the synchronous reluctance machine for traction applications is increasing very fast due to the fact that this class of the electrical machine is capable of meeting most of the properties of the IM and BLDC, but at a lower cost. Despite having the excellent above mentioned advantages, the SynRM has some drawbacks that are important for traction applications. These drawbacks are summarized as below:

- low power factor (0.55-0.7)
- Low speed range
- Torque ripple

Since the major operation characteristics of high performance SynRM relies on the anisotropic structure of the rotor which is called “Saliency”, the rotor geometry is the main concern to achieve a proper design of the synchronous reluctance machine for traction applications.

1.3 Selection of Motor Drive for Research Work

Currently permanent magnet machines with rare-earth magnets are widely used for the traction drives of electric and hybrid electric vehicles because of their high efficiency and power density. However, there exists a concern regarding limited supply or increased prices of rare-earth magnets, as China controls the global supply of rare-earth magnet production, supplying over 97% of the world’s rare-earth production, and consuming most of its production locally. Due to the possibility of future shortage of rare-earth materials, the use of rare-earth permanent magnet motors in electric vehicles may not be economic or technically feasible in the future. Therefore, it is essential for the future electric vehicle industry to find alternative motor technologies that do not depend on rare-earth magnets.

Synchronous reluctance machines (SynRM) is used in industries owing to their unique merits such as high efficiency, fast dynamic response, high torque to current ratio, and low cost. However, considering the major requirements of traction systems, such as high torque and power density, low torque ripple, wide speed range, proper size, and the capability of meeting specific torque envelop, this machine is under intensive research work for development. In this machine,

the anisotropic structure of the rotor that is the source of reluctance torque can eliminate use of magnet, cage, and winding from rotor structure. Consequently, compared to the IM, by elimination of the rotor cage's relative copper losses, the efficiency and compactness will be increased. The possibility of achieving required power and torque with lower losses and temperature rise compared to the same size IM, improves the lifetime of the motor insulation and bearings and decreases maintenance demands and failures as a result. Since, the choice of motor for traction is generally determined based on three factors by manufacturers: cost, weight, and size, the SynRM can be considered as a strong alternative compared to IM due to its considerable high efficiency and low cost in middle and high power ranges.

On the other hand, without magnets in the rotor structure, the SynRM is similar to the conventional salient pole synchronous motor, but does not have an excitation in the rotor. In this condition, only the rotor is constructed by flux barriers (air) and flux carriers (steel). With the absence of magnets, start-up and drive's control is performed by power electronics which will be simpler than PMSM owing to the simplification of the vector control. Because, In SynRM, there's only one vector, the stator field vector, which needs to be controlled versus rotor position angle as well as, no need for flux weakening by injecting the negative I_d, and no concern about demagnetization issues. Besides lower price compared to the PMSM, canceling the magnets removes back-emf voltage induced in the stator of the SynRM which can eliminate the overvoltage protection of the power electronics stages as well as over current challenges in the case of inverter failure. Also, the machine's rugged structure refers to its capability of high speed operation. Therefore, the mechanical variable speed power transmission such as gearbox can be eliminated in powertrain system. Thus, the SynRM can also be a strong competitor to PMSM for traction applications.

Compared to the SRM, except the extended speed range that is a superior property of the SRM, the SynRM offers all other its properties. Moreover, the sinusoidal flux distribution produced by stator winding and the rotor flux carriers in SynRM refers to a lower torque ripple which distinguishes this machine from the SRM. Whereas, high torque ripple is the highlighted drawback of the SRM. In this research work, development of methods, algorithms, and software for the design of the synchronous reluctance motors (SynRM) for traction applications is proposed. The key motivations of the research work are summarized as follows:

- The need for new alternative technologies for EVs and HEVs motor drives which do not depend on rare-earth permanent magnet materials and can achieve similar performance.

- The need to enhance the energy efficiency of the electric motor drives for EVs and HEVs with lower cost that helps reducing air pollution and increasing the public interest in using this green technology.

- The need for diversity of products in order to be flexible with different economic condition and customer's satisfaction.

To pursue these goals in this research work, the electric motor proposed to be designed for traction applications is based on the concept of the synchronous reluctance machine that is a strong alternative as an efficient, less expensive, and reliable motor technology. This machine offers superior advantages that have been mentioned in (1.2.3.5).

1.3.1 Potential Issues of the SynRM as an Electric Powertrain

1.3.1.1 Sizing Method

Considering today's compact passenger vehicles in which the size and weight are the design limitations, proper size of the SynRM is an important challenge for the design. Regarding to the major requirements of the traction motors such as high torque and power density, low torque ripple, wide speed range, and proper size, this machine is still under investigation to be developed for high performance in traction applications. In general, the choice of electrical machine for traction application is determined by manufacturers with respect to three dominant factors; cost, weight, and size. Hence, the machine proper size estimation is the major step of the design procedure before attempting to design of the rotor geometry. Many investigations reported in the literature are mostly focused on performance optimization by rotor geometry [17-19, 21, 23-26], control strategy [27-33], and comparison of the SynRM to different machines [9, 17, 34]. Whereas, there is no particular work on sizing methods of the SynRM based on the traction application requirements.

1.3.1.2 High Torque Ripple

High torque pulsation is one of the most common problems of the SynRM that is caused by the interaction between the spatial harmonics of the electrical loading and the rotor anisotropic geometry. The torque ripple causes additional losses, reduces the efficiency when the machine needs to operate at constant power region, decreases average torque, produces audible noise, and imposes mechanical pulsation on the shaft all of which are intolerable in most applications particularly in traction [19, 25, 35, 36]. To solve these inherent problems, the stator winding is chorded to reduce the lower order MMF space harmonics. However, it has been shown in [35] that this technique reduces the output power of the machine. The rotor or stator is skewed by

numbers of stator slot pitch to reduce the torque slot harmonics, but it has been shown in [19, 35] that, it is not a proper solution due to reduction of the output torque. Over the past decade, intensive work has been done on torque ripple optimization techniques [24, 25, 37, 38] to increase the torque quality in SynRM drives. Today, these machines need to have more improvements with respect to the torque quality in order to meet the EVs and HEVs standards and be considered as a strong alternative for electrified propulsion systems in automotive industries.

1.3.1.3 Low Speed Range

Low flux weakening or low speed range reduces the capability of the SynRM to operate at constant power beyond the base speed for a wide range. This drawback is harmful when the machine is proposed to run as electrical propulsion in EVs and HEVs. In general, differing from the industrial applications of the electric motors, the traction motors usually require a wide speed range in which the desired performance characteristics of the powertrain is to deliver constant output power over the full speed range. The SynRM's flux weakening capability may refer to adequate speed range in industrial applications [1, 16]. However, it cannot satisfy the traction requirement regarding the wide speed range of 3 to 6. Over the past decades, there has been intensive work to improve performance of the SynRM reported in the literature, but very few studies have been performed on the traction applications capability of this machine in particular, on its drawback such as low speed range. In [39], the performance of EVs and HEVs using SynRM was investigated and lower speed range of the SynRM compared to the IM and SRM was reported. It was shown in [26] that; the speed range (base speed/ maximum speed) of a high power SynRM cannot exceed beyond 1.5. However, this number for PMSM and SRM is more

than 3 and 6 respectively. Therefore, extending the speed range of the SynRM for automotive applications is still an interesting area of investigation.

1.4 Research Objectives

The goal and objectives of this research work are to:

- Analytically design and perform calculations using the mathematical model of the proposed machine.
- Propose a sizing methodology of the SynRM for the automotive applications considering initial data, assigned parameters, and specific torque envelope.
- Identify the key parameters which affect the SynRM's performance for traction applications.
- Develop finite element software in order to have appropriate flexibility with respect to the machine's geometry in particular, the rotor to analyze performance of the proposed machine using different geometries and key parameters.
- Improve the performance of the proposed SynRM using computer aided analysis in order to meet the desired requirements of automotive applications such as torque envelop, proper size, and converter rating.
- Examine prototypes and compare performances of the proposed SynRMs to evaluate the design methods.

1.5 Organization of this Thesis

The organization of this Thesis is as follows:

Chapter 2: Operation of synchronous reluctance machine; fundamental operation of the synchronous reluctance machine based on anisotropic concept and saliency effect is reviewed. The equivalent circuit and mathematical model in conjunction with the machine's main characteristics are described. Different rotor geometry classifications, the proposed rotor structure, and the design parameters are discussed.

Chapter 3: Analytical Design; presents the analytical method and development of the relevant codes for design procedure in order to propose a sizing method. The sizing methodology is used to design a SynRM to meet a specific torque-speed envelope for traction application. The method criteria is based on the machine's mathematical model, equivalent circuit, initial data, and assigned parameters. The electric and magnetic parameters of the proposed machine in conjunction with the core dimensions are calculated. Finally, the proposed method's evaluation and validity are investigated using FE analysis and experimental test.

Chapter 4: Torque Analysis; presents a design method to improve the machine torque by minimizing the torque ripple for a given magnetic material based on the rotor geometry. Furthermore, the possibility of using anisotropic magnetic material (cold roll grain oriented/CRGO) for the rotor core in order to improve the machine electromagnetic torque is investigated. The proposed methods are evaluated through the FEA and experimental examinations.

Chapter 5: Core Analysis; discusses a core analysis focusing on the magnetic and mechanical performance. A computer aided analysis on the core with multiple magnetic material and different core structures is performed to identify dominant parameters which affect the machine performance with respect to the output torque and mechanical robustness for automotive applications. A new design based on variable ampere-turns method is proposed and discussed to extend the machine speed range at high speed operation. The proposed methods evaluation is supported by FEA and experimental test.

Chapter 6: Conclusions and future work; Discusses improvements to the design and future perspectives of the research work.

1.6 Contributions of this Thesis

The specific contributions of this Thesis are summarized as follows:

1.6.1 The Main Contribution of Chapter 3

1) Propose a sizing methodology for design of synchronous reluctance machines for automotive applications by taking into consideration specific size, converter rating, and torque envelop as the design limitations.

1.6.2 The Main Contributions of Chapter 4

1) Propose a geometrical method for the rotor design to improve the machine output torque and reduce the torque ripple significantly without skewing or chording pitch winding.

2) Propose an innovative method for the rotor poles assembly and lamination to increase the machine output torque by 5-10 percent using cold rolled grain oriented electrical steel as the rotor core material.

1.6.3 The Main Contributions of Chapter 5

1) Identify and address the most important geometrical, magnetic, and mechanical design parameters of the SynRM's which have not been verified yet for automotive applications. These design parameters affect strongly the machine performance with respect to the output torque and torque ripple at high and low speed operations.

2) Develop a new method using variable ampere-turns concept by which the SynRM's flux weakening capability controlled under conventional flux weakening method (FWC) improves and the speed range can be extend more than three times in high speed operations which is desirable for automotive applications.

1.6.4 Industrial and Experimental Contributions

1) Design and manufacturing of a 50hp prototype in industrial level in collaboration with TM4 company as the industrial partner of the research project. This machine is used for real vehicle load test under actual city and highway driving cycles at TM4. Due to the IP issues, the design procedure, specifications, and the test results are not included in the thesis.

2) Design and manufacturing of 7.5hp prototypes with three different rotors for laboratory level examinations in order to validate the design methods at Concordia University. Owing to the geometrical and parametrical nature of the design, the design validation can be generalized for machine with higher ratings.

1.6.5 Patent

Parts of Chapter 4 including sections 4.4 and 4.5 are in the process of the US Patent, No: 05015656-82USPR, entitled: "A Novel Rotor Design Method and Lamination for High Performance Synchronous Reluctance Traction Motors" and currently is patent pending.

1.6.6 Publications

Journal papers published, accepted or submitted:

1) S. Taghavi and P. Pillay, "A Sizing Methodology of the Synchronous Reluctance Motor for Traction Applications," *Emerging and Selected Topics in Power Electronics, IEEE Journal of,* vol. 2, pp. 329-340, 2014.
2) S. Taghavi and P. Pillay," Rotor Core Parameters Sensitivity of Synchronous Reluctance Traction Motors," *in IEEE Trans. On Energy Conversion, 2015 (Accepted).*
3) S. Taghavi and P. Pillay, "A Mechanically Robust Rotor with Transverse-Lamination for a Wide Speed Range Synchronous Reluctance Traction Motor," *in IEEE Trans. On Ind. App., 2015(Accepted).*
4) S. Taghavi and P. Pillay, "Torque Analysis of Synchronous Reluctance Traction Motor Using Rotor Slot Pitch and a Novel Rotor Poles Assembly," *in IEEE Trans. On Energy Conversion, 2015 (Submitted).*

Conference papers published or accepted:

1) S. Taghavi and P. Pillay, "A mechanically robust rotor with transverse-laminations for a synchronous reluctance machine for traction applications," in *Energy Conversion Congress and Exposition (ECCE), 2014 IEEE*, 2014, pp. 5131-5137.
2) S. Taghavi and P. Pillay, "A core analysis of the synchronous reluctance motor for automotive applications," in *Electrical Machines (ICEM), 2014 International Conference on*, 2014, pp. 961-967.

3) S. Taghavi and P. Pillay, "A comparative study of synchronous reluctance machine performance with different pole numbers for automotive applications," in *Industrial Electronics Society, IECON 2014 - 40th Annual Conference of the IEEE*, 2014, pp. 3812-3818.

4) S. Taghavi and P. Pillay, "An Innovative Rotor Core Assembly for High Performance 4-Pole Synchronous Reluctance Traction Motor Using Grain Oriented Lamination, " *in International Electrical Machines and Drives, IEMDC 2015, International Conference on, (Accepted).*

5) S. Taghavi and P. Pillay, "Geometrical Design Aspects of Low Torque Ripple Synchronous Reluctance Traction Motor Using Rotor Slots Pitch Angles, " in *Energy Conversion Congress and Exposition (ECCE), 2015, IEEE, (Accepted)*.

1.7 Summary of Chapter 1

This chapter presented the research background of the synchronous reluctance machine and related investigations of the research work regarding to the automotive applications, described the research goal and objectives, the thesis organization, and the research contributions. Also, in this chapter the electric machine topology for automotive applications was proposed and the proposed machine's potential problems were addressed.

Chapter 2 Operation of Synchronous Reluctance Machine

The first theoretical and technical introduction of this motor with reluctance torque production and sinusoidal magnetic motive force (MMF) using the conventional IM motor stator was made by Kostko in 1923[15]. However, this machine suffered from stability and start up torque during the direct lineup start. Later on, it was shown by Vagati in 1990s that the SynRM can be controlled easily using a closed-loop control technique and the above-mentioned drawbacks can be overcome with both filed oriented and direct torque control methods. Furthermore, this machine is capable of operating with considerable power and torque density [27-29].

2.1 Fundamental Operation of the Synchronous Reluctance Machine

The main idea of the variable reluctance concept is shown in Figure 2.1. Object (a) and (b) are made by isotropic magnetic material and are exposed to a magnetic field (Ψ). Object (a) has different geometric dimensions in d and q-axis which refers to different reluctances, this is called anisotropic object whereas, object (b) has the same geometric dimensions in all directions and hence the same reluctances in the d-axis and q-axis. This is called an isotropic object.

If the d-axis of the object has misalignment angle of (δ) with the magnetic field, this will introduce a field distortion which is aligned with q-axis and will increase the reluctance in d-axis. As a result, an electromagnetic potential energy is created that can develop an electromechanical torque to force the object to be aligned with the minimum reluctance at field direction (d-axis). According to this concept which describes fundamentals of the SynRM, if the angle (δ) which is called load angle is kept constant by applying a constant mechanical load, the electromagnetic potential energy can be converted to mechanical energy on the shaft of the SynRM.

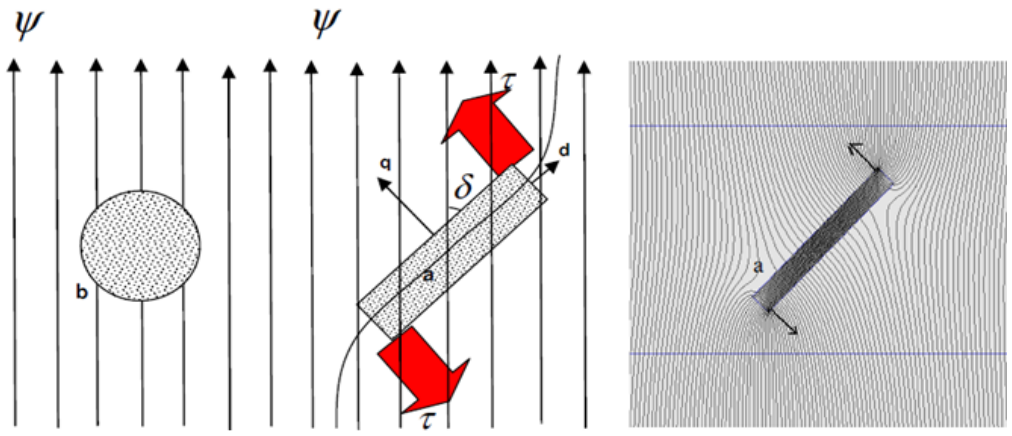

Figure 2.1. Isotropic and anisotropic objects in magnetic field (Ψ), (ABB).

Figure 2.2a shows a basic three phase two-pole synchronous reluctance motor. In principle, the SynRM is similar to the conventional salient pole synchronous motor but does not have an excitation winding in the rotor. Therefore, the rotor is only constructed by salient poles. The stator inner surface is cylindrical and typically retains many of the benefits of the variable reluctance motors and at the same time eliminates its several disadvantages.

Developments in machine design, control methods, and power electronics allow the machine designers to remove the starting cage from the rotor structure and to achieve a better performance by using vector oriented control technique. In vector controlled drives, two crucial parameters are the difference and ratio of the inductances in d-q axis which refer to the saliency or anisotropy property.

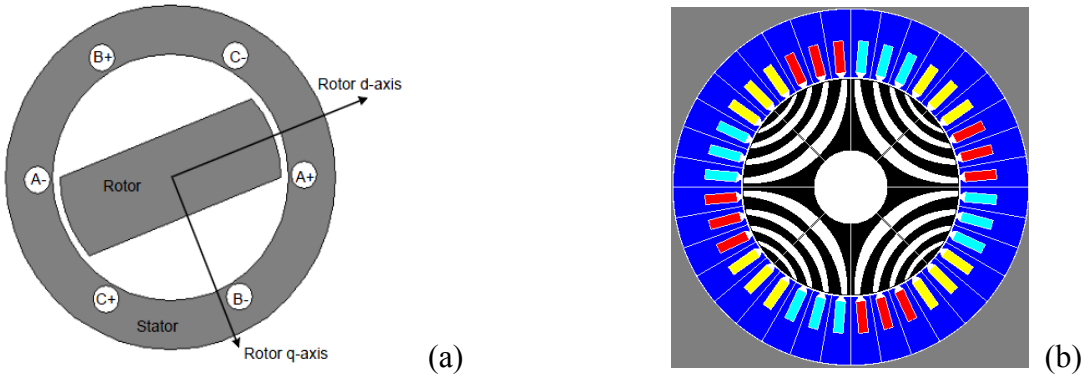

Figure 2.2. Basic three phase two-pole (a) and a modern 4-pole SynRM (b).

This ratio which is the most important parameter to evaluate the SynRM's performance is called saliency ratio and is expressed as equation (2.1). Therefore, in order to design high performance SynRM, the main goal is to obtain both high L_d and low L_q. This refers to having maximum and minimum flux in d and q-axis, respectively[18]. Figure 2.2b shows a typical configuration of a modern 4-pole SynRM in which the proper design of the rotor structure is adapted for a high saliency ratio.

$$\xi = \frac{L_{dm}}{L_{qm}} \qquad \text{Saliency ratio} \tag{2.1}$$

2.1.1 Equivalent Circuit and Mathematical Model

In synchronous reluctance motor the stator winding is identical to IM's in which the flux is distributed in sinusoidal form. Therefore, the machine's equations which define the behavior of the SynRM can be derived based on the conventional wound field synchronous machine while taking into account two important properties; 1- the excitation winding is nonexistent 2- the machine's rotor does not have cage or windings. Figure 2.3 and Figure 2.4 show the vector diagram and equivalent circuit of the SynRM respectively when the iron losses is taken into account [40].

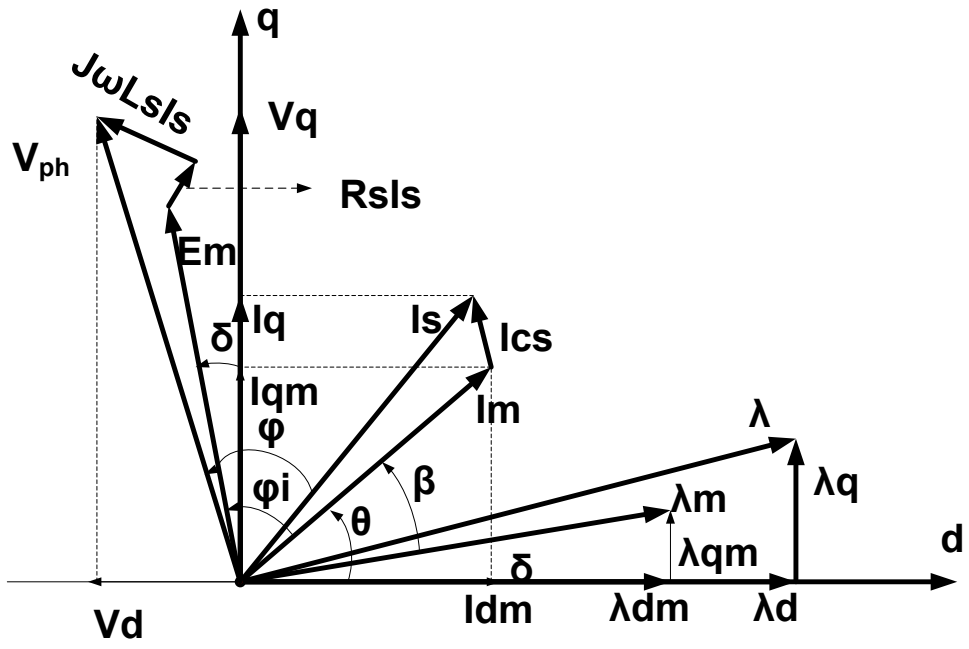

Figure 2.3. Vector diagram of the SynRM including iron losses.

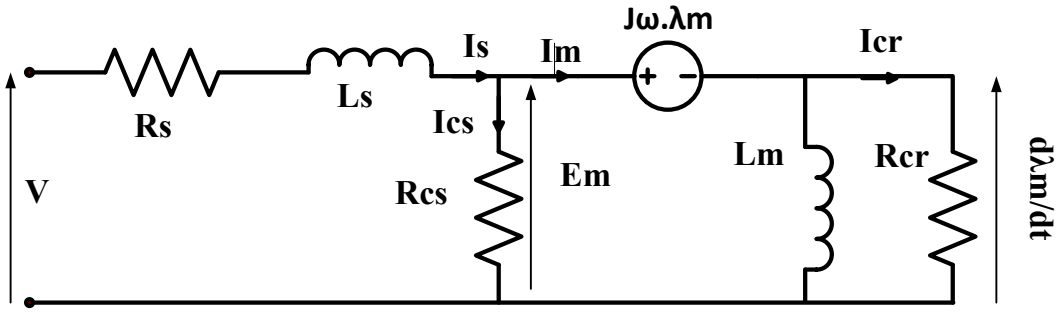

Figure 2.4. The equivalent circuit of the SynRM including iron losses

Considering the above-mentioned figures and by eliminating the rotor excitation caused by winding or cage from the equations, the mathematical model of SynRM in the rotating reference frame (d-q axis) at base speed can be expressed as follows:

$$V_{ph} = E_m + R_s i_s + j\omega_{be} L_s i_s \quad (2.2)$$

$$E_m = \frac{d\Lambda_m}{d_t} + j\omega_{be}\Lambda_m \quad (2.3)$$

Where; $\omega_{be} = \omega_b P_o \frac{2\pi}{60}$ is the electrical base speed, V_{ph} is the phase voltage, i_s is the phase current, E_m is the phase electromagnetic motive force (emf), R_s is the phase resistance, L_s is the phase leakage inductance, λ_m is the phase magnetizing flux, and P_o is the pole pairs.

Neglecting the cross coupling effect allows us to express the magnetizing flux as in (2.4).

$$\Lambda_m = L_{dm} i_{dm} + jL_{qm} i_{qm} \quad (2.4)$$

Where; i_{dm}, i_{qm}, L_{dm}, and L_{qm} are the d-axis and q-axis magnetizing current and magnetizing inductance in rotary reference frame respectively.

Therefore, in steady state in which $\frac{d\lambda_m}{dt} \cong 0$, by substituting (2.3) and (2.4) into (2.2) we can rearrange the machine's phase voltage, (2.2), and its d-q components as follows:

$$V_{ph} = (-\omega_{be} L_q I_{qm} + R_s I_{dm}) + j(\omega_{be} L_d I_{dm} + R_s I_{qm}) \quad (2.5)$$

$$V_d = -\omega_{be} L_q I_{qm} + R_s I_{dm} \quad (2.6)$$

$$V_q = \omega_{be} L_d I_{dm} + R_s I_{qm} \quad (2.7)$$

The vector equations (2.6) and (2.7) can sufficiently operate as the machine mathematical model in order to characterize the magnetic and electric parameters of the proposed SynRM during the analytical design. This will be discussed in more details in the next chapter.

2.2 Main Characteristics

In order to design and evaluate the performance of the SynRM, it is quite necessary to verify its most important parameters and characteristics. These parameters and characteristics that are mainly targeted during design process can be summarized below:

- Electromagnetic torque
- Power factor
- Efficiency
- Torque per kVA
- Torque ripple
- Speed range (field weakening range)
- Iron losses

2.2.1 Electromagnetic Torque

In synchronous reluctance machine the electromagnetic torque is produced by the interaction between air gap flux and its corresponding magnetizing current. Hence, referring to Figure 2.3and equations (2.1), (2.3), and (2.4), different expressions of the electromagnetic torque can be obtained as in equations (2.8) to (2.11) [16, 40].

$$Te = \frac{3}{2}\frac{P}{2}\lambda_m i_m \sin\beta \tag{2.8}$$

$$Te = \frac{3}{2}\frac{P}{2}\left(L_{dm} - L_{qm}\right) i_{dm} i_{qm} \tag{2.9}$$

$$T_e = \frac{3}{2}\frac{P}{2}\left(L_{dm} - L_{qm}\right) Im^2 \sin 2\theta \tag{2.10}$$

$$T_e = \frac{3}{2}\frac{P}{2}(\xi - 1)(\frac{E_m}{\omega L_{dm}})^2 \sin 2\delta \quad (2.11)$$

The strong message from the above-mentioned equations is that; for a certain voltage and operating speed, the developed torque on the shaft depends on the saliency ratio (ξ) and reaches to its maximum at a proper load angle (δ) or current angle (θ). Since during the machine operation, direct control of the load angle is not practically feasible, the current angle is the selected parameter to regulate the rotor position at the proper value. Equations (2.1), (2.4) and the resultant equations (2.12), (2.13), from vector diagram of Figure 2.4 lead to identify the relation between load and current angle as in (2.14).

$$\tan\delta = \frac{\lambda_{qm}}{\lambda_{dm}} \quad (2.12)$$

$$\tan\theta = \frac{I_{qm}}{I_{dm}} \quad (2.13)$$

$$\theta = \tan^{-1}(\xi \tan\delta) \quad (2.14)$$

2.2.2 Power Factor

The machine vector diagram (Figure 2.4) allows identifying the air gap or apparent power factor which is also called internal power factor (IPF). This characteristic can be expressed in different forms as in (2.15) [41, 42] which yield the final expression of IPF as in (2.16).

$$IPF = \cos(\varphi_i) \text{ or } \quad IPF = \sin(\beta) \text{ or } \quad IPF = \cos(\frac{\pi}{2} + \delta - \theta) \quad (2.15)$$

$$IPF = (\xi - 1)\sqrt{\sin(2\theta)/2(\tan\theta + \xi^2 \cot\theta)} \quad (2.16)$$

Equation (2.16) shows that, IPF is a function of current angle which depends on the machine saliency ratio and reaches to its peak at $\theta = \tan^{-1}\sqrt{\xi}$. Therefore, the maximum internal power factor can be expressed as shown in (2.17). This, again, confirms the dependency of the power factor on the saliency ratio in SynRM [42].

$$(IPF)max = \frac{\xi - 1}{\xi + 1} \quad (2.17)$$

It must be mentioned that the terminal power factor which is derived in (2.18) is not identical to the air gap power factor in steady state. Hence, considering the vector diagram, there is a small deference between the two that is caused by machine's losses [21, 31].

$$\cos(\varphi) = \frac{V_d i_d + V_q i_q}{|V||i_s|} \quad (2.18)$$

2.2.3 Efficiency

Efficiency is one of the most important characteristics of the SynRM design, particularly, in vehicle applications. Since the iron losses are negligible compared to the copper losses in low speed [29], the efficiency can be expressed in (2.19) and rearranged in (2.20).

$$\eta = \frac{\omega T_e}{\omega T_e + 3R_S {I_s}^2} \quad (2.19)$$

$$\eta = \left(1 + \frac{3R_S {I_s}^2}{\omega T_e}\right)^{-1} \quad (2.20)$$

Equation (2.20) shows that in order to maximize the efficiency up to base speed, the (T_e/I_s) ratio needs to be maximized which refers to a high saliency ratio requirement. Since the iron losses directly depends on the flux fluctuation and torque ripple, the assumption due to negligible iron losses compared to copper losses is not valid in high speed, but high saliency ratio still remains a dominant factor in achieving high efficiency.

2.2.4 Torque per kVA

Torque per kVA describes the machine's torque production associated with the absorbed apparent power from supply [29]. A SynRM which is properly designed exhibits higher torque per kVA ratio. This is due to the effect of the saliency ratio on the torque per kVA that can be approximated as in (2.21).

$$\frac{T_e}{KVA} \cong \frac{P}{\omega}\left(1-\frac{1}{\xi}\right)\sin\theta \tag{2.21}$$

2.2.5 Torque Ripple

Torque ripple causes mechanical vibration, acoustic noise, and additional iron losses. If torque harmonics of different rotor slot barriers in the air gap eliminate each other, the torque harmonics amplitude are directly proportional to the flux harmonics when a pure sinusoidal current is applied to the stator winding. Considering the first harmonic of the torque ripple due to the stator slotting, the torque equation in (2.9) can be modified as below [36, 40]:

$$T_e(\vartheta) \cong \frac{3}{2}\frac{P}{2}\left(\lambda_d i_q - \lambda_q i_d\right) + \frac{1}{2}\left(i_d \frac{\partial \lambda_d}{\partial \delta} + i_q \frac{\partial \lambda_q}{\partial \delta}\right) \tag{2.22}$$

Equation (2.22) shows that the d-q axis inductances depend on rotor position (δ). Therefore, an additional term is added to the torque equation that represents torque pulsations. However, the average value of this term is zero. Equation (2.23) shows how the inductances depend on the rotor position.

$$\begin{bmatrix}\lambda_d\\ \lambda_q\end{bmatrix}=\begin{bmatrix}L_d(\delta) & L_{dq}(\delta)\\ L_{dq}(\delta) & L_q(\delta)\end{bmatrix}\begin{bmatrix}i_d\\ i_q\end{bmatrix} \tag{2.23}$$

The torque equation in (2.22) can be rearranged by taking into account the dependency of inductances as in (2.24).

$$\begin{aligned}T_e(\delta)=\frac{3}{2}\frac{P}{2}\left(\frac{3q}{\pi}\sin\frac{\pi}{3q}\right)&\left((L_{d-}L_q)i_di_q+(\Delta L_d+\Delta L_q)i_di_q\cos(3pq\delta)\right.\\&\left.-\Delta L_{dq}(i_d^2-i_q^2)\,sin(\,3pq\delta)\right)\end{aligned} \tag{2.24}$$

Equation (2.24) shows that the torque ripple has two components. The first component which is proportional to average torque (i_di_q) caused by oscillation of Carter's factor and circulating flux component (L_{cq}). These two oscillations create a considerable variations of d-q inductances (ΔL_d, ΔL_q) respectively. However, these can be eliminated by distributed anisotropic structure of the rotor. The second component is due to the stator slots effect which can introduce ΔL_{dq} and consequently produces torque ripple.

2.2.6 Iron Losses

Similar to the other synchronous ac drives, in SynRM, iron losses are composed of different components that can be divided into 1- Hysteresis losses, 2- Eddy current losses (Joule losses), and 3- High frequency hysteresis losses. For an area with constant flux density, the total iron losses per weight (W/kg) can be calculated for each flux harmonic as in (2.25). This is while the flux density in rotor body can oscillate due to the space harmonic of the stator slotting and the rotor anisotropic nature [40].

$$\frac{P_{tot}}{kg} = K_h B_{om}^2 f_o + \frac{\pi^2}{6} d^2 \sigma (B_m^h(h_{f1}))^2 + K_e (B_m^h(h_{f1}))^{3/2} \quad (2.25)$$

In high speed the iron losses in the rotor is comparable to the stator. As a result, it can change the design strategy from maximizing the average torque to maximizing the power factor or efficiency. In general, some solutions such as using low loss magnetic material, reducing the lamination thickness, and filling the stator slots opening (wedge area) with semi-magnetic material are used to sufficiently reduce the iron losses.

2.2.7 Field Weakening Range

It is previously mentioned in 1.2.2 that wide field weakening range in constant power operation is one of the most important requirements of the vehicle applications. In general, differing from the industrial applications, the motors used in EVs and HEVs usually require a very wide speed range in which the desired performance characteristics of the powertrain is to deliver the constant output power over the full speed ranges. Similar to most specifications of the

SynRM, the field weakening range also depends on the saliency ratio which can be expressed as in (2.26) [43].

$$\frac{\omega_r}{\omega_b} = \left(\frac{V_{ph}}{\omega_{be}}\right)^2 \frac{3P_o(L_d - L_q)}{2L_d L_q T_{em}} \tag{2.26}$$

Survey in specifications of the SynRM highlights the effect of the saliency ratio (L_d/L_q) on the machine's performance that shows this parameter can be considered key in the machine design. Since the saliency ratio is directly associated with the anisotropic nature of the rotor structure, identification and analysis of the rotor geometry is a highly required aspect of this study.

2.3 Rotor Structure and Geometry

In general, the SynRM is similar to the conventional salient pole synchronous motor, but does not have an excitation winding in the rotor structure. In this machine only, the rotor is constructed by barriers (air) and segments (steel). The main advantage of the SynRM relies on the absence of the rotor copper losses that permits to obtain a continuous torque that is higher than other wound or cage rotor machines of the same size. Developments in machine design and power electronics allow designers to achieve direct start up and better performance by using vector oriented control methods. In this technique two crucial parameters are difference and ratio of the d-q inductances that needs to be as high as possible. In order to fulfill these requirements, the rotor geometry has to be designed for maximum L_d and minimum L_q [16, 42].

2.3.1 Rotor Geometry Classifications

Anisotropic property of the SynRM can be achieved through different rotor structures that may be classified into three types as follows:

- Traditional simple rotor
- Axially laminated rotor (ALA)
- Transversally laminated rotor (TLA)

Figure 2.5 shows three different structures of (a) simple salient pole, (b) axially laminated, ALA, and (c) transversally laminated, TLA, rotor of the synchronous reluctance machine.

In the ALA type (Figure 2.5b) the laminations are suitably shaped at each pole and are insulated from each other by using electrically and magnetically insulation materials while all stacks are connected by pole holders to the central region or shaft.

In the TLA type rotor (Figure 2.5c), the laminations are identical and punched or cut in the traditional way. Some thin connections which are called “Rib” connect the ends of the segments to each other axially and transversally. These joints maintain enough mechanical integrity in the rotor structure against rotational forces in high speed operations.

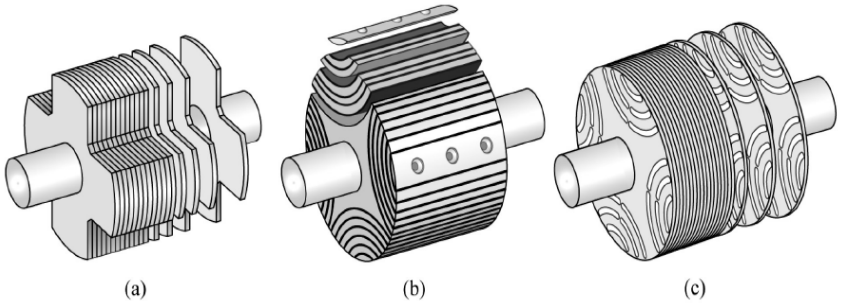

Figure 2.5. Typical configurations of different anisotropic structures of the rotor [2].

2.3.2 Comparison between TLA and ALA Structures

Figure 2.6 shows two commonly used anisotropic structures of the rotor that are a) ALA and b) TLA types which can be distinguished by following technical and manufacturing properties [17].

- In TLA type, the rotor laminations can be punched by the same cutting technology as the other conventional machines. Therefore, these laminations are easy to manufacture. Whereas in ALA type, each lamination needs to be formed by a certain shape that makes the manufacturing process difficult. However the ALA type presents a higher mechanical stability.
- Torque ripple is produced in both TLA and ALA types which are due to stator slots harmonics effects on rotor magnetic reaction. The TLA types are capable of skewing to minimize the torque ripple. Whereas, it is unpractical for the ALA type to do so and the stator skewing method is also avoided when, the automatic winding facility is being used [19, 36].
- The ALA type presents additional iron losses that are due to flux oscillations in the rotor laminations which are much ticker than that of the TLA type [29].

It was reported in previous investigations [44, 45] that the saliency ratio higher than 10 can be mostly achieved by ALA rotor, whereas the TLA rotor presents $\xi \leq 10$. However, the TLA type is preferable in many applications due to its simple manufacturing and lower iron losses. Hence in this study, considering the traction application requirements, the TLA type rotor is the proposed rotor structure.

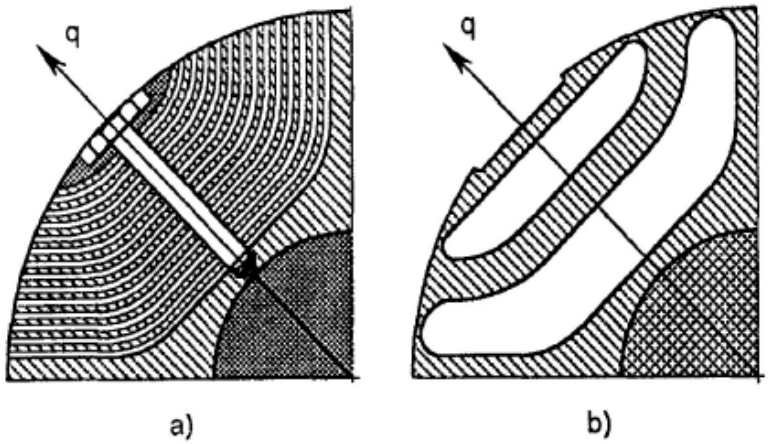

Figure 2.6. ALA (a) and TLA (b) lamination types of the SynRM rotor [18].

2.3.3 TLA Rotor Structure and Design Parameters

As it was previously mentioned, in order to achieve a proper design of the TLA rotor, two crucial parameters, (L_d-L_q), (L_d/L_q), need to be treated. Thus, the rotor design methodology is aimed at increasing the value of these two parameters based on rotor geometry. Hence, for the design procedure and evaluation of the rotor structure, the design and target parameters need to be identified which can be divided into two different categories as follows:

1) Design parameters
    - Rated power
    - Maximum torque
    - Number of poles
    - Number of flux barriers and segments (layers)
    - Insulation ratio

- Position and size of barriers and segments
- Tangential and radial ribs
- Air gap length

2) Target parameters

- Torque per current ratio
- Efficiency
- Torque ripple
- Power factor
- Field weakening range
- Iron losses

Since the target parameters have been briefly discussed in section 2.2, in the next section a summary of the design parameters and their effects on machine's performance will be addressed.

2.4 Design Parameters

Figure 2.7a shows a typical configuration of a 4-pole, 36 slots, 4 layers, and TLA rotor type SynRM in which the most important geometric design parameters are zoomed in the Figure 2.7b.

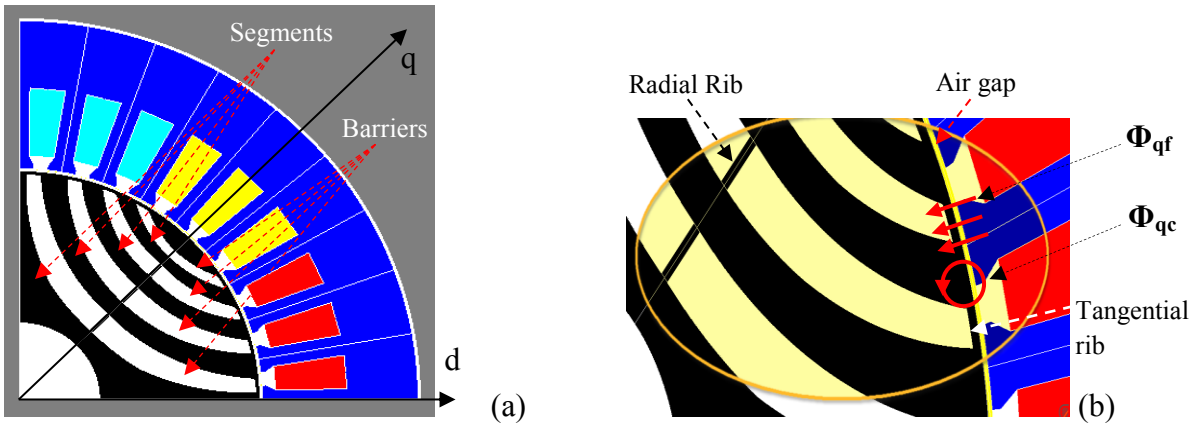

Figure 2.7. Typical configuration of a 4-pole, 36-slot SynRM with 4-layer TLA rotor.

2.4.1 Rated Power and Maximum Torque

Today, SynRM is manufactured in wide power range from 0.2kW to more than 300kW in different industrial applications. This rating for EVs and HEVs may differ from 30kW to 60kW (from 150Nm to 450Nm) which depends on powertrain's mechanism [10, 22, 23, 39]. The rated power and maximum torque affect strongly the machine's size and rotor outer diameter which will be discussed in further chapter.

2.4.2 Number of Poles

Since the design of a high performance SynRM is aimed at maximizing the saliency ratio (L_{dm}/L_{qm}), minimization of the q-axis magnetizing inductance is a potential way to achieve this goal. For a given air gap, L_{qm} is related to the sinusoidal MMF that is produced by its corresponding flux in q-axis.

Figure 2.7b shows the q-axis flux which is composed of circulating flux across the segment ends and stator teeth which leads to L_{qc} and the flux that is flowing throw the segments and

barriers which leads to L_{qf}. The following equations express the relations of L_{qm} and its components [17, 18]:

$$L_{qm} = L_{qc} + L_{qf} \tag{2.27}$$

$$\frac{L_{qc}}{L_{dm}} = \frac{\pi^2}{12 n_r} \tag{2.28}$$

$$\frac{L_{qf}}{L_{dm}} = kp \frac{g}{L_a} \tag{2.29}$$

P is the number of poles, L_{dm} is the d-axis magnetizing inductance, L_{qm} is the q-axis magnetizing inductance, i_d and i_q are the d and q-axis components of the phase current, g is the air gap length, L_a is the total width of the segments (steel) in the q-axis direction (Figure 2.7a), K is a constant, and n_r is the number of layers in each pole of the rotor structure. Equation (2.29) shows dependency of L_{qm} on the number of poles through which a SynRM with lower pole numbers exhibits a smaller L_{qm} and a higher saliency ratio.

2.4.3 Number of Layers

Number of layers per pole (n_r) is the total numbers of a couple of the flux barriers and segments in rotor anisotropic structure (Figure 2.7a). This parameter has to be selected properly due to its effect on machine's q-axis inductance [42]. The number of layers doesn't have much effect on L_d, but it highly affects L_q due to the fact that the higher number of layers decreases the circulating flux (L_{qc}) in q-axis and reduces the L_q consequently (2.28).

Due to mechanical and manufacturing issues, increasing of n_r is much more limited in TLA type rotor than in ALA type. This is why the ALA type exhibits a higher saliency ratio. Hence, in order to either avoid the ALA type rotor or minimize the q-axis flux density in SynRM design, it is necessary to minimize the L_{qf} (2.29). Therefore, the number of poles and the insulation ratio are the selective parameters to treat the saliency ratio in TLA type rotor.

2.4.4 Insulation Ratio

Insulation ratio is a good tool for adjusting the width of barriers that refers to maximizing the iron utilization in the rotor structure and saliency ratio as well. This parameter is defined by the ratio of the total width of the air to total width of the steel through the q-axis (Figure 2.7a) which can be expressed as in (2.30).

$$K_w = \frac{W_{air}}{W_{st}} \tag{2.30}$$

Therefore, K_w= 0 means the rotor does not have any barriers and is only made by steel, while K_w=1 means that the total width of barriers (air) and segments (steel) are equal [21]. Since for a proper design, the maximum saturation in the segments has to be lower than saturation in the stator back (yoke), in this situation, the value of W_{air} can affect the flux density in q-axis significantly. In general, for proper range of the insulation ratio, L_q will be minimized which consequently refers to a maximum (L_d-L_q) and a higher torque production [21, 40].

2.4.5 Position and Size of Barriers and Segments

In the ideal case in which the rotor core losses and the stator slotting effect are assumed negligible, the d-axis magnetic motive force (MMF_d) has sinusoidal shape with peak value in d-axis alignment. In order to obtain constant flux density through all segments, the size of each segment may be proportional to its corresponding average MMF_d. Therefore, the width of each segment is also necessary to vary in a sinusoidal form through the rotor body in q-axis. On the other hand, the variations of co-energy in non-uniformed air gap caused by interaction of rotor and stator slots create torque pulsation when each barrier end tends to go into or out of the slots opening area.

Figure 2.8 and Figure 2.9 show the k_{th} barrier position and the q-axis flux distribution versus the barrier's end position (α) of a typical two-pole SynRM in which f (α) is the flux distribution in q-axis and f_k (shaded area) is the circulating flux in q-axis. Equations (2.31) to (2.34) show how the size and position of the barrier's end (α) contribute to value of L_q and consequently the saliency ratio [40, 43]:

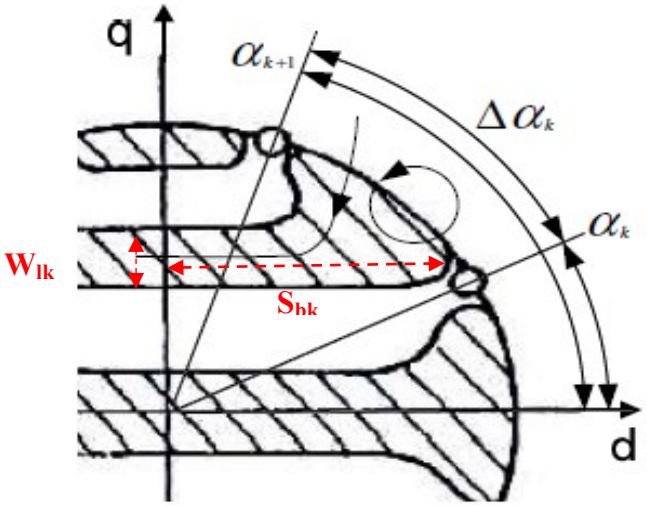

Figure 2.8. The position of the k_{th} barrier in one lamination of 2-pole SynRM .

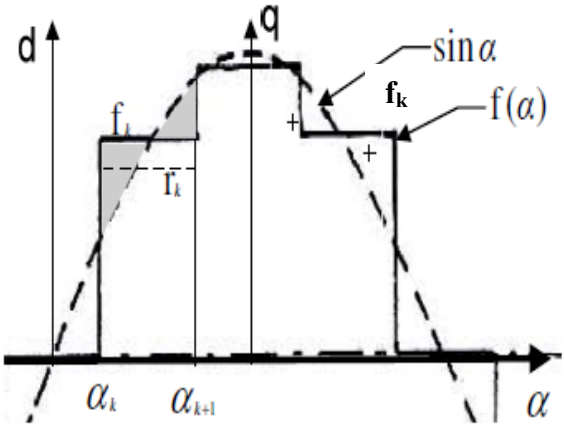

Figure 2.9. The q-axis flux distribution of the SynRM [31].

$$f_k = \frac{1}{\Delta\alpha_k}\int_{\alpha}^{\alpha+1} \sin\alpha d\alpha = \frac{\cos\alpha_k - \cos\alpha_{k+1}}{\alpha_{k+1} - \alpha_k} \tag{2.31}$$

$$\frac{L_{qc}}{L_{dm}} = 1 - \frac{4}{\pi}\sum_1^k f_k^2\,\Delta\alpha_k \tag{2.32}$$

$$\frac{L_{qf}}{L_{dm}} = \frac{4}{\pi}\sum_1^k f_k^2(f_k - r_k)\Delta\alpha_k \tag{2.33}$$

$$\frac{L_{qf}}{L_{dm}} = \frac{4}{\pi}\left(\frac{P}{2}\frac{2g}{D_{ro}}\right)\sum_1^k (P_k \Delta f_k^2) \qquad \text{where;} \quad P_k = S_{bk}/W_{lk} \tag{2.34}$$

2.4.6 Tangential and Radial Ribs

In TLA type rotor, the laminations are identical and some thin connections which are called rib connect the middles and ends of the segments to each other. These joints maintain enough mechanical integrity in the rotor structure to resist rotational and magnetic forces in high speed. However, as a drawback, they allow an increase in the flux in q-axis and a decrease in the saliency ratio. As a result, they reduce the machine developed torque by ΔT_e. The torque reduction caused by tangential rib is dominant due to the number of tangential ribs. This can be expressed in (2.35).

$$\Delta T_e = \frac{4}{\mu_0} W d B_s P^2 B_d \tag{2.35}$$

Where; (W) is rib's width, (d) is the laminations thickness, B_s is the rib's flux density which is assumed constant for all ribs, P is pole pair, and (B_d) is the d-axis flux density. Equation (2.35)

shows the torque reduction caused by tangential ribs is proportional to (p^2) and (d). Therefore, for a given pole numbers this reduces when the ribs width are designed as thin as possible.

2.5 Summary of Chapter 2

This chapter reviewed fundamental operation of the synchronous reluctance machines. The machine's mathematical model, vector diagram, and the main design characteristics were presented. Different rotor geometries with respect to the anisotropic structure were introduced and compared to propose the rotor type. The electrical, mechanical, magnetic, and geometrical parameters and their influences on the machine's performance were discussed. Moreover, the machine's key parameters which are dominant for the SynRM design were addressed.

Chapter 3 Analytical Design

3.1 Sizing Method Algorithm

Sizing of the SynRM refers to the electric, magnetic, and thermal aspects. In traction applications, in order to develop the required torque in critical times such as start-up and maximum power demand at maximum speed, the machine needs to be designed for high current density and high frequency operations. Hence, the heat caused by copper or iron losses is a concern that cannot be transferred by air cooled system. Since, the cooling system of the electric machine is supplied through the vehicle's cooling system; the thermal issue depends on both machine and vehicle cooling system capacity. The stator outer surface area and volume are two parameters that lead to the machine cooling capacity at a certain operating temperature (120-150) ˚C. Practically, by selecting the proper number of cooling jacket around the outer surface of the stator, the cooling system would be capable of cooling down the machine in continuous or transient mode of operations properly. Therefore, in this design procedure after meeting the torque and power capability, the vehicle cooling system is supposed to cool the machine properly. On the other hand, the electromagnetic design strongly depends on the application. Therefore, it is necessary to perform the whole procedure of sizing with taking into account the maximum output power, torque-speed profile, initial data, and assigned parameters. The proposed method algorithm may be explained by the flow diagram in Figure 3.1.

The sizing process of the proposed machine begins with preparing initial data and assigning the key parameters. These will be used in calculations of geometric, magnetic, and electric parameters in conjunction with the mathematical model of the machine. In this step the pre-design output parameters will be the stator geometry and rotor outer diameter. A new iteration

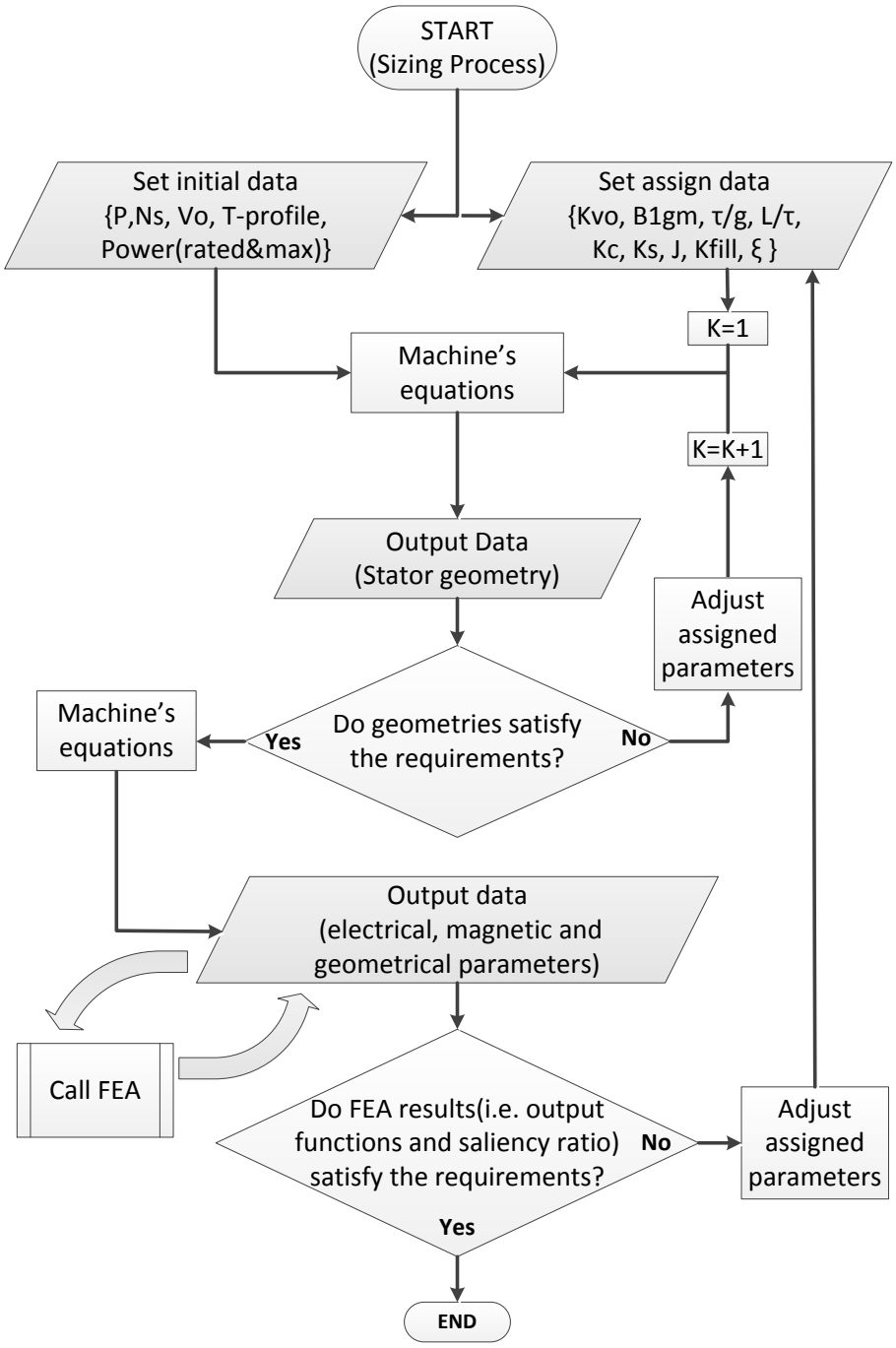

Figure 3.1. Flow diagram of the sizing algorithm.

with updated assigned parameters will be done if the geometries such as stack length or stator outer diameter cannot satisfy the design requirements i.e., specific stack length or outer diameter.

Otherwise, the electrical, magnetic, and geometrical parameters i.e., stator geometry, windings specifications, inductances, saliency ratio, maximum torque, and etc. will be characterized for further steps.

Finite element software is called to analyze the machine's performance regarding to the output functions such as maximum developed torque, torque ripple, and output power as well as magnetic characteristics e.g., flux density and saliency ratio that are known as the design requirements. The process will be ended if the finite element results satisfy the design requirements. Otherwise, the new process will be carried out by updating the assigned parameters such as magnetic and current loading, stack aspect ratio, and pole pitch to air gap ratio to obtain the proper size.

3.2 Analytical Pre-design and Calculations

As per the method algorithm described in Figure 3.1, the first step of the sizing process is to analytically determine the solution of the proposed machine. This step leads to the identification of the stator geometry, rotor outer diameter, machine's electrical and magnetic parameters i.e., inductances, resistances, windings specifications as well as the output functions such as maximum developed torque, power factor, and efficiency. The proposed approach uses the machine's mathematical model including the equivalent circuit, vector diagram, and mathematical equations in conjunction with initial data, desired torque envelope, and assigned parameters.

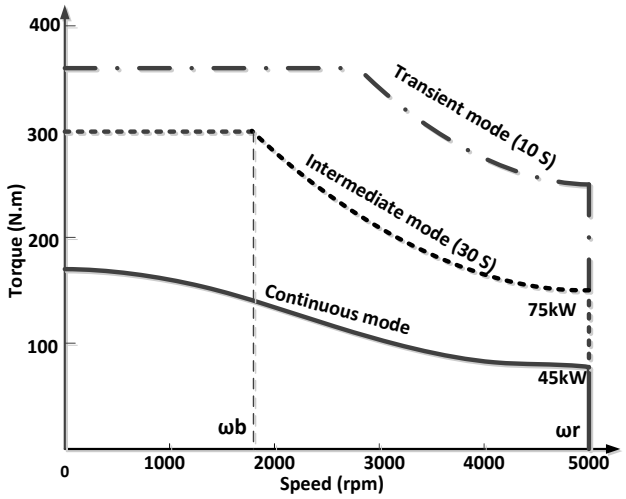

Figure 3.2. Torque profile of powertrain

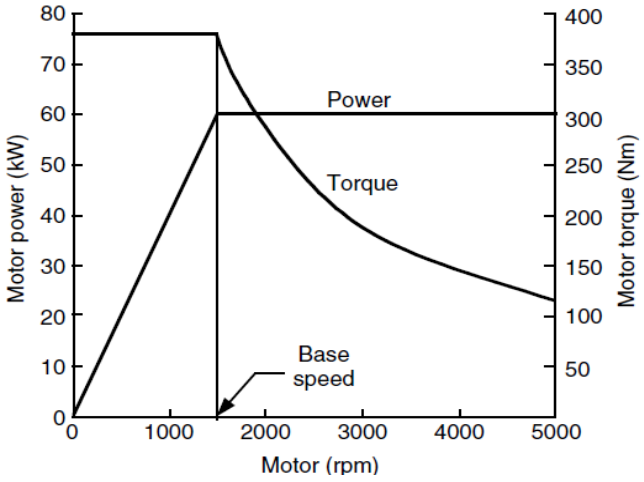

Figure 3.3. Electric motor characteristics for traction [1].

Figure 3.2 and Figure 3.3 show examples of the torque envelope and its corresponding traction motor desirable characteristics respectively in which the base and maximum speed have important effects on electric machine's parameters [43]. It should be noted that these

characteristics present information in the motor side. Therefore, in order to have the final drive characteristics the gearbox ratio (transmission system) needs to be taken into account.

3.3 Initial Data

The Initial data is provided based on the desired torque-speed envelope (Figure 3.2) and manufacturer's requirements. In general, only the continuous torque-speed mode of operation is imposed on the machine design, but in traction applications, the motor needs to take over the high current demand in the intermediate mode of operation from zero up to base speed, in which the maximum torque needs to be developed during a critical time such as start-up or over taking time (about 30sec.). Table 3.1shows an example of the initial data in which the key parameters will be used in further calculations. This data can be extracted from design requirements such as torque envelope in Figure 3.2.

Table 3.1. Initial Data

Symbol	Parameter	Quantity
P_{mo}	Continuous output power	45kW
T_{em}	Peak torque in intermediate mode	300 Nm
T_{ep}	Peak torque in continuous mode	170 Nm
ω_b	Base speed	1800 rpm
P_o	Number of pole pairs	2
N_s	Number of stator slots	48
V_o	DC-bus voltage	600 V

3.4 Assign Parameters

Some parameters need to be assigned which are important during calculations. However, some of them can be modified during design process [46];

1) Converter factor (K_{vo}): K_{vo} is due to the limitation of available maximum voltage through VSI. Generally, K_{vo} is between 0.9> Kvo< 1. In this study, K_{vo} is selected 0.98.

2) Magnetic loading (B_{1gm}): B_{1gm} is selected based on the core type to provide enough flux density without unwanted saturation. In this study, the core type is M15 and B_{1gm} =1 Tesla, which gives enough boundary before core saturation.

3) Pole pitch to air-gap ratio (τ/g): this ratio has a strong effect on the magnetizing coefficients (K_{dm1}, K_{qm1}). It is obtained during sizing algorithm for a sufficient value of saliency ratio in order to satisfy the geometrical and torque envelope requirements. In this study, ξ=10 and the obtained value of τ/g is (345).

Equations (3.1), (3.2), and (3.3) show the relations as follows:

$$L_{dm} = L_m K_{dm} \tag{3.1}$$

$$L_{qm} = L_m K_{qm} \tag{3.2}$$

$$\xi = \frac{L_d}{L_q} \; Then; \; \xi = \frac{L_{dm}+L_{\sigma s}}{L_{qm}+L_{\sigma s}} \tag{3.3}$$

Where d-axis is the direct and q-axis is the quadrature axis of rotor reference frame and L_{dm} and L_{qm} are their corresponding magnetizing inductances respectively.

4) Stack aspect ratio ($\lambda = L/\tau$, $0.6 < \lambda < 3$): this ratio leads to the machine's stack length. It is obtained through the sizing method. The higher ratio refers to longer stack length and shorter pole pitch that is suitable for higher speed applications. In this study $\lambda = 0.9$.

5) Current density (J): It can be selected from 3.5 A/mm2 to 8 A/mm2 for axial or axial-radial air cooled machines [46]. However, in traction applications, by employing an advanced cooling system, a higher value would be applicable. This system is composed of cooling jacket located around the outer surface of the stator, coolant such as water-glycol or oil, cooling pump, and temperature control devices that is supplied via vehicle's cooling system. According to this, the stator outer surface area and volume are two parameters that lead to the machine cooling capacity at certain operating temperature (120-150) ˚c. In this study, J=10 A/mm2 is assigned for continuous mode of operation. It is increased to twice in peak torque. Table 3.2 shows summary of the assigned data.

Table 3.2 Assign Data

Symbol	PARAMETER	Quantity
B_{1gm}	Magnetic loading	1.0 T
τ/g	Pole pitch to air gap ratio	345
λ	Stack aspect ratio	0.9
ξ	Saliency ratio	10
J	Current density	10 A/mm^2
K_{fill}	Fill factor	0.7
K_c	Carter factor	1.2
Ks	Saturation factor	0.4
K_{vo}	Converter factor	0.98

3.5 Rotor Core Dimensions

In order to obtain the rotor outer diameter, machine's pole pitch is the leading parameter. Equations (3.4), (3.5), and (3.6) show this approach using fundamental component values e.g., B_{1dm} [43, 46].

$$B_{1dm} = \frac{B_{1gm}}{\sqrt{1+\left(\frac{K_{qm1}}{K_{dm1}}\right)^2 \frac{L_d}{L_q}}} \tag{3.4}$$

$$\tau = \sqrt[3]{T_{em} \frac{K_{dm1}\mu_o\left(\frac{\tau}{g}\right)\left(\frac{\tau}{L}\right)}{B_{1dm}{}^2 P_o{}^2\left(1-\frac{K_{qm1}}{K_{dm1}}\right)K_c(1+K_s)\sqrt{\frac{L_d}{L_q}}}} \tag{3.5}$$

$$D_{ro} = 2P_o \frac{\tau}{\pi} \tag{3.6}$$

In the above-mentioned equations, it is illustrated that the two key parameters are K_{dm1} and K_{qm1}. Since the flux leakage is unknown, it may be necessary to assume the leakage inductance ($L_{\sigma s}$) is approximately equal to the q-axis magnetizing inductance (L_{qm}). This assumption helps to simplify the solution process. It means that even if the actual L_{qm} is higher than the calculated one, the torque and machine's performance will remain approximately the same [43]. Therefore, we are still on the safe side of the design. Considering this assumption along with substituting the assigned saliency ratio (ξ=10) in equation (3.3) gives $\frac{K_{dm1}}{K_{qm1}} = 19$ and then $K_{dm1} = 0.95$. These two key parameters can be substituted again into (3.4), (3.5), and (3.6) that consequently give the pole pitch and the rotor outer diameter. On the other hand, the machine's pole pitch, pole pitch to air gap ratio, and stack aspect ratio give the air gap and stack length respectively.

The reason behind assigning the saliency ratio of 10 is that, from the machine performance point of view, this value is at the boundary of the two rotor types (ALA, TLA). Previously, it was reported in investigations [44, 45] that the saliency ratio higher than 10 can be mostly achieved by ALA rotor, whereas the TLA rotor presents $\xi \leq 10$. However, the TLA type is preferable in many applications due to its simple manufacturing and lower iron losses. In the TLA type rotor, Figure 2.6b and Figure 2.7b, the laminations are identical and punched or cut in the traditional way. Some thin connections which are called "Rib" connect the ends of the segments to each other axially and transversally. These connections maintain enough mechanical integrity in the rotor structure against rotational and magnetic forces in high and low speed operations.

General speaking, in this chapter achieving the desired torque profile while taking into account the assigned saliency ratio, proper stake length, stator outer diameter, and converter current limitations is the key in selecting the rotor type and designing the machine's geometry.

3.6 Stator Geometry

Electromotive forces for all coils which are distributed along pole pitch are not the same. Therefore, the torque includes all odd harmonics. In general, chorded pitch winding is a solution to improve the torque quality. However, it has been reported in [35] that, chording of the stator winding in SynRM is not necessary to reduce the amplitude of the lower-order MMF space harmonics when the round rotor with uniformly internal flux barriers is used. Because "the lower order harmonic generated fluxes are attenuated by the flux barrier rotor". Furthermore, it reduces the machine power rating by 5 to 10%. Therefore, chorded winding is neglected and the chording factor, K_y, is eliminated in (3.7) below which gives the machine's winding factor.

$$K_{w1} = \sin(\frac{\pi}{6})/(q \sin\frac{\pi}{6q})K_y \quad , \quad q = \frac{N_s}{3(2P_o)} \tag{3.7}$$

3.6.1 Ampere-turns per Slot

The flux in machine's magnetic circuit is deemed to be proportional to the resultant ampere-turns. In other word, we assign the magnetic loading such that the machine operates in the linear portion of the magnetization characteristic. Therefore, the major part of the exciting ampere-turns is required to maintain the proper flux density across the air gap. Equations (3.8) to (3.10) show approaches to obtain the d-q components and total value of the ampere-turns per slot respectively [43].

$$n_s I_{dm} = \frac{B_{1dm}\pi g K_c(1+K_s)}{3\sqrt{2}\mu_o q K_{w1} K_{dm1}} \tag{3.8}$$

$$n_s I_{qm} = (n_s I_{dm})\sqrt{\frac{\mathrm{L_d}}{\mathrm{L_q}}} \tag{3.9}$$

$$n_s I_m = \sqrt{(n_s I_{dm})^2 + (n_s I_{qm})^2} \tag{3.10}$$

3.6.2 Stator Slots Dimensions and Core Size

In order to design the stator core geometry, all dimensions of the stator slots need to be obtained, Figure 3.4 shows the detail:

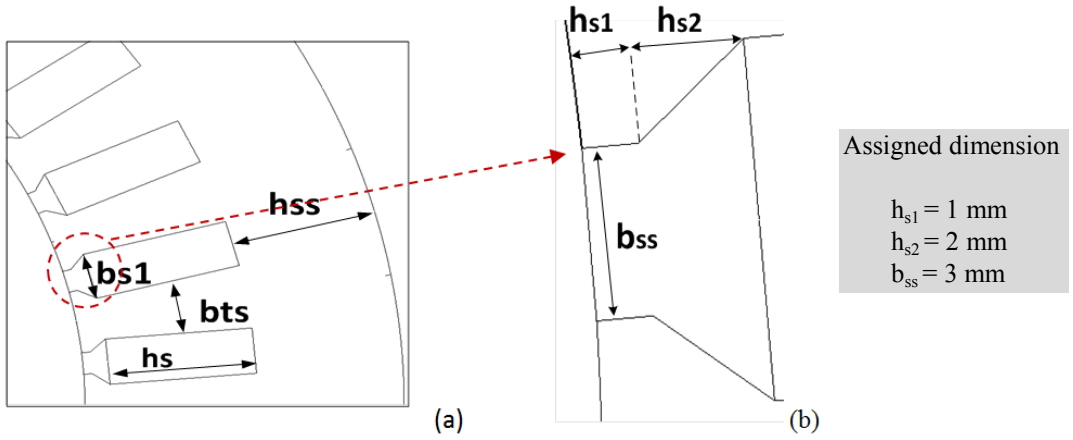

Figure 3.4. Typical dimensions of the stator slot (a) and wedge area (b).

The ampere-turns per slot and pole pitch allow calculating the useful area and slot pitch through equations (2.11) and (2.12) [43].

$$A_s = \frac{n_s I_m}{J K_{fill}} \tag{3.11}$$

$$\tau_s = \frac{\tau}{3q} \tag{3.12}$$

Equations (3.13) to (3.15) yield the dimensions of each slot as follows:

$$b_{ts} = \frac{B_{1gm}}{B_{ts}} \tau_s \cong \frac{B_{1gm}}{2B_{1dm}} \tau_s \tag{3.13}$$

$$b_{s1} = \pi \frac{D_{ro}+2(h_{s1}+h_{s2})}{3\times 2P_o q} - b_{ts} \quad (3.14)$$

$$h_s = A_s / b_{s1} \quad (3.15)$$

In order to reduce the air gap flux pulsations, it is quite necessary to select minimum possible dimensions for slots opening. Therefore, in this study bss = 3mm, hs_1=1mm, and hs_2= 2mm. On the other hand, b_{s1} and b_{s2} will be identical if rectangular wire is used. Consequently, the fill factor and heat transferring capability from winding to the stator's body will be increased. It should be noted that, according to the wire gage standards, if the calculated gage of the flat wire is not available, some modifications might be applied to the slot's dimensions and the closest gage can be selected. In this condition, the new slot's area has to be very close to the calculated useful area in order to maintain the assign current density.

Stator back iron or yoke width can be obtained through (3.16) in which the yoke flux density, $B_{ss,}$ is considered to be 70% higher than the air gap flux density.

$$h_{ss} = \frac{B_{1gm}}{B_{ss}} \frac{\tau}{\pi} \quad (3.16)$$

Now, all parameters that are required to calculate the stator geometry are calculated. Therefore, the stator inner and outer diameter can be found using (3.17) and (3.18).

$$D_{si} = D_{ro} + 2g \quad (3.17)$$

$$D_{so} = D_{si} + 2(h_{s1} + h_{s2} + h_s + h_{ss}) \quad (3.18)$$

3.7 Machine Parameters

In order to analyze performance of the proposed machine by 2D FEA, its electric and magnetic parameters need to be identified. According to the approaches outlined below, the machine's dimensions, initial data, and assigned parameters lead to the characterization of all the required parameters as a function of the number of conductor turns per slot (n_s) [43, 46]. Therefore, n_s is one of the key parameters in the design.

3.7.1 Phase Resistance and Inductances

The leakage inductance can be expressed as in (3.19).

$$L_{s\sigma} = 2\mu_o n_s^2 q P_o(\lambda_s + \lambda_z + \lambda_f) \tag{3.19}$$

Where;

$$\lambda_s \cong \frac{2h_s}{3(b_{s1}+b_{s2})} + \frac{2h_{s2}}{b_{s1}+b_{ss}} + \frac{h_{s1}}{b_{ss}} \qquad \text{(slots permence)}$$

$$\lambda_z = \frac{5g}{5b_{ss}+4g}$$

$$\lambda_f = \frac{0.34q}{L}(l_f - 0.64\tau) \tag{3.20}$$

$$l_f = \pi\frac{\tau}{2} \qquad \text{(stator end winding length)}$$

Substituting all data into (3.20) and then the resultant into (3.19) yield the leakage inductance as in equation (3.21).

$$L_{\sigma s} = 8.5518 \times 10^{-6}(n_s)^2 \tag{3.21}$$

Equation (3.22) shows the phase resistance as a function of n_s in which $\rho = 2.3 \times 10^{-8}$ Ωm is the copper resistivity.

$$R_s = \rho l_c P_o q (n_s)^2 \frac{J}{n_s I_m} \qquad \text{where;} \quad l_c = 2\left(L + l_f\right) \tag{3.22}$$

Consequently, we can express the phase resistance as in (3.23).

$$R_s = 3.292 \times 10^{-3}(n_s)^2 \ (\Omega) \tag{3.23}$$

For uniform air gap the magnetizing inductance can be expressed in equation (3.24).

$$L_m = 6\mu_o \tau L \frac{(P_o q K_{w1} n_s)^2}{\pi^2 P_o g K_c (1+K_s)} \tag{3.24}$$

Consequently, we can also define the magnetizing inductance and its d-q components as a function of n_s as follows:

$$L_m = 7.3211 \times 10^{-4}(n_s)^2 \quad \text{(H)}$$

$$L_{qm} = 3.6605 \times 10^{-5}(n_s)^2 \quad \text{(H)} \tag{3.25}$$

$$L_{dm} = 6.955 \times 10^{-4}(n_s)^2 \quad \text{(H)}$$

As previously mentioned, to simplify the solution process, the q-axis magnetizing inductance is considered equal to the leakage inductance. However, it is always bigger. Therefore, we can express the d-q axis inductance of the machine as in equations (3.26).

$$L_d = L_{dm} + L_{\sigma s} \cong L_{dm} + L_{qm}$$

$$L_q = L_{qm} + L_{\sigma s} \cong 2L_{qm}$$

$$L_d = 7.3211 \times 10^{-4}(n_s)^2 \quad \text{(H)} \tag{3.26}$$

$$L_q = 7.3211 \times 10^{-5}(n_s)^2 \text{(H)}$$

3.7.2 Number of Turns per Slot

The number of turns per slot depends on the available voltage across the stator phases. It is varied based on the stator connection and the converter type. Since in this study the machine has

delta connection and is assumed to be supplied by a SVPWM power converter, supply voltage can be obtain as in equation (3.27).

$$V_{ph} = \frac{\sqrt{6}}{\pi} K_{vo} V_o \tag{3.27}$$

In order to identify n_s, the machine equivalent circuit and its relevant vector diagram at base speed are used to define the machine's mathematical model through voltage equations. Considering the machine's vector diagram, Figure 2.4b we can express the voltage equations as follows:

$$V_d = -\omega_{be} L_q I_{qm} + R_s I_{dm}$$

$$V_q = \omega_{be} L_d I_{dm} + R_s I_{qm}$$

$$\omega_{be} = \omega_b P_o \frac{2\pi}{60} \qquad \text{(electrical speed, rad/s)} \tag{3.28}$$

$$V_{ph} = \sqrt{{V_d}^2 + {V_q}^2}$$

Substituting the values of d-q components of the ampere-turns from (3.8) and (3.9) into (3.28) yields the number of turns per stator slot of the conductor which is the key in identifying

all machine's required parameters. Those parameters have been previously characterized as a function of n_s. Therefore, n_s = 9.54 turns which can be approximated as n_s = 10 turns.

Table 3.3 shows a summary of the design specifications of the proposed machine which were obtained through the design process based on the sizing method:

Table 3.3 Design Parameters

Parameter	Quantity		Parameter	Quantity
τ	191.4 mm		R_s	0.3256 Ω
L	172.0 mm		L_d	73.2 mH
g	0.6 mm		L_q	7.3 mH
D_{ro}	244.0 mm		I_{dm}	16.10A
b_{ts}	8.0 mm		I_{qm}	50.91 A
b_{s1}	8.4 mm		I_m	53.40 A
h_s	15.0 mm		$I_{dph(\omega_r)}$	6.40 A
h_{ss}	30.0 mm		$I_{qph\ (\omega_r)}$	64.08 A
D_{si}	245.2 mm		$I_{ph(\omega_r)}$	64.40 A
D_{so}	341.2 mm		$N_s.I_m$	533.99 A.turns
Volume	15.70 dm^2		$L_{\sigma s}$	0.855 mH
$\eta cos\phi$	0.7938		ω_r/ω_b	1.85
n_s	10 turns		V_{ph}	462.2 V
W_{co}	10.77 kg		W_{ir}	51.40 kg
P_{co}	2578.6 W		P_{ir}	488W

3.7.3 Electromagnetic Torque and Speed Range

The maximum torque developed by the electrical machine is a major requirement in traction applications. This parameter is basically defined in torque envelope of the powertrain (Figure 3.3a). Hence, it is expected to be developed by electric machine and remain constant up to base speed. We can express the machine torque production as in equation (3.29).

$$T_{em} = 1.5P_o\left(L_d - L_q\right)I_{dm}I_{qm} \tag{3.29}$$

Using the required data from Table 3.3 yields T_{em} = 324N.m. Since the machine is supposed to be designed to develop 300 Nm in intermediate mode of operation up to base speed, the difference between calculated and assigned torque can be adjusted by supply voltage and phase current. On the other hand, it may be necessary to make another adjustment on the supply voltage with regards to the approximation on calculated n_s. Therefore, the new phase voltage and current that can be used in further calculations are;

$$V_{ph}{}^{*} = 458.46\frac{10}{9.54}\sqrt{\frac{300}{324}} = 462.2\ \ (V) \tag{3.30}$$

$$I_m{}^{*} = 56 \times \sqrt{\frac{300}{324}} = 53.4\ \ (A) \tag{3.31}$$

The maximum speed range, the corresponding phase current, and its d-q components can be expressed as follows (the results are included in Table 3.3);

$$\frac{\omega_r}{\omega_b} = \left(\frac{V_{ph}}{\omega_{be}}\right)^2 \frac{3P_o(L_d - L_q)}{2L_d L_q T_{em}} \tag{3.32}$$

$$I_{dph} = \sqrt{\frac{T_{em}\, L_q}{3P_o(L_d - L_q)L_d} \frac{\omega_b}{\omega_r}}$$

$$I_{qph} = I_{dph} \frac{L_d}{L_q} \tag{3.33}$$

$$I_{ph} = \sqrt{{I_{dph}}^2 + {I_{qph}}^2}$$

The product of power factor and efficiency over speed range is a leading parameter of the SynRM to justify the machine's performance with respect to speed variations.

$$\eta cos\, \varphi = \frac{T_e \omega_i}{3P_o V_{ph} I_m} \tag{3.34}$$

As is illustrated in equation (3.34), the efficiency and power factor depend on each other. Their product remains constant at any operating speed (ω_i) over speed range and its corresponding electromagnetic torque (T_e). This means improving one can decline the other. Therefore, proper values for both parameters can improve the machine performance with regards to output power and losses and lead designers to select the machine control strategy of maximum power factor or maximum efficiency techniques accordingly [28, 30, 31].

3.8 Proposed Method Validity and Evaluation

The dimensions, electrical, and magnetic parameters of a 45kW SynRM were identified based on the proposed sizing methodology. To validate the size obtained through the design process as well as evaluation of the machine's performance, a comparison between previously examined machine data with the same characteristics and 2D FEA using designed parameters are performed as follows;

3.8.1 Comparison of the Designed and Examined Machines

The performance of a 45kW SynRM with the same characteristics e.g., rated power, maximum torque, pole pairs, and number of stator slots has been examined and reported previously in [35]. Table 3.4 shows the tested machine's specifications (reference machine) compared to the parameters of the machine which is designed using analytical and FE method trough the sizing algorithm. The volume ratio of two machines, V_{ratio} = 15.7/15.9, indicates the size of the designed machine is very close to that of the reference machine's (V_{ratio} = 0.987). Furthermore, two dimensions i.e., stator outer diameter and stack length that may be the major limitations of the machine's size in today's compact EVs and HEVs, meet the requirements of the reference machine sufficiently, this confirms the validity of the proposed method.

It may be noted that the final geometries identified through this method are not unique and the proposed method is quite flexible to adapt to proper initial data e.g., stack aspect ratio and pole pitch to air gap ratio, in order to introduce the machine with longer stack length or larger bore diameter while the stack volume remains constant. Besides geometric limitations, these two parameters are important in traction applications due to their effects on the machine's electric and dynamic response. The longer length refers to faster dynamic response and lower starting

torque whereas the larger bore diameter exhibits higher starting torque and slower dynamic response. A considerable difference is indicated between rotor's outer diameters of two machines that distinguish the design for traction from industrial applications. This is due to higher current density ($10A/mm^2$) and magnetic loading (1Tesla) assigned for the proposed machine. These lead to shorter teeth and smaller yoke size and consequently, larger rotor diameter and higher torque production at the same phase current. Today, electric powertrains equipped with advanced cooling system, allow electric machines to operate with heavy current loading to maintain the maximum torque and power requirements at different modes of operation.

Table 3.4 Comparison between the Parameters of the Reference and Designed Machines

Parameters of 45kW SynRM	Reference	Designed
Stator outer diameter (mm)	340	341.2
Stator inner diameter (mm)	199	245.2
Rotor outer diameter (mm)	197.76	244
Stack length (mm)	175	172
Stack volume (dm^2)	15.9	15.7
Air gap length (mm)	0.62	0.6
Number of poles	4	4
Number of stator slots	48	48
Maximum torque (N.m)	300	301.6
Torque ripple (%)	10	12

3.8.2 FE Analysis and Results

The finite element analysis (FEA) is necessary to verify and evaluate the proposed machine's performances in different modes of operation. The geometry of the machine which is designed through the proposed method has been modified properly in order to be used in 2D FEA software. Since the rotor optimization techniques is not discussed in this chapter, a TLA type rotor with four layers was adapted [18, 19, 21, 25, 36, 41, 42, 47]. The geometry of the rotor lamination has been modified several times to meet the maximum possible saliency ratio and output torque and then, the proposed machine with proper rotor geometry was examined by FEA to evaluate its performance.

The simulations are done using current source operation to realize the machine performance at different loads. The circuit diagram of the simulation is shown in Figure 3.5 in which (I_1,I_2, I_3) are the current source inverter supply, (R_1, R_2, R_3) are the end winding resistors, (L_1, L_2, L_3) are the end winding inductances, and (B_1, B_2, B_3) are the magnetizing coils including resistance and inductance.

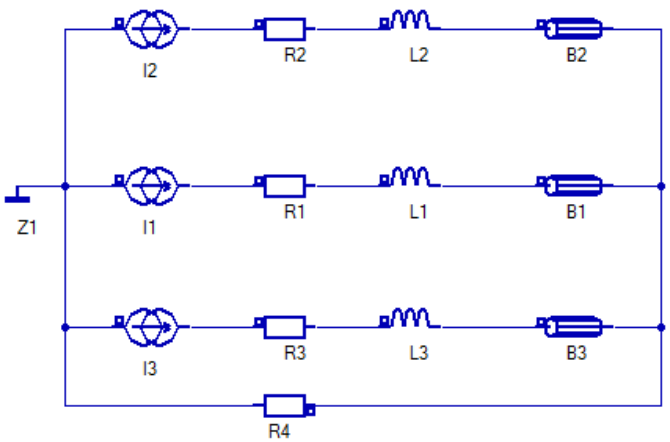

Figure 3.5. Circuit diagram of the current source simulation method.

The single pole mesh profile of the proposed machine is shown in Figure 3.6. As is illustrated, due to the dynamic behavior of the rotor versus the stator, the air gap has been modeled based of two layers. Since the machine's most important electromagnetic parameters such as the electromagnetic torque, electromotive force, and flux depend on the air gap's characteristics, a very fine mesh was defined in the air gap area to improve accuracy. However, this increases somehow the simulation time.

To identify the effects of saturation and increase the accuracy of the FE calculations at the critical points such as stator teeth, tangential ribs, and radial ribs, all the corresponding region have been modeled by fine mesh.

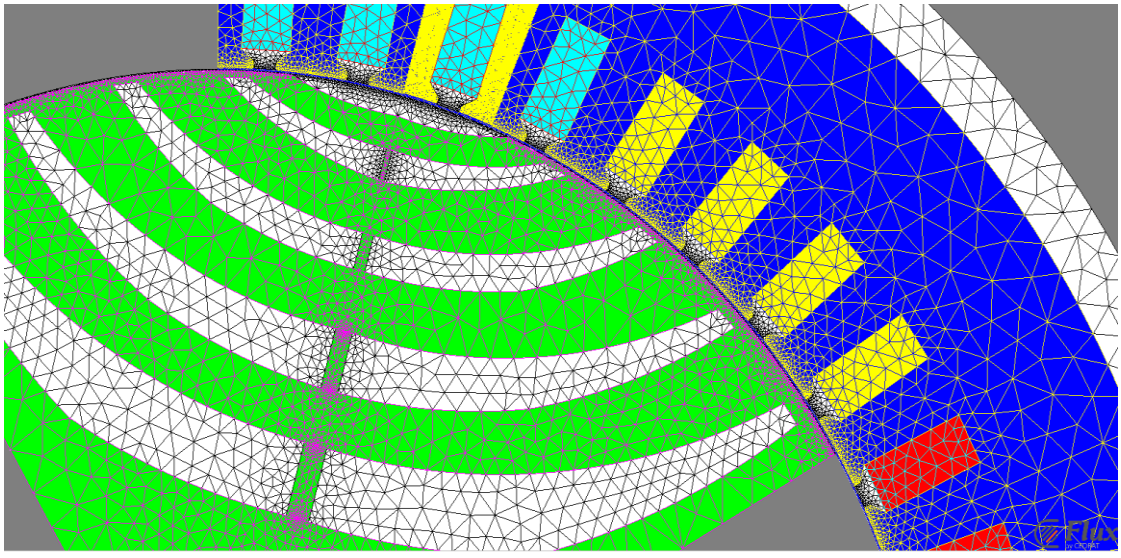

Figure 3.6 Single pole mesh profile of the proposed machine.

Figure 3.7 shows the d-axis flux distribution and Figure 3.8 shows the torque profile versus rotor position of the proposed SynRM. The machine is simulated under direct current control while the DC-bus voltage is 600v and the current and its angle (ϕ_i in Figure 2.4b) are adjusted at 220A and 32 degrees electrical respectively. Referring to Figure 2.4b, the relation between θ, ϕi, and the rotor angle δ can be described as; $\pi/2 + \delta = \theta + \varphi i$. This gives θ and leads to the torque-θ characteristic while taking into account the rotor angle which can be obtained through the FEA ($\delta = 10^{\circ}$ when $\varphi i = 32^{\circ}$ electrical). If θ is required, it can be calculated as; $\theta = \pi/2 - 32 + 10$ therefore, $\theta = 68^{\circ}$. Compared to θ, ϕi is easier to be controlled during the FEA because, information of the d and q-axis parameters are not required.

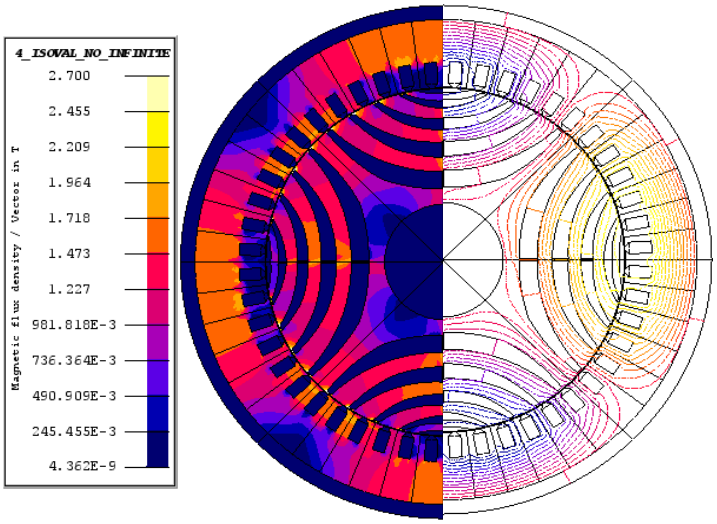

Figure 3.7. D-axis flux density and distribution at base speed (continuous mode).

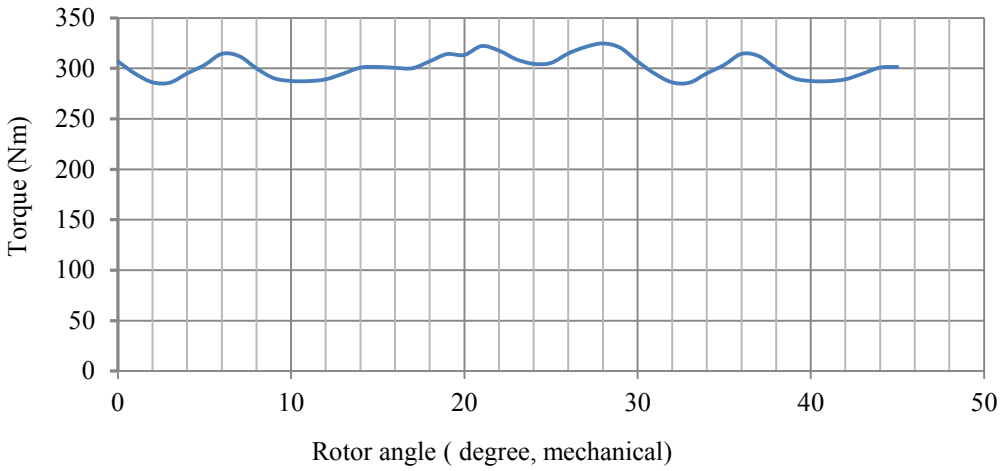

Figure 3.8. Torque- angle characteristics of the proposed SynRM in intermediate mode.

As it is illustrated in Figure 3.8; the machine equipped with a rotor constructed by 4 layers is capable of developing required torque (300N.m) at the base speed with low ripple (12%). This situation is compatible with the intermediate mode of operation in desired torque profile (Figure 3.3a). Since the machine is supposed to operate in low speed with maximum torque, the dominant loss would be the stator copper loss that imposes a high temperature shock to the stator winding. In traction applications, an advance cooling system which is integrated in vehicle cooling system and composed of coolant such as water-glycol can transfer heat from stator body sufficiently and regulate the temperature at its rated. These results confirm that the SynRM which is characterized by the proposed algorithm is capable of meeting the torque profile.

As it was previously mentioned, from traction application point of view, the maximum developed torque at base speed and the maximum output power at maximum speed are two crucial operating points.

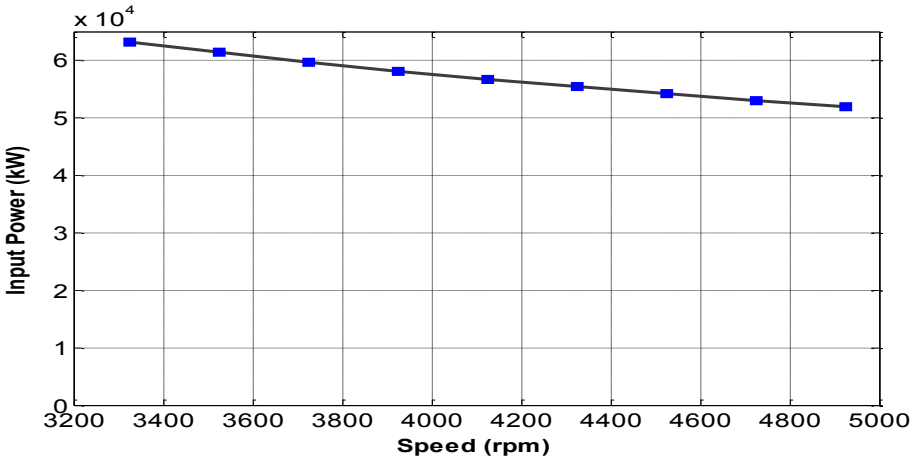

Figure 3.9. Input power-speed characteristic of the SynRM.

Figure 3.9 shows the machine input power characteristic beyond the maximum speed (1800x1.85=3300rpm, ω_b=1800rpm). According to equation (3.32), the speed range is 1.85 within which a constant power operation using vector control technique is expected. Reductions in both saliency ratio and power factor will degrade the machine performance at speed higher than the designed maximum speed (ω_r > 3300rpm) and reduce the input power significantly. Therefore, in order to deliver 45kW on the shaft at 5000rpm in continuous mode of operation (Figure 3.3a), we need to design the machine with higher power rating (63kW). This is another reason why the SynRM is bigger than the PMSM with the same power rating.

Figure 3.10 shows that the performance of the SynRM is sensitive to air gap length. In order to achieve a higher T/A (torque per ampere), a shorter air gap length is required. However, higher air gap length is limited by the converter rating due to the fact that the machine needs to draw more current at the same torque.

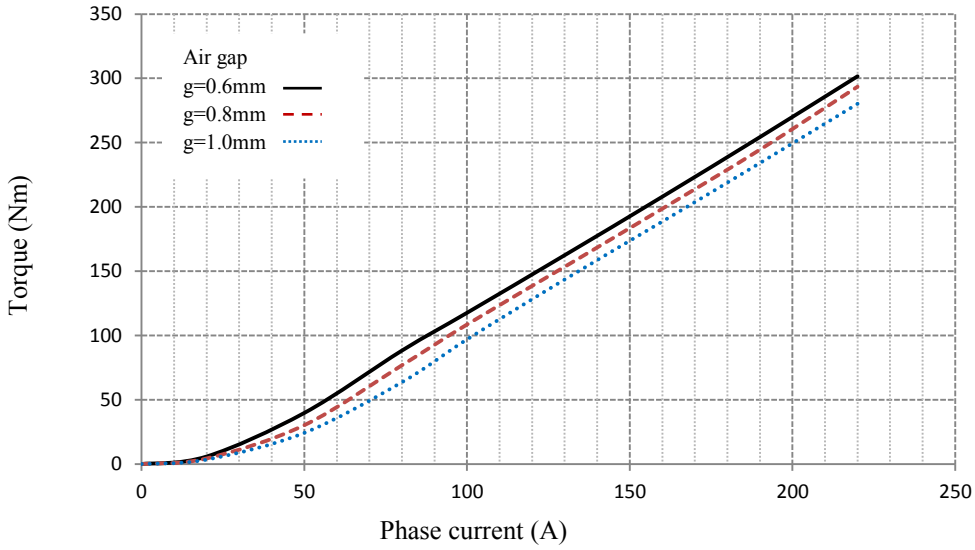

Figure 3.10. Torque – current profile of the SynRM for different air gap lengths.

Figure 3.11 shows the characteristics of the flux versus phase current for different rotor positions (64˚, 0˚, 54˚, mechanical in stationary reference frame) which is also called magnetic curves. In order to evaluate the machine performance in continuous mode of operation, the phase current information is necessary. Referring to Figure 3.3a, continuous mode of operation, and Figure 3.10, the machine with 0.6mm air gap needs to draw 90A-125A to satisfy the torque requirement (90-160 Nm). As is illustrated in Figure 3.11, when the rotor angle is at 54˚ mechanical, the machine can operate around linear part of magnetic curve that leads to less saturation and higher saliency ratio. As opposed to this, when the rotor position is at 0˚ or 64˚ the machine operates in the nonlinear region and it is expected to have lower saliency ratio caused by saturation. Therefore, the designed machine is capable of satisfying the desired torque envelope Figure 3.3a when the rotor position is adjusted at 54˚. It highlights the importance of the rotor position in SynRM operation.

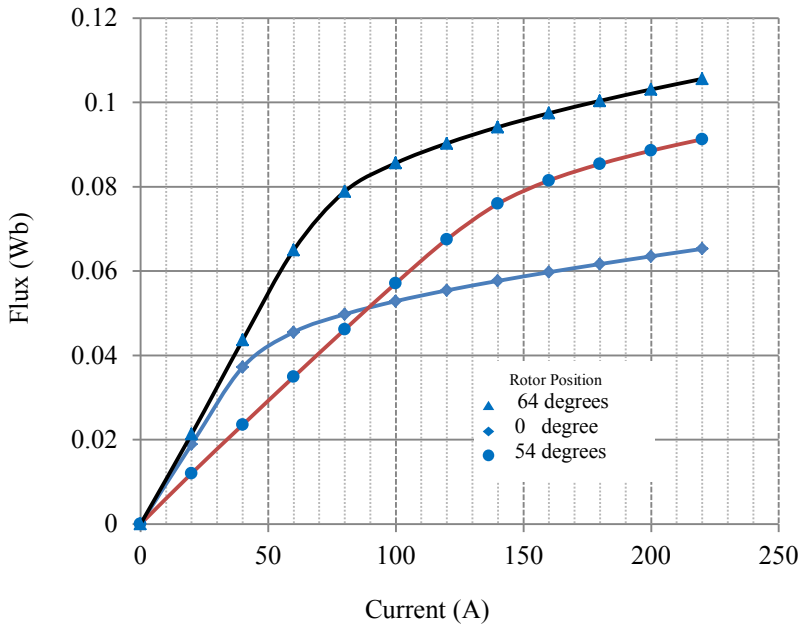

Figure 3.11. Magnetic characteristics of the SynRM for three different rotor positions.

Figure 3.12 shows the torque-current angle profile of the SynRM at maximum current (220A) during intermediate mode of operation in which the developed torque is maximized when the current angle (ϕ_i) is adjusted at 32 electrical degrees. The current control technique is necessary to control the machine from zero up to base speed when it operates as traction. Therefore, the knowledge of the proper current angle is necessary to maximize the torque magnitude. This angle is not a unique parameter. It is current-dependent and varies with respect to the magnitude of the phase current. This is due to the fact that, for a specific rotor, the saliency ratio is not only sensitive to rotor position, but it also depends on phase current.

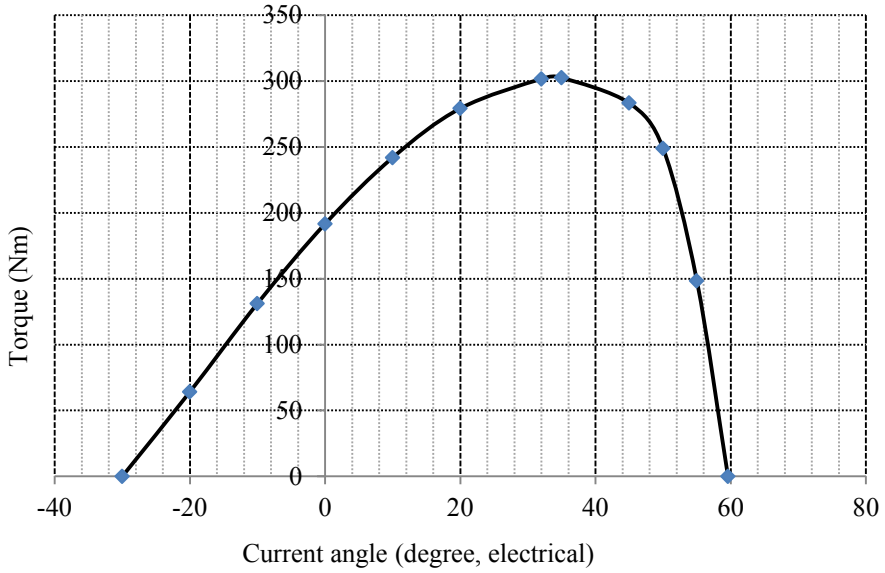

Figure 3.12. Torque – current angle (ϕi) characteristic of the proposed SynRM.

Figure 3.13 and Figure 3.14 show the saliency ratio versus current ratings and the d-q inductances of the proposed SynRM respectively. The importance of the results in Figure 3.13 are that the saliency ratio of 10 can be achieved for current rating in continuous mode (100A) while the rotor position is aligned at the proper angle (54 mechanical degrees). This yields maximum power at maximum speed in continuous mode of operation which is compatible with vehicle highway driving scheme. It has to be noted that the previously-mentioned operating point and saliency ratio are two leading parameters (Figure 3.3a, Table 3.3) in the sizing method. On the other hand, the rotor alignment which can be practically defined by the current angle is the key parameter in achieving the proper saliency ratio in different current ratings or mode of operations.

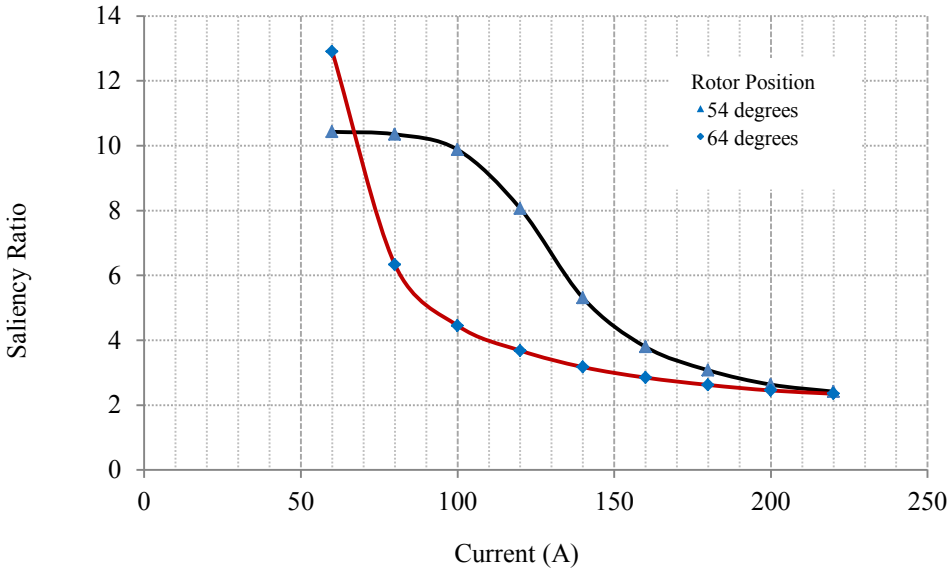

Figure 3.13. Saliency ratio of the SynRM.

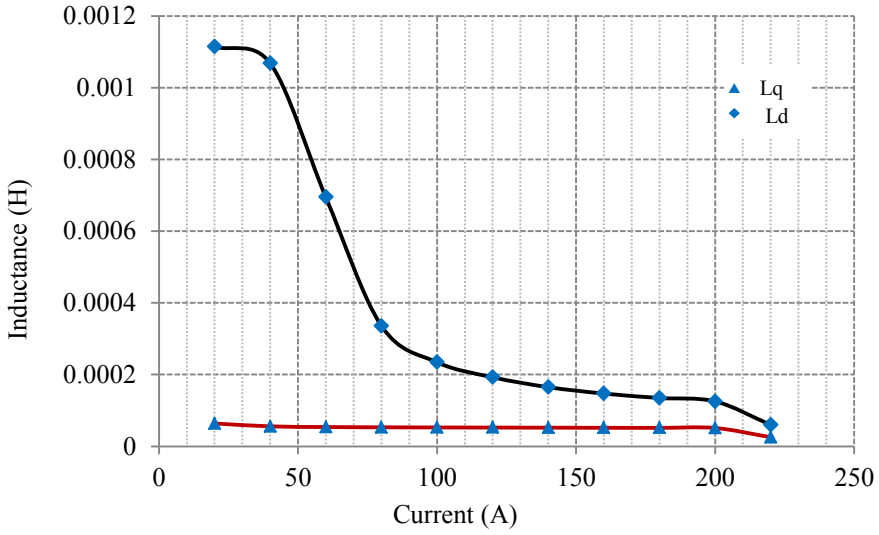

Figure 3.14. D-Q inductances versus phase current at φi =32˚ and θ = 68˚electrical.

3.9 Prototype and Experimental Results

In order to evaluate the method, a 7.5hp SynRM has been designed and manufactured. The design specifications which have been characterized by the proposed sizing method are summarized in Table 3.5. An existed DC machine rated at 3400rpm, 50A, and 250V is selected to be connected back to back to the proposed machine as mechanical load. The prototype machine operates as the prime mover and designed for low base speed (850rpm) to avoid over speed issues in the DC machine during the test procedure.

Table 3.5 The Prototype Design Specifications

Parameters	Quantity
Rated power	7.5hp
Peak torque	60 Nm
Rated voltage	230 Δ
Air gap	0.4 mm
Magnetic load	0.8 T
Stator outer diameter	204.8 mm
Rotor outer diameter	134 mm
Stack length	200 mm
Standard frame	IEC132 (208, 200)mm
Number of pole	4
Number of stator slots	36
Number of turns per slot	25
Number of rotor internal layers	4
Rated current	20 A
Stator slot opening	3 mm
Shaft diameter	43 mm
Winding type	distributed
Minimum/maximum rib width	1/1.5 mm
Skew	no
Coil pitch	full
Core steel type	M19
Max speed (electrical limit)	2400 rpm
Base speed	850 rpm
Saliency ratio	5

3.9.1 Prototype

The rotor was design by four poles and four internal layers which is shown in Figure 3.15. The rotor geometry has been modified according to the design criteria discussed in 3.8.2 to improve the machine's magnetic performance. The stator windings are designed by two layers, 18 and 7 turns per slot, to verify the effects of the number of turns per slot on the machine's performance which will be discussed in Chapter 5. This gives the possibility of operating the machine in 25 and 18 turns per slot configurations. In this chapter, examinations have been carried out using the stator winding with full turns (25 turns) per slot. Figure 3.16 shows the stator frame, core, and windings before finishing isolations and final painting. Figure 3.17 shows details of the encoder installation on the shaft to measure the rotor position.

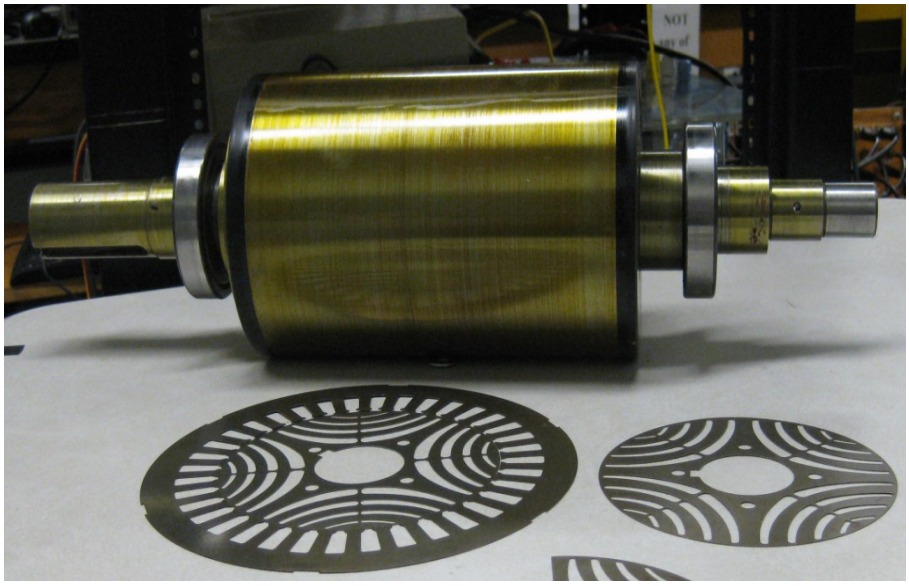

Figure 3.15. Prototype rotor and laminations from M19 steel.

Figure 3.16. The stator windings.

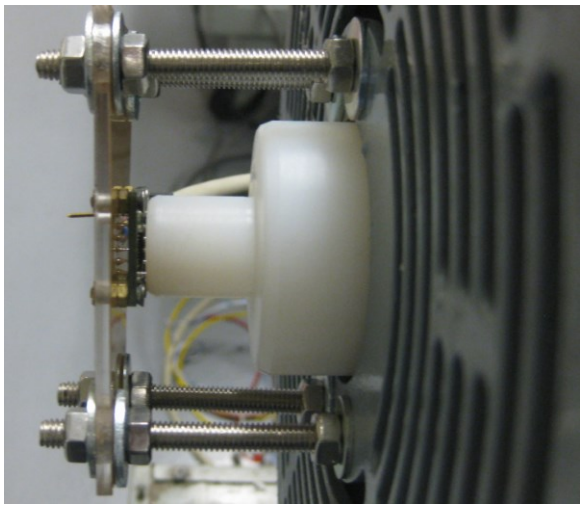

Figure 3.17. Installation of the encoder on the shaft.

3.9.2 Load Test

The proposed machine was examined under the load test at different speed in the steady state as well as the Multi-Static test in the locked rotor condition. To prevent over current issues due

to the low speed operation of the DC machine, the test has been performed at 40% of the nominal load. Figure 3.18 shows the experimental setup.

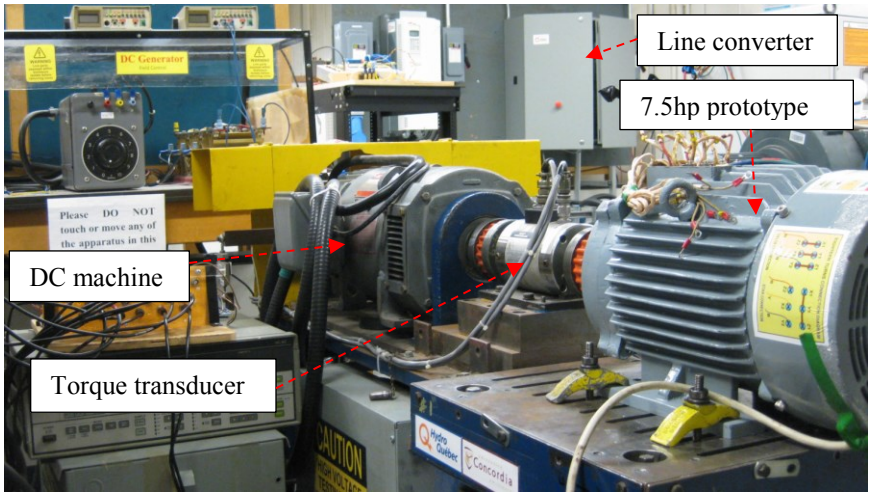

Figure 3.18. Experimental setup using back to back DC machine as the load.

The goal of this examination is to verify the proposed sizing method validation. Hence, the important performance characteristics of the prototype i.e., the torque profile, maximum power, and the saliency ratio has been characterized. The load test has been performed at 40% of the nominal power. This helps to limit over current of the DC machine in low speed operation, Figure 3.19 shows the torque and power profiles of the prototype at 9.0A which were measured in steady state.

As is illustrated, the machine took over 42% of the rated load, 27.3Nm and 2300 W, successfully at 9.0A and 820rpm which is quiet close to the design base speed. The maximum speed at which the constant power operation is terminated can be characterized at1450rpm. The speed range of 1450/820 is less than the design requirement. This confirms low speed range operation which is a potential issue of the SynRM for traction applications. This will be discussed in Chapter 5. The measured torque and power which were characterized at 9A shows

that the machine is capable of handling more load and developing more torque at rated current which is designed based on 20A.

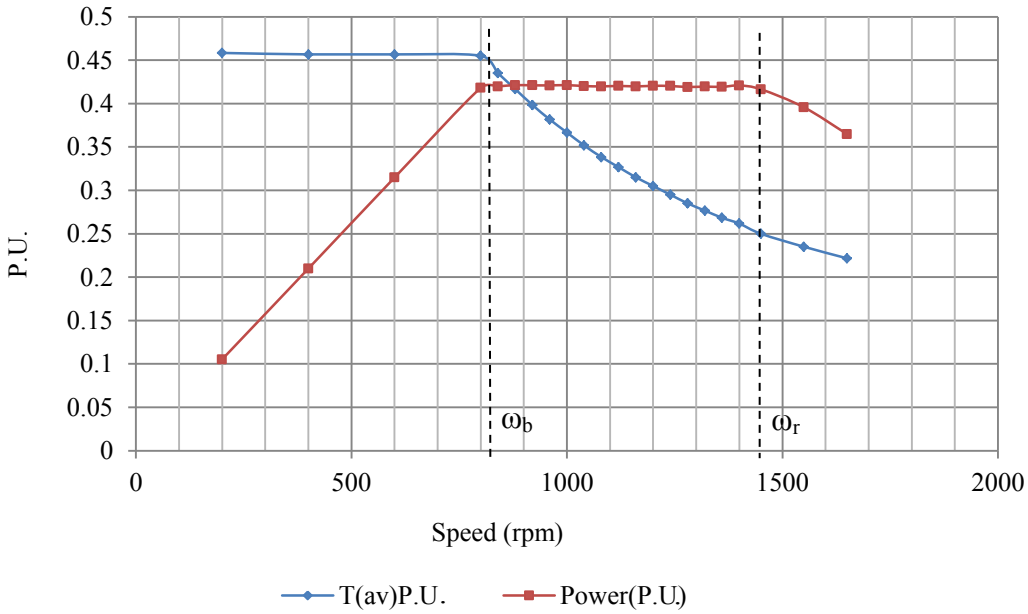

Figure 3.19. Measured torque- speed characteristic of the proposed machine.

3.9.3 The Locked Rotor Test

To verify the machine's peak torque, the Multi-Static test has been performed due to the previously-mentioned limitations of the load (DC machine). In this test; the rotor is locked, a DC current pulses equivalent to the rated current (20A) would be applied to the machine's windings, and the output torque would be measured at different rotor positions. Figure 3.20 and Figure 3.21 show the locked rotor setup and measured output torque-angle characteristics at the current corresponding to the base speed (850rpm) respectively. As is illustrated, the trend line which is extrapolated from the output torque data confirms the prototype machine is capable of developing 60Nm at 74° and 41° of the rotor position and the peak torque of 70Nm can be achieved at about 61°.

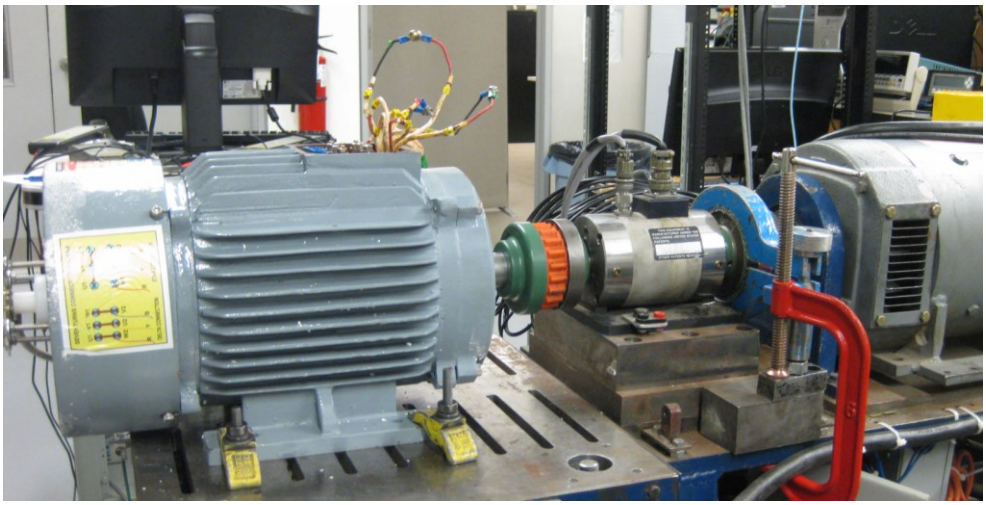

Figure 3.20. The locked rotor setup for torque-angle characteristic.

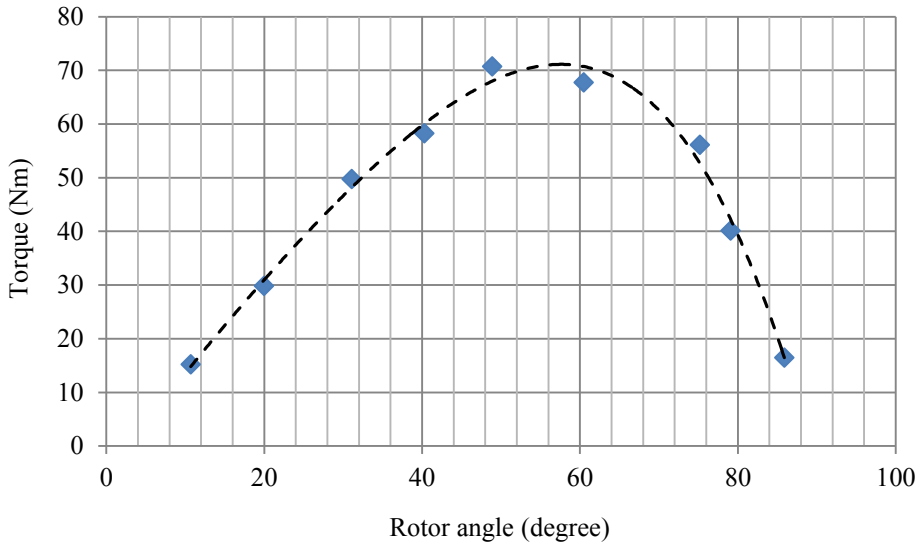

Figure 3.21. Measured torque-angle characteristic of the prototype.

To identify the machine's saliency ratio, the d-q axis inductances have been measured at different current loadings and rotor's proper angle corresponding to the maximum torque, using the AC test in the locked rotor condition. In this case the rotor has been locked before torque

transducer. Figure 3.22 and Figure 3.23 show the corresponding d-q axis inductances. The ratio of 4.58 (275/60) can be obtained at 9.5A which is 9% lower than that of the design specification.

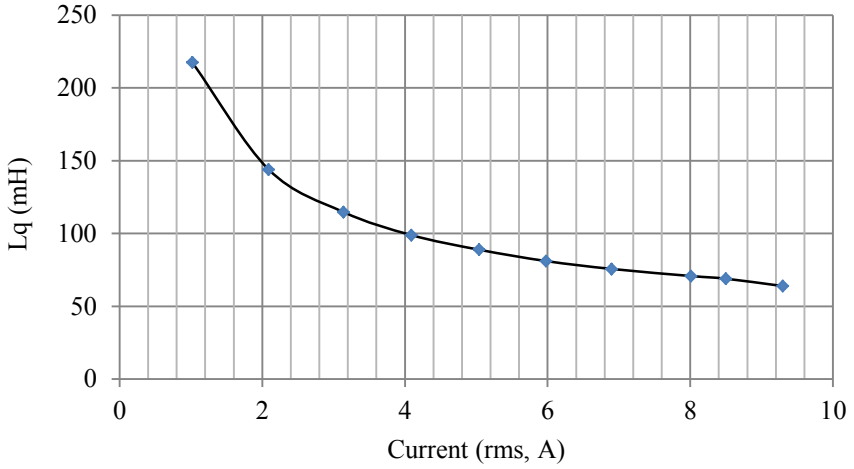

Figure 3.22. Measured q-axis inductance of the prototype for different currents.

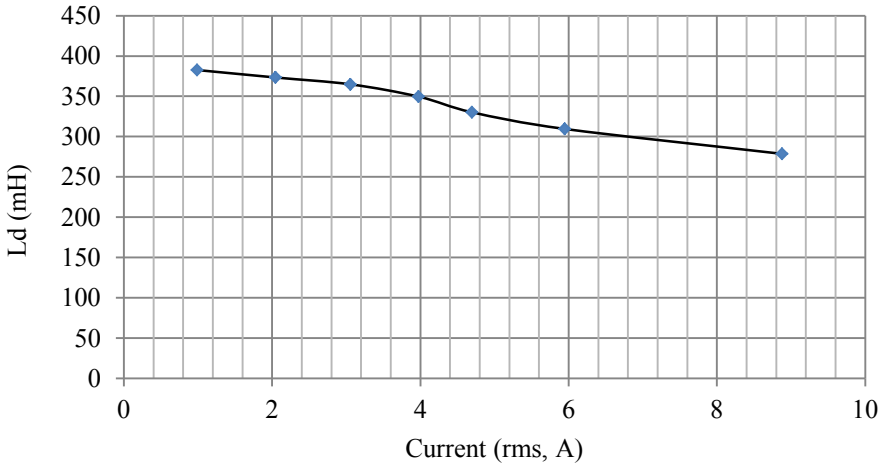

Figure 3.23. Measured d-axis inductance of the prototype for different currents.

The most important parameters which have been targeted through the sizing method are summarized in Table 3.6. As illustrated, the experimental results show good agreement with the design specifications. This confirms that; the proposed sizing method can be used as a fast and

reliable approach to identify proper size of the machine corresponding to the design requirements.

Table 3.6 Comparison of the Prototype and Designed Machine Specifications

Parameters	Measured	Designed
Peak torque (Nm)	60	70
Peak power at base speed (W)	5670	5500
Saliency ratio	4.58	5
Base speed (rpm)	810	850

3.10 Summary of Chapter 3

This chapter discussed the proposed sizing methodology and analytical design process of a SynRM for traction applications through which the stator geometry, rotor outer diameter, machine's electrical and magnetic parameters i.e., inductances, resistances, winding specifications as well as the output functions such as maximum torque, power factor, and efficiency were identified. The proposed approach uses the machine's mathematical model i.e., the equivalent circuit, vector diagram, and mathematical equations in conjunction with the initial data, desired torque envelope, and assigned parameters. Proposed sizing method was evaluated successfully by comparison between FE analysis and experimental test results. It was shown that this method can be sufficiently used as a fast and reliable procedure to identify the most important parameters of the SynRM based on the design specifications. Therefore, it can be performed prior to the rotor geometry design and machine final design procedure.

Chapter 4 Electromagnetic Torque Analysis

A major requirement in various industries, such as automotive, is for electrical machines to have high performance and low price. In order to enhance the performance of a synchronous reluctance motor for automotive applications, it is desirable to minimize torque ripples which may cause troubles, such as noise or unwanted machining patterns. Such torque ripples are predominantly caused by rotor and stator slot harmonics and depend on the position of the stator slots opening relative to the rotor slots. Although several solutions have been proposed to reduce torque ripples, several magnetic, mechanical, and electrical limitations remain as obstacles to achieve a proper design with desired torque. This chapter presents a geometrical method to identify a proper rotor slot pitch angle and their final fine tuning for minimizing the torque ripple using a given core material when the machine is equipped with transversal anisotropic laminated rotor (TLA). Furthermore, a novel rotor core design and assembly with cold rolled grain oriented magnetic material is proposed to investigate further improvement to the motor torque quality for traction applications. Prototypes with different rotors have been fabricated and examined. The results are compared to the finite element analysis for evaluating the methods.

4.1 Introduction

Despite having superior merits [16, 48], SynRM suffers from higher torque ripple compared to the IM and PMSM in traction applications, which is its inherent characteristic caused by the rotor anisotropic structure (Figure 4.1).

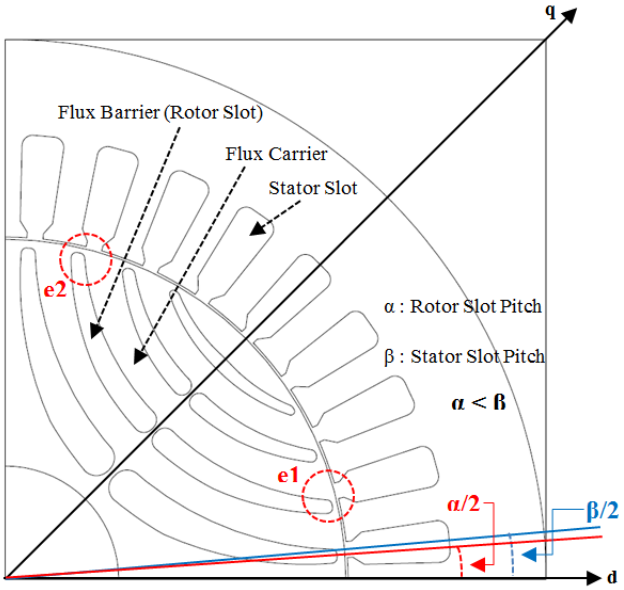

Figure 4.1. General perspective of the rotor and stator slot pitch angles in 4-pole SynRM.

A methodology for low torque ripple SynRM based on the concept of positive and negative complete rotor geometry [19] and a design criteria of high performance SynRM with higher torque per current capability [18] have been reported and considered as the foundation of many further investigations. Intensive works have been performed on torque harmonic compensation methods [37] based on the rotor flux barrier design [25] and sensitivity analysis of the rotor barriers [49]. It has been shown that the chording pitch method for stator winding is not necessary and a distributed multi-layer rotor is capable of eliminating the low order slotting harmonics from electromagnetic torque [19, 35]. To achieve a proper design of the SynRM, the magnetic performance related to the rotor geometry needs to be improved. This has been reported in different investigations recently [20, 47, 50].

Today, compactness and efficiency of the passenger vehicles imply that the size and weight are the design limitations. Thus, more attention needs to be paid to the type and size of the

traction motor [9, 39, 51, 52]. In this chapter the torque quality of SynRM consist of the average torque and torque ripple is investigated. A geometrical method based on rotor and stator slot pitch angle is presented to minimize the torque ripple which can be generalized to any SynRM with different number of stator slots and rotor flux barriers. A novel rotor core design and assembly with cold rolled grain oriented magnetic material (CRGO) is investigated for further improvement to the machine torque for traction applications. A 7.5hp prototype with different rotors is manufactured and examined; the results are compared to the finite element analysis for evaluating the methods.

4.2 Torque Ripple Principles in SynRM

In SynRM the electromagnetic torque is produced by interaction between air gap flux and its corresponding magnetizing current as is expressed in (4.1).

$$T_e = \frac{3}{2}\frac{P}{2}\lambda_m i_m \sin\beta \tag{4.1}$$

Where; P, λ_m, i_m, and β are the machine pole number, magnetizing flux, magnetizing current, and their corresponding angle respectively.

In general, the main sources of torque ripple in SynRM are categorized into two types;

1) Low order MMF space harmonics caused by non-sinusoidal stator current

2) Slots harmonics caused by non-uniform air gap

Internal flux barrier distribution in rotor structure implies a sinusoidal magnetic motive force (MMF) and its corresponding phase current and mainly minimizes the torque pulsation of the

first category. Therefore, adjusting the winding factor by chording the winding pitch is not necessary [35]. Chording reduces the output power consequently, increases the machine size, weight, and cost that are not desirable for automotive applications. If the torque harmonics of type one are minimized, the torque harmonics amplitude are directly dictated by the flux harmonics caused by the slots effects and non-uniform air gap which depend on the rotor position. Taking into consideration the first harmonic of the torque ripple due to the rotor and stator slotting, (4.1) can be modified as follows [36, 40];

$$T_e(\vartheta) \cong \frac{3}{2}\frac{P}{2}\left(\lambda_d i_q - \lambda_q i_d\right) + \frac{1}{2}(i_d \frac{\partial \lambda_d}{\partial \delta} + i_q \frac{\partial \lambda_q}{\partial \delta}) \tag{4.2}$$

Where; λ_d, λ_q, i_d, i_q are the d-q axis flux and current respectively and δ is the rotor angle. An additional term is added to the torque equation that represents torque pulsations. However, the average value of this term remains zero. Considering dependency of the d-q inductances on the rotor position, which is expressed as (4.3), the torque equation in (4.2) can be rearranged as (4.4).

$$\begin{bmatrix}\lambda_d \\ \lambda_q\end{bmatrix} = \begin{bmatrix}L_d(\delta) & L_{dq}(\delta) \\ L_{dq}(\delta) & L_q(\delta)\end{bmatrix}\begin{bmatrix}i_d \\ i_q\end{bmatrix} \tag{4.3}$$

$$\begin{aligned} T_e(\delta) = \frac{3}{2}\frac{P}{2}(\frac{3q}{\pi}\sin\frac{\pi}{3q})((L_{d-} L_q) i_d i_q \\ +(\Delta L_d + \Delta L_q) i_d i_q \cos(3Pq\delta) \\ -\Delta L_{dq}\left(i_d^2 - i_q^2\right) \sin(3P\, q\delta) \end{aligned} \tag{4.4}$$

where, q is the number of slots per pole per phase.

Equation (4.4) shows that the torque ripple has two components. The first component which is proportional to the average torque ($i_d i_q$) caused by oscillation of Carter's factor and circulating flux component (L_{cq}). These two oscillations create a considerable variations of d-q inductances (ΔL_d, ΔL_q) respectively. However, these can be reduced by skewing of the stator or rotor slots. The second component is due to the stator and rotor slots mutual effects. This introduces ΔL_{dq} and an additional torque ripple which needs to be minimized for high performance SynRM in electric powertrain. This is one of the objectives of this study in this chapter.

4.3 Rotor and Stator Slot Effects

The principal of the torque pulsation relative to slot harmonics lays on the fact that, in SynRM the rotor is forced to be aligned with the minimum reluctance by electromagnetic field. Any change on this alignment causes variations of stored energy at the slots opening area in the rotor and stator, results in changes in their equivalent co-energy. These variations which depend on the rotor angle are the potential sources for creating torque pulsations. Equations (4.5) and (4.6) show the analytical expression of the co-energy and its effect on the torque ripple [36];

$$W_{Co} = \int \left(\frac{B_\delta^2}{2\mu_0}\right) dV_r \tag{4.5}$$

$$T_r = \frac{dW_{Co}}{d\delta} \tag{4.6}$$

Where; V_r is the volume of the region of interest, δ is the rotor angle, and T_r is the torque pulsation amplitude.

As is illustrated in (4.6), in order to reduce the above-mentioned torque pulsation, the variation of co-energy versus rotor position needs to be minimized. During the past recent years, an intensive works have been performed and many investigations have been reported to improve

the SynRM torque ripple. From an automotive applications point of view, this section presents a new look at the torque ripple minimization in which the concepts of either rotor or stator slots pitches as well as the number of rotor internal layers as an important geometrical parameter, are taking into consideration. Moreover, a final fine tuning method is discussed to gain further improvement to the machine torque quality. Due to the parametrical nature of the approach, the method can be generalized for different designs with various numbers of rotor and stator slots and rotor internal flux barriers.

4.4 Torque Ripple Analysis Based on the Rotor Slot Pitch

Compactness in powertrain design in today's automotive industries requires high torque and power density of the electric machines. Therefore, torque ripple minimization using chorded pitch winding and skewed rotor or stator, that cause reduction in output power and torque by 5-10 percent [35] and simply increase the size, weight, and cost are not desirable.

4.4.1 Geometrical Method Criteria

Rotor and stator slot pitches in a single pole of a 4-pole, 36-slot stator, and 4-layers rotor are shown in Figure 4.1 and zoomed in Figure 4.2 in which R_{so} and S_{so} are the rotor and stator slots width respectively. Referring to the SynRM operation principal, when the stator core are magnetically energized, a magnetic flux waveform is produced and the rotor attempts to be aligned with the direction of the minimum reluctance. This is achieved by displacing the rotor d-axis until alignment of the magnetic fields in the motor's poles is obtained. This in turn results in rotary motion of the rotor at the same speed as the rotating magnetic field.

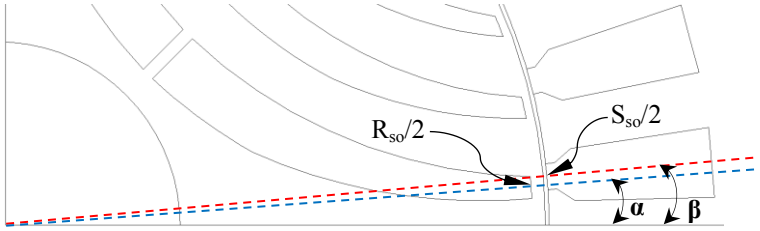

Figure 4.2. Presentation of the rotor and stator slots pitch angle.

Referring to Figure 4.1, the geometry of the rotor lamination is designed such that, for all barriers, when one end of a given barrier moves towards the opening of a corresponding stator slot, the opposite end of the barrier moves away from the opening of a corresponding stator slot. In this manner, during operation of the motor, a negative torque pulsation is generated by the end (e_1) while a positive torque pulsation is at the same time generated by the end (e_2) of the barrier leaving the opening of the corresponding stator slot. The positive and negative torque pulsations in turn cancel each other, thereby reducing the total amount of torque ripples generated by the rotor and stator slots mutual effects. Thus, average torque is also maximized.

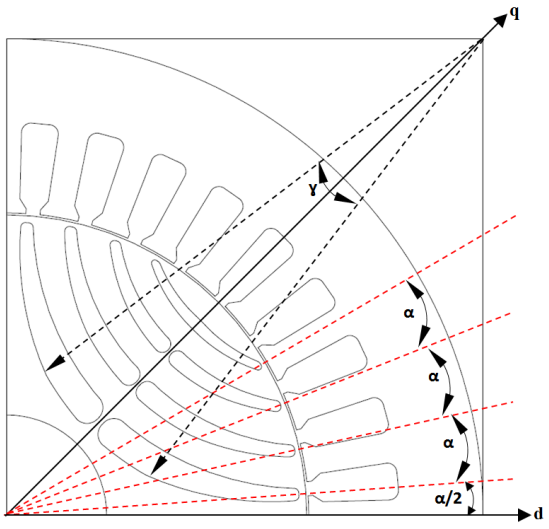

Figure 4.3. Rotor slot pitch angles of different rotor flux barriers.

As is shown in Figure 4.3, in order to achieve such reduced torque ripple characteristic, the angular spacing between two neighboring barriers ends needs to be set to a predetermined value which is called rotor slot pitch. It is easier to define the barriers end position by translating the rotor slot pitch from an angular space to an angle relative to d-axis (Figure 4.2). The ends of the barriers may then be aligned relative to each other and to the stator slots at the rotor slot pitch angle correspondingly. In addition, each barrier ends are necessary to be designed with the same width as the stator slots opening. Mathematical definition of the proper rotor slot pitch angle has been developed considering the number of pole pairs (P), the number of rotor internal layers (n_l), the number of stator slots (n_s), the number of rotor slots (n_r), the stator slot opening width (S_{so}), and the rotor slot end width (R_{so}) which is expressed in (4.7).

$$\alpha = \frac{180}{P} \frac{1}{\frac{n_s}{n_r}(n_l + \frac{R_{so}}{S_{so}})} \tag{4.7}$$

Amongst the above-mentioned parameters, the number of rotor internal layers which can be characterized by the number of flux barrier has strong role in average torque and torque ripple. Minimizing interaction between the stator and rotor slots is the key in designing proper rotor geometry for high performance SynRM. As is reported in [19], to achieve a low torque ripple characteristic, the number of rotor slots needs be specified based on the given number of stator slots as in (4.8) where, both n_s and n_r must be even.

$$n_s = n_r \mp 4 \tag{4.8}$$

Therefore, considering (4.8), the proposed condition can be generalized by (4.7) for different rotor geometries.

4.4.1.1 Different Rotor Geometries and Selection of the Reference Machine

As is shown in (4.7), to achieve a lower torque pulsation, the rotor slot pitch angle needs to differ from that of the stator. Rotor slot pitch angles are characterized using (4.7) and (4.8) for different motors with various internal layers and slots end width when two numbers of stator slots (36 and 48) are taking into consideration for a 4-pole machine, the results are summarized in Table 4.1.

Table 4.1 Rotor Slot Pitch Angles for Different Designs

Parameters						
n_s	n_r	n_l	S_{so}	R_{so}	α	β
-	-	-	mm	mm	degree	degree
36	24	3	3	3	7.5	10
				2	8.2	
				1	9.0	
	32	4	3	3	8.0	
				2	8.6	
				1	9.2	
	40	5	3	3	8.3	
				2	8.8	
				1	9.4	
48	32	4	3	3	6.0	7.5
				2	6.4	
				1	6.9	
	40	5	3	3	6.3	
				2	6.6	
				1	7.0	
	48	6	3	3	6.4	
				2	6.7	
				1	7.1	

According to 4.4.1, the worst case with respect to the torque ripple production is when the rotor and stator slot pitch angles are identical. In this circumstance, the torque pulsations produced at the ends of each barrier are either positive or negative when they move towards or away the stator slots opening respectively. Therefore, they boost each other, results in the highest torque ripple on the shaft. Referring to the Table 4.1, to evaluate the method, a machine rated at

7.5hp with a stator including 36 slots and a rotor with 4 internal flux barriers is selected as the reference. In this manner either (4.7) or (4.8) are satisfied. Table 4.2 shows the reference machine's specifications.

Table 4.2 Reference Machine Specifications

Parameters	Quantity
Rated power	7.5hp
Peak torque	20 Nm
Rated voltage	230 Δ
Air gap	0.4 mm
Magnetic load	0.8 T
Stator outer diameter (frame IEC132)	208 mm
Rotor outer diameter	134 mm
Stack length	200 mm
Number of pole	4
Number of stator slots	36
Number of rotor internal layers	4
Rated current	20 A
Stator slot opening	3 mm
Shaft diameter	43 mm
Winding type	distributed
Minimum/maximum rib width	1/1.5 mm
Skew	no
Coil pitch	full
Core steel type	M19
Max speed (electrical limit)	2400 rpm

Since the aim of current study in this section is to verify the mutual effects of the rotor and stator slot pitch angle on the torque pulsation, the rotor geometrical parameters such as flux carriers and barriers width, shape, and the radial and tangential ribs width have been designed such that to obtain the maximum possible saliency ratio and output torque [47, 50, 51], which is not described in detail in this section. The proposed machine with proper rotor geometry has been examined by FEA to identify its performance. It is while different alternatives of the rotor

slot pitch angle and flux barrier ends width are taking into consideration. It is the subject of the next section.

4.4.2 Computer Aided Analysis and Results

Simulations have been performed using current source mode of operation and lumped parameters. Due to the symmetrical nature of the rotor and stator geometries, the machine operated for 45 degrees mechanical to verify its performance for different rotor geometrical specifications. As opposed to voltage source operation, this method eliminates the effects of current harmonics on the output torque, results in a torque ripple caused by the no uniformed air gap that is only dictated by the rotor geometry. The circuit diagram of the simulation is shown in Figure 4.4 in which I_1, I_2, and I_3 are the current source inverter supplies, R_1, R_2, and R_3 are the end winding resistors, L_1, L_2, and L_3 are the end winding inductances, B_1, B_2, and B_3 are the magnetizing coils including resistance and inductance. The geometry of the reference machine has been coded in the software. The software is modified to obtain full control of the rotor and stator geometries. All parameters are kept the same for different alternatives except the rotor slot pitch angle and ends width.

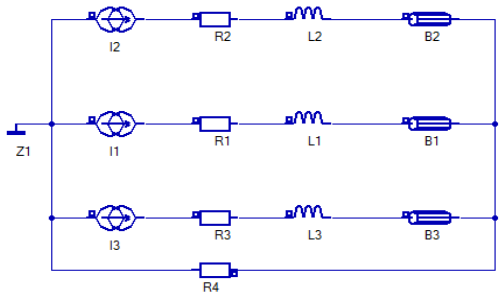

Figure 4.4. Circuit diagram of the current source simulation.

4.4.2.1 Reference Machine Performance

As is previously discussed, an equal rotor and stator slot pitches is the condition in which the torque pulsation is maximized. Figure 4.5 shows the single pole configuration of the machine where, the stator slot openings and the rotor barrier ends are the same and equal to 3mm. FEA results in Figure 4.6 show poor torque qualities with respect to the torque ripple in which 72.1% ripple (Peak to Peak) at the average of 26.9 Nm for either high or low current are evidenced. In this figure the machine operated for 45° mechanical degrees at base speed and the results have been translated to time domain for torque ripple harmonics analysis.

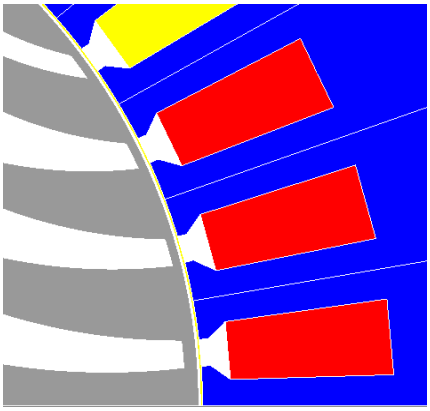

Figure 4.5. Location of the barriers end at α=β.

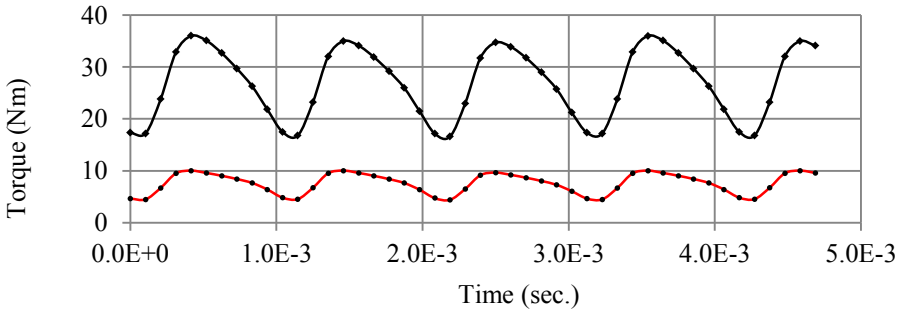

Figure 4.6. Torque- angle characteristics at rated and 30% torque in time domain (α = β).

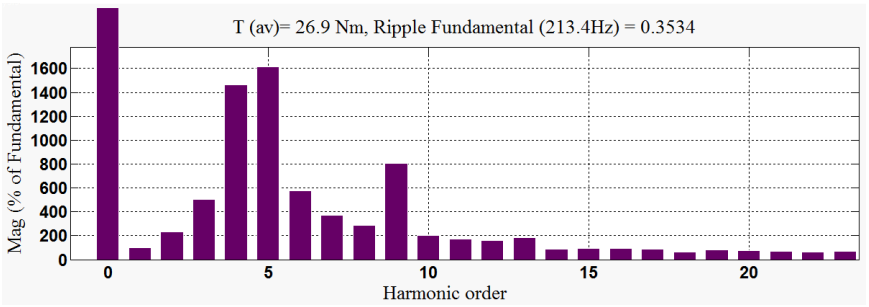

Figure 4.7. Torque ripple harmonics for α=β.

As is illustrated in Figure 4.7; the third to ninth order harmonics have strong effects on the torque pulsation. Amongst them the fourth and fifth harmonics are dominant compared to the DC component that represents the average torque (26.9 Nm).

4.4.2.2 Effects of the Rotor Slot Pitch Angle

To evaluate the rotor barriers end adjustment scheme based on (4.7), the geometry of the rotor has been modified as is shown in Figure 4.8 in which the rotor slot pitch angle is 8 degrees (Table 4.1).

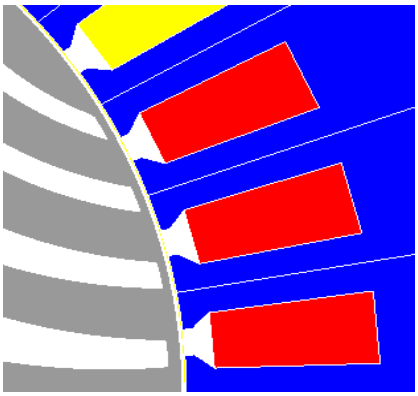

Figure 4.8. Location of the barriers end at α sketched by (4.7).

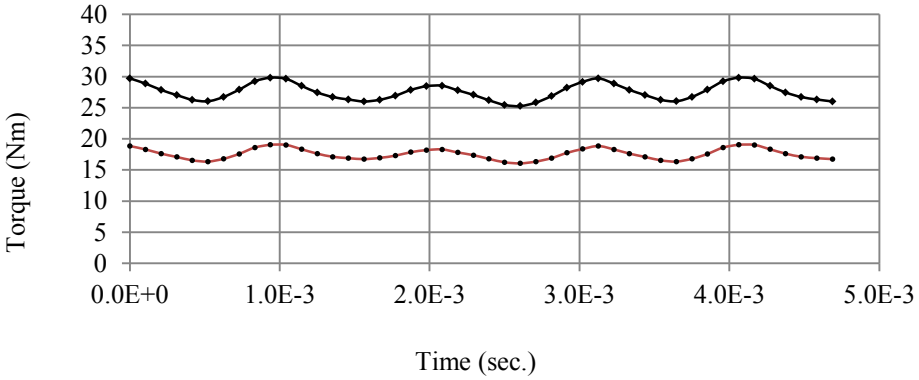

Figure 4.9. Torque-angle characteristics at rated and 50% torque in time domain (α = 8°).

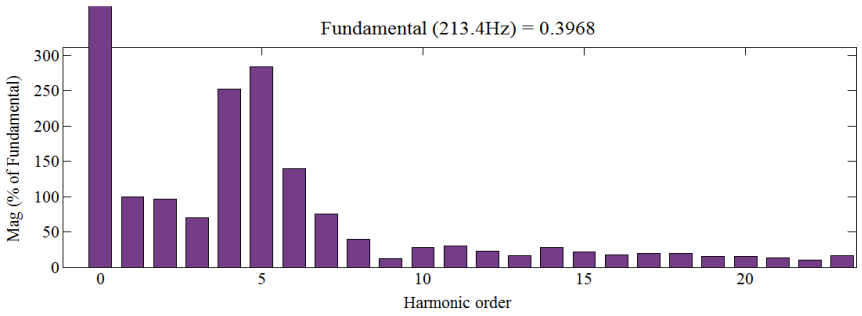

Figure 4.10. Torque ripple harmonics for α= 8°.

The FEA results of the new rotor barriers end arrangement show considerable reduction in torque ripple. As is illustrated in Figure 4.9, the torque ripple is reduced to 16.4% which is 78% less than that of in Figure 4.6 with the average of 27.6 Nm. To validate the results, the torque harmonics is shown in Figure 4.10 correspondingly. As is illustrated, the magnitudes of the dominant harmonic are reduced from 1600% to 275 % and the ninth order harmonic mostly removed. These results confirm that; using (4.7) for SynRM's rotor barrier ends adjustment allows designer to reduce the magnitude of the torque ripple significantly. However, the low order harmonics (2_{cd}-7_{th}) are still produced.

High torque operation in traction motors occurs in short transient time (10-30 sec.). From a traction point of view, to verify the effect of the different rotor slot pitch angles on the proposed machine's performance, it is necessary to compare various alternatives for medium torque (15A) and at maximum speed that is compatible with high speed operation and maximum power (cruising mode). The results are summarized in Table 4.3.

Table 4.3 Proposed Machine Performance with Different Rotor Slot Pitches

Unit	$\beta = 10°$	alternatives			
degree	α	7.5	8	8.5	9
Nm	Average torque	17.6	17.6	17.5	17.4
%	Torque ripple	15.5	16.4	10	21.9
A	Phase current	15	15	15	15
Nm/A	Torque/Current	1.17	1.17	1.17	1.17

As is shown in Table 4.3 and Figure 4.11; the torque ripple has been reduced to 10% (Peak-Peak) as the rotor slot pitch angle was adjusted at 8.5 degrees. It is while; the average torque did not change considerably. Figure 4.12 also confirms reduction of the low order harmonics magnitude in the machine torque. The importance of these results is that; the rotor slot pitch angle adjustment can reduce torque ripple significantly without any considerable change in average torque and output power. Furthermore, (4.7) is a fast and reliable approach to find the proper rotor slot pitch angle. Also, final fine tuning may be necessary to find the proper angle.

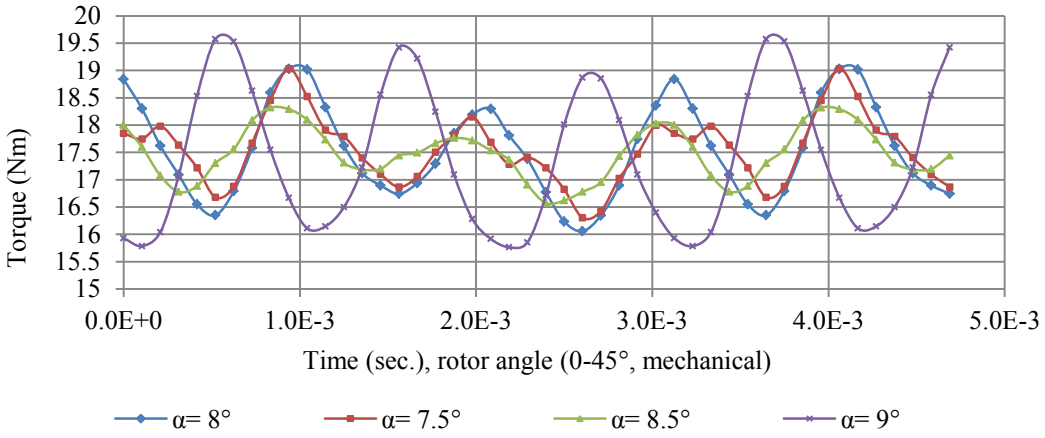

Figure 4.11. Torque-angle characteristics of different rotor slot pitch angles.

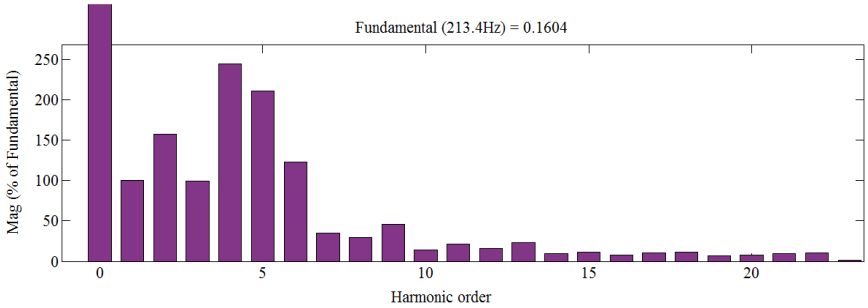

Figure 4.12. Torque ripple harmonics for α= 8.5°.

4.4.2.3 Effects of the Flux Barrier Ends Width

The rotor flux barrier ends width affect the stator and rotor mutual magnetic reaction. Therefore, this can introduce additional torque pulsations. In this section, the effects of the rotor barrier ends width are investigated. In order to achieve such a reduced torque ripple characteristic described in 4.4.1, an identical stator slot opening and rotor flux barrier end is selected. The machine with rotor slot pitch angle of 8.5° exhibits a better performance with respect to the torque ripple (Table 4.3). Therefore, it has been selected as the reference machine

in this section for FEA. The FEA results for different rotor barriers end widths (BEW) are summarized in Table 4.4.

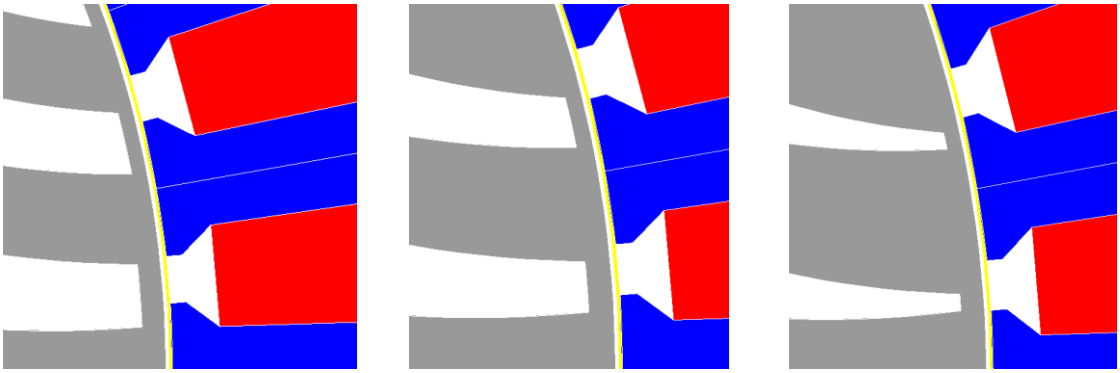

BEW=5mm BEW=3mm BEW= 1mm

Figure 4.13. Rotor geometry with different barriers ends width (BEW).

Table 4.4 Proposed Machine Performance with Different Rotor Barrier End Widths

Unit	β = 10°, α=8.5°	alternatives			
mm	BEW	1	2	3	5
Nm	Average torque	17.0	17.4	17.5	17.3
%	Torque ripple	9.5	9.6	10	10.18
A	Phase current	15	15	15	15
Nm/A	Torque/Current	1.13	1.17	1.17	1.15

As is illustrated, reduced barrier end width affects the average torque and torque ripple (0.5%) slightly when the rotor slot pitch angle is adjusted at the proper angle (8.5°) for all four examinations. Thus, the same width for the stator slots opening and the rotor flux barriers end is

a proper solution to achieve the maximum torque at lower ripple. However, to prevent unwanted saturation and critical stress, round shape is desired at the rotor barrier end edges.

4.5 Torque Analysis Based on a Novel Rotor Poles Assembly

Design of a high performance SynRM requires maximizing the anisotropic property of the rotor geometry in which either high L_d or low L_q are desired. This implies higher saliency ratio, results in a larger output torque on the shaft. The multi-layer structure of the rotor geometry is the key in achieving a proper design of the TLA rotor type which has been discussed in 4.4 previously. Recent advantages of high quality anisotropic magnetic materials such as Cold Rolled Grain Oriented (CRGO) steel has contributed to new energy efficient, compact, and high performance static electric machines such as transformers. From the rotor core point of view, the circular geometry of the rotor in SynRM remained as an obstacle to take advantage of these advanced magnetics material for the motors with number of poles higher than two.

CRGO is a specialty steel having a grain surface in which the grain's magnetization direction is aligned with a rolling direction of the steel sheet. This is due to a tight control of crystal orientation during processing of the electrical steel. As a result, the CRGO shows improved magnetic properties in the rolling direction. In particular, higher induction or flux density and lower core loss are developed.

By cutting the rotor laminations from CRGO, the magnetic properties of the rotor core are further improved compared to a proper anisotropic geometrical design of the TLA rotor, thereby improving overall performance. Figure 4.14 shows a typical magnetic characteristic of the CRGO electrical steel. This chart illustrates the difference of magnetic properties in the rolling direction (straight up and down) and at angles up to 90º from the rolling direction (left to right).

The maximum performance is achieved by application of the material with the strip in the same direction that flux is expected. In contrast, isotropic magnetic steel shows only a slight variation in properties within the plane of the strip and can be used in any orientation. A new rotor poles assembly for a 4-pole SynRM using CRGO is proposed in this section to improve the magnetic performance of the SynRM for traction applications.

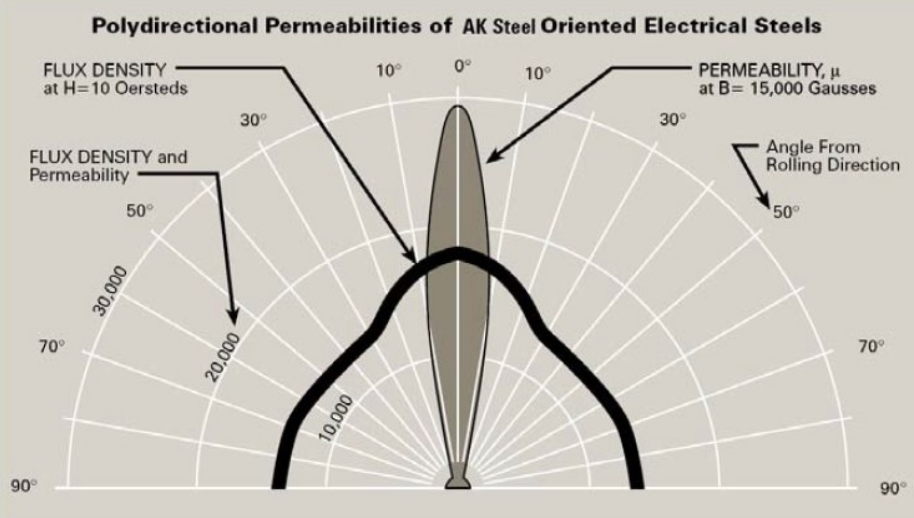

Figure 4.14. Flux density and permeability of the CRGO, (AK Steel courtesy).

4.5.1 Method of the New Rotor Poles Assembly

For this purpose, the rotor poles may be split to obtain individual one-pole rotor laminations, which are cut from the CRGO sheet. As shown by the cutting layout illustrated in Figure 4.15, the one-pole rotor laminations may be aligned with the rolling direction such that the direction of the q-axis of each one-pole rotor lamination is substantially perpendicular to the rolling direction. In this manner, both ends of any given insulating barrier of the one-pole rotor lamination may be positioned on an axis, which is parallel to the rolling direction. In addition, the cutting layout of

the one-pole rotor laminations may reduce the material loss of the sheet during the cutting process. For instance, a staggered cutting pattern which minimizes material scrap may be used. Therefore, the cutting process can then be simplified and more efficient.

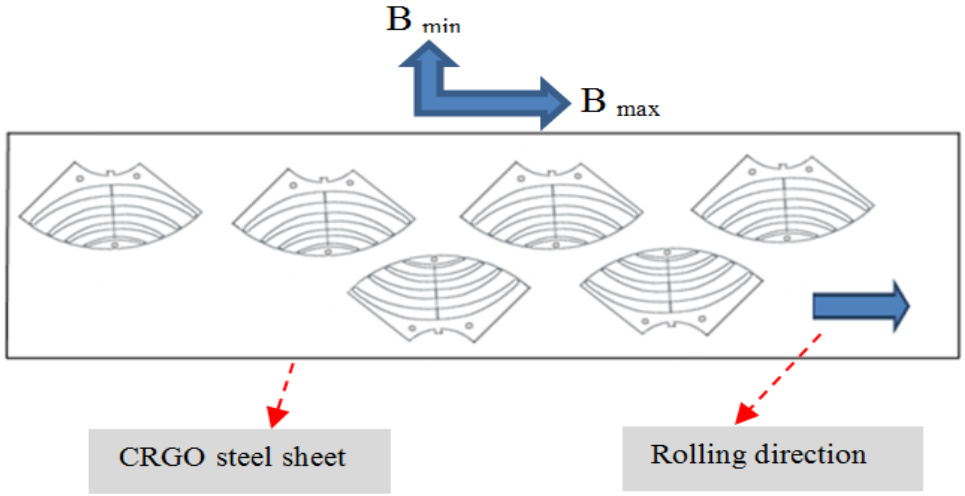

Figure 4.15. Cutting method of the one-pole lamination.

Once the one-pole rotor laminations have been obtained, a bonding technique is used to clamp the one-pole rotor laminations together and provide proper mechanical strength to the resulting rotor. For this purpose and as shown in Figure 4.15, each one-pole rotor lamination may comprise bolt holes and a guide pine which provide positioning guidance during the clamping process. The bolt holes and the guide pine ensure proper alignment of the one-pole rotor laminations relative to one another during their assembly into the individual rotor laminations. As are illustrated in Figure 4.16 and Figure 4.17, asymmetrical design of one-pole lamination in which on arm of the first flux carrier is thicker than the other arm, allows overlapping between two consecutive layers that is the key in proper bonding of the whole rotor laminations.

Referring to Figure 4.3 and as is shown in Figure 4.17; the flux barriers span angle, ɣ, is widened compared to Figure 4.3. This increases the length of flux carrier in the direction aligned with the maximum excitation of the CRGO (rolling direction) with constant width. This further improves the corresponding flux density and maximum steel utilization.

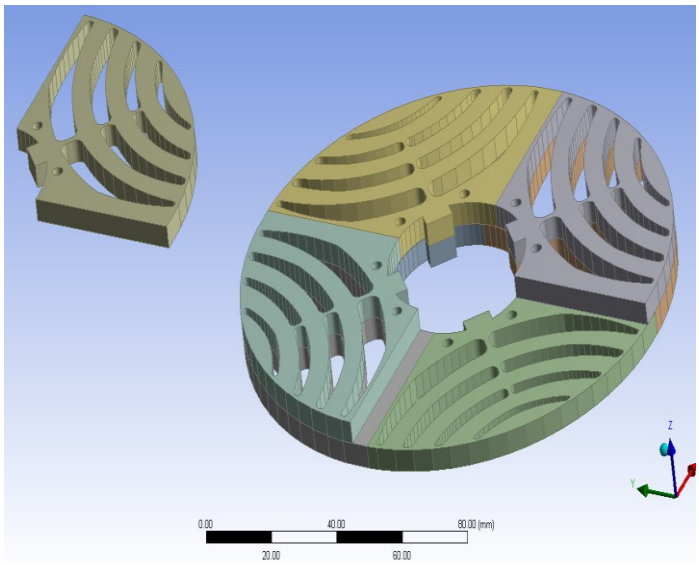

Figure 4.16. General perspective of the segmented one-pole laminations assembly.

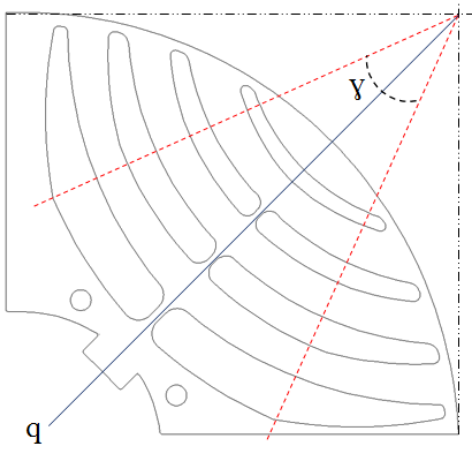

Figure 4.17. One pole configuration of segmented pole SynRM using CRGO steel.

4.5.2 Simulation Results

Simulation has been performed using the same criteria as 4.4.2. The rotor slot pitch angle, α, of the prototype was designed with the proper value that has been discussed previously in 4.4.2.2. The machine run at base speed, 45% load (9A), and other specifications were kept the same as the reference machine. The anisotropic material is considered only for rotor core. The magnetic characteristic (B-H curve) of the rotor core is defined based on two different perpendicular axis using Figure 4.14 which is equivalent to the M5 from AK electrical steel specifications. Due to rotary behavior of the field relative to the stator core, use of the grain oriented material for stator is not advantageous. As opposed to this, the rotor at synchronous speed remained stationary relative to the fundamental component of the rotating filed which leads to take advantage of the CRGO material in the machine operation. The simulation results will be presented and compared to the experimental test results in the next section.

4.6 Experimental Test and Results

In order to evaluate the methods in 4.4 and 4.5, a 7.5hp SynRM has been designed and manufactured with three different rotors. The prototype machine has been described in 3.9.1 and 3.9.2 previously and the design specifications were summarized in Table 3.5. Figure 4.18 a, b, and c show three different rotor's laminations including rotor with identical stator and rotor slots pitch angle, rotor with modified slot pitch angle, and single pole segmented rotor using CRGO (M5) respectively. Figure 4.19 a, b, and c show different rotors assemblies correspondingly. As is discussed in Chapter 3, A DC machine rated at 3400rpm, 50A, and 250V has been considered as load and connected back to back to the prototype mechanically, and to the grid electrically.

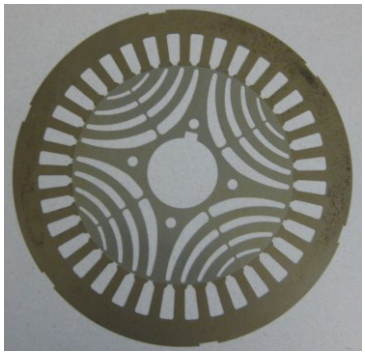

(a)

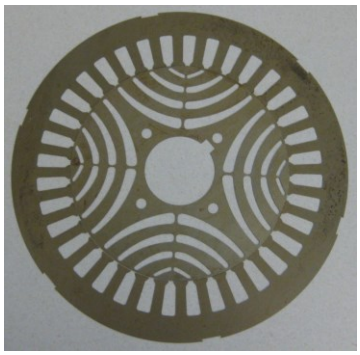

(b)

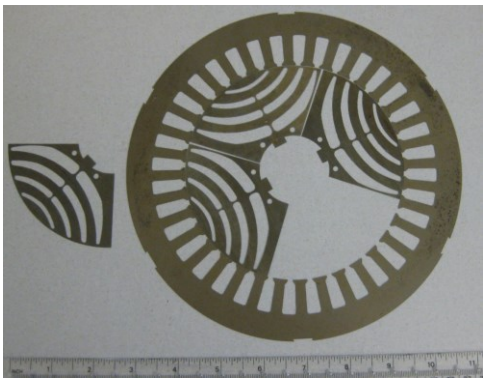

(c)

Figure 4.18. Different rotors lamination.

(a) (b) (c)

Figure 4.19. Different rotors assembly.

The prototype operates as the prime mover and designed for low base speed (850rpm) to avoid over speed issues in DC machine during the test. The goal of this examination is to verify and compare performances of the prototype using three different rotors shown in Figure 4.18 and Figure 4.19 with respect to the torque ripple using rotor (a) and (b) as well as, with respect to the output torque or saliency ratio using the rotor (a) and (c) . The load test has been performed at 45% of the nominal power at base speed to limit over current of the DC machine in low speed operation. The test setup is the same as Figure 3.18. The first examination was performed under load test at based speed using rotors (a) and (b). Figure 4.20 shows the current profiles of the prototype at 9.0A which were measured in steady state for two electrical cycles. Correspondingly, Figure 4.21 and Figure 4.22 show the torque profiles of the prototype equipped with rotor (a) and (b) versus time.

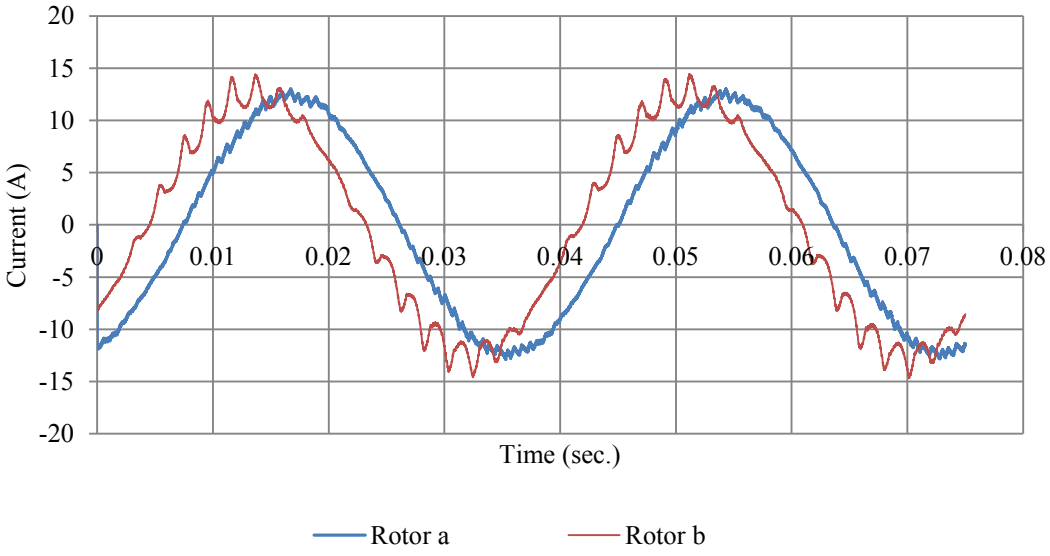

Figure 4.20. Measured current profiles of the prototype equipped with rotor (a) and (b).

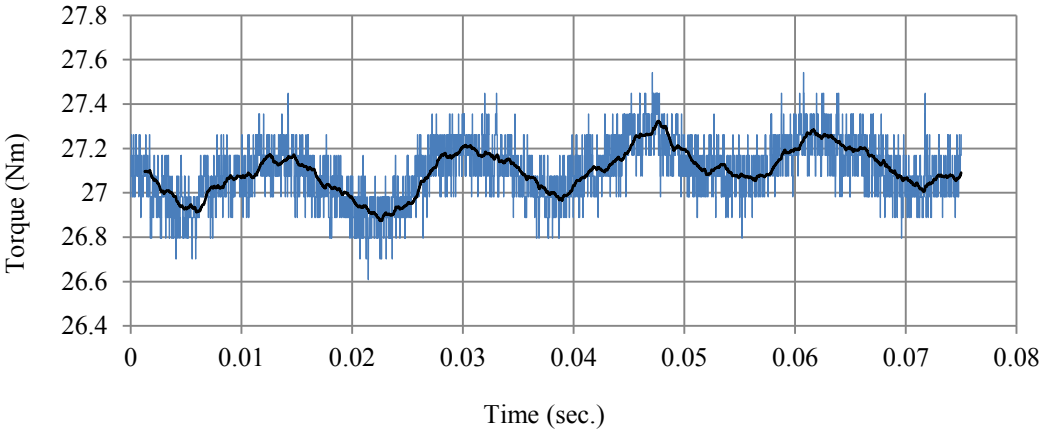

Figure 4.21. Measured torque characteristic of the prototype equipped with rotor (a)

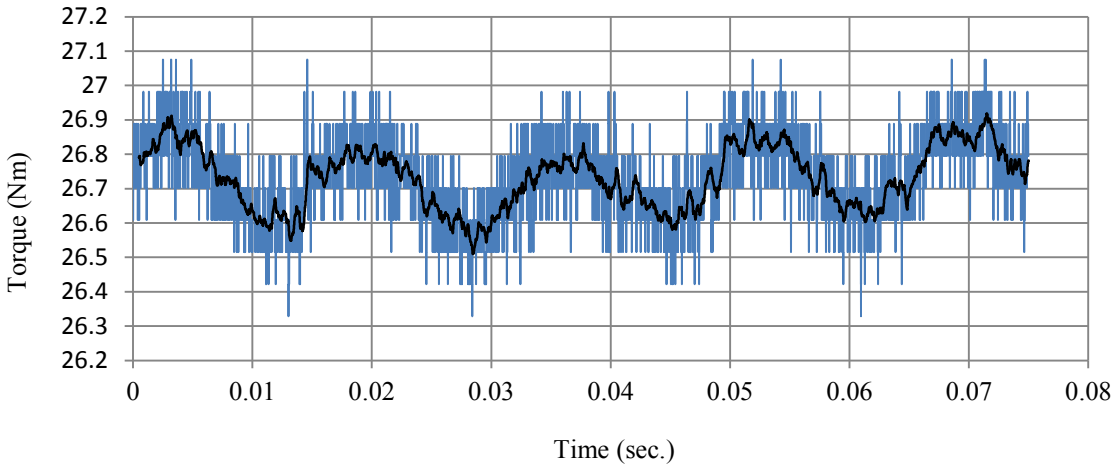

Figure 4.22. Measured torque characteristic of the prototype equipped with rotor (b).

As is illustrated in Figure 4.20, the measured current of the machine equipped with rotor (b) is much more distorted compared to that of the machine equipped with rotor (a). This implies a higher torque distortion and lower average torque using rotor (b) which are shown in Figure 4.21 and Figure 4.22 with approximately 1.5Nm (5.5%) reduction in average torque and 24.5% increase of the torque ripple.

The second test was carried out to verify the performance of the prototype machine equipped with rotor type (c) with respect to the saliency ratio and peak torque. The AC test at locked rotor

condition was performed for both machines. The test procedure has been described in 3.9.3 and the setup shown in Figure 3.20. Figure 4.23 and Figure 4.24 show the measured and calculated d-q axis inductances of the machines equipped with the rotors type (a) and (c).

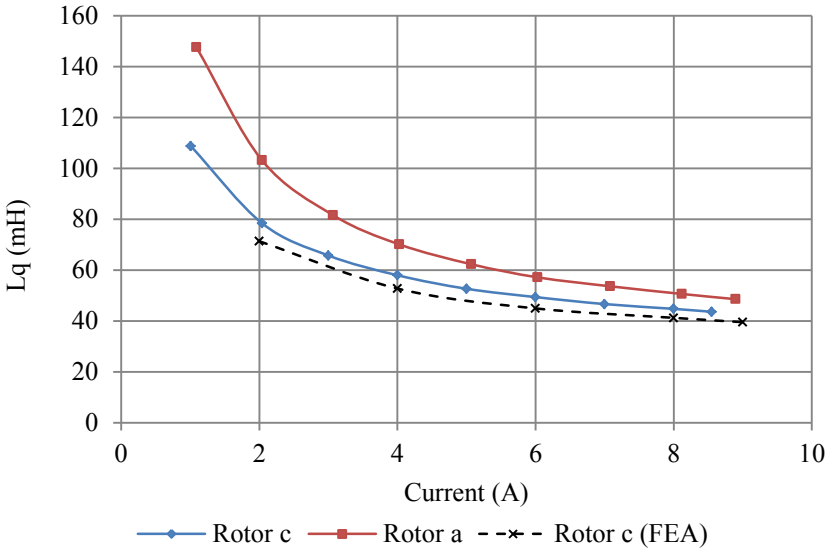

Figure 4.23. Measured and calculated L_q versus current for the rotor (a) and (c).

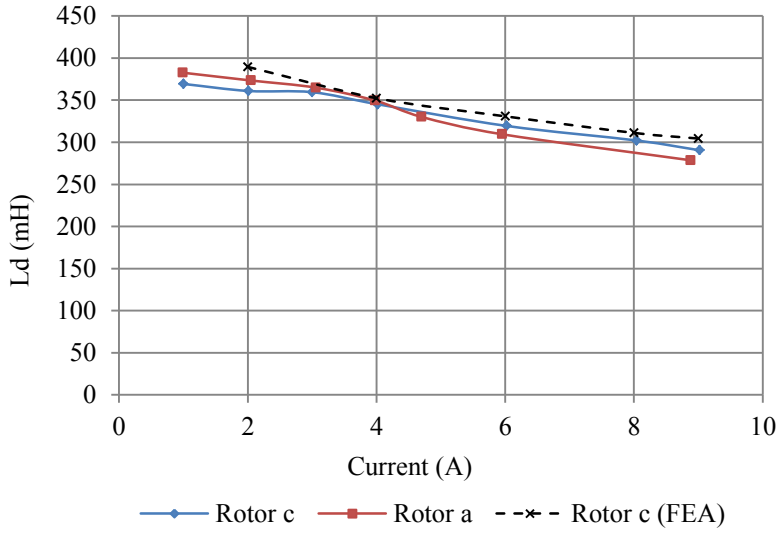

Figure 4.24. Measured and calculated L_d versus current for the rotor (a) and (c).

As is illustrated, the machine equipped with the rotor type (c) made by CRGO steel exhibits higher induction in d-axis and lower induction in q-axis at operating point (9A) which implies higher performance, but in general, there is a good agreement between FEA and measurements. Table 4.5 summarizes the output functions of the proposed machines. Accordingly, the use of CRGO steel in the rotor core improves the machine's saliency ratio and magnifies the output torque; consequently, reduces the size at the same operating load which all of them are desirable for automotive applications.

Table 4.5 Test and FEA Results of the Proposed Machines Using CRGO (M5)

Unit	Parameters	Rotor a (measured)	Rotor c (measured)	Rotor c (FEA)
A	Current	8.9	9	9
V	Line voltage	401	403	400
Degree	Rotor angle	55	51.5	54
W	Output power	2300	2300	2300
-	Saliency ratio	4.6	6.8	7.6
Nm	Power factor	0.5	0.52	0.6
Nm	Output torque (T)	27.3	29	31.5
%	ΔT compared to rotor (a)	0	6	15.4
Nm/A	Torque/Current	3.07	3.22	3.5
rpm	Operating speed	850	850	850

4.7 Summary of Chapter 4

This chapter discussed torque ripple principles of the synchronous reluctance machines and proposed a geometrical method to identify a proper rotor slot pitch angle and their final fine tuning approach for minimizing the torque ripple using a given core material. The proposed machine is equipped with transversal anisotropic laminated rotor (TLA). Different machines with various rotor slot pitch angles and rotor barrier ends widths have been examined by FEA and experimental test to evaluate the method. It is shown that; in order to achieve such reduced torque ripple, the angular spacing between two neighboring barriers ends needs to be set to a predetermined value which is called rotor slot pitch angle. The rotor slot pitch angle adjustment can reduce torque ripple significantly without any considerable change in the average torque and output power. Furthermore, an innovative rotor core design and assembly with cold rolled grain oriented magnetic material was proposed to investigate further improvement to the motor torque quality for automotive applications. It was shown that; the machine equipped with the segmented rotor made by anisotropic magnetic steel exhibits higher induction in d-axis and lower induction in q-axis at operating point compared to the isotropic magnetic steel. As a result, use of the oriented material in the rotor core improves the machine saliency ratio, magnifies the output torque, and reduces the machine size at the same operating load which all of these are desirable for automotive applications.

Chapter 5 Core Analysis

Considering the major requirements for automotive applications that are high torque and power density, low torque ripple, wide speed range, and high speed operation capability, the synchronous reluctance machine is still under intensive investigations. As a traction motor, the proper operation of this machine at low and high speeds is desired. Hence, the magnetic and mechanical performances of the core structure are important challenges. Thus, prior to the final design, they need to be analyzed with regards to the core magnetic behavior and mechanical robustness which cause degradation in torque quality and harmful deformation at critical points in the rotor structure. At low speed, the high current demand at maximum torque makes the core magnetic performance dominant, whereas at high speed the mechanical behavior of the rotor core structure limits the machine performance. This chapter presents a computer aided comparative analysis of different core characteristics to improve the core magnetic and mechanical performance of the synchronous reluctance machine equipped with a transversal laminated anisotropic rotor type for automotive applications.

5.1 Introduction

Referring to the major requirements of the traction motors in 2.2, high start-up torque of the SynRM is desired. To maximize the output torque, the saliency ratio (L_d/L_q) needs to be maximized. This parameter is the key in proper design which depends strongly on the rotor geometry. Figure 5.1 shows the general perspective of a 6-pole SynRM with TLA rotor.

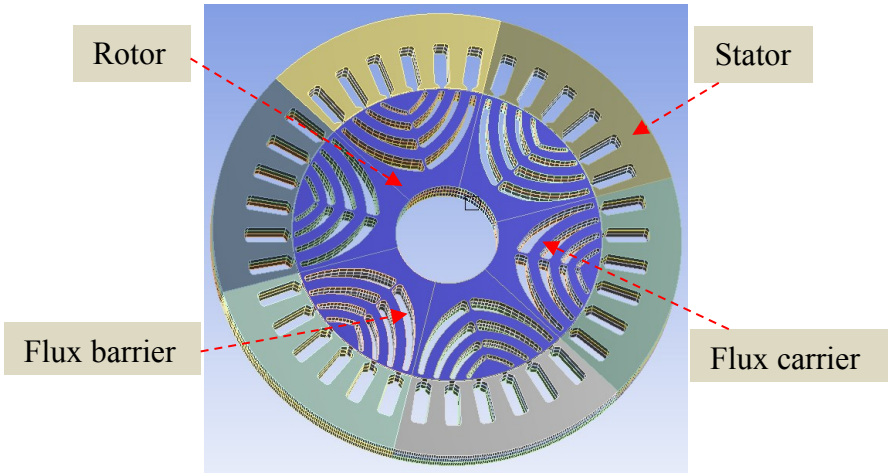

Figure 5.1. General perspective of 6-pole SynRM with TLA rotor.

Recent investigations reported in the literature are mostly focused on control strategy [27-29, 53, 54], comparison of SynRM to different machines [34, 52], and axially laminated anisotropic (ALA) rotor type for high speed operation [55-57] due to its higher saliency ratio [44, 45] and rigid structure. However, the transversal laminated anisotropic rotor (TLA) type is preferable in many applications because of its simple manufacturing process and lower iron losses [17]. To achieve a proper design of the SynRM, the magnetic performance related to the rotor geometry needs to be improved. This has been reported in different investigations previously [18, 20, 25, 47, 50]. Furthermore, considering today's compact passenger vehicles in which the size and weight are the design limitations, special attention must be paid to the rotor and stator core with regards to the magnetic and mechanical aspects. These may guarantee the design for a higher performance and structural integrity in high speed operation when the SynRM is used in automotive applications.

5.2 TLA Rotor Structure

In the TLA rotor type shown in Figure 5.1 and Figure 5.2, the most important design parameters which have significant effects on the saliency ratio are the number of poles, number of flux barriers and segments (layers), insulation ratio (ratio of total air to total steel in rotor q-axis), position and size of the barriers and segments, air gap length, and the width of tangential and radial ribs. Among them the parameters, "width of the tangential and radial ribs," also affect the rotor mechanical integrity in high speed operations.

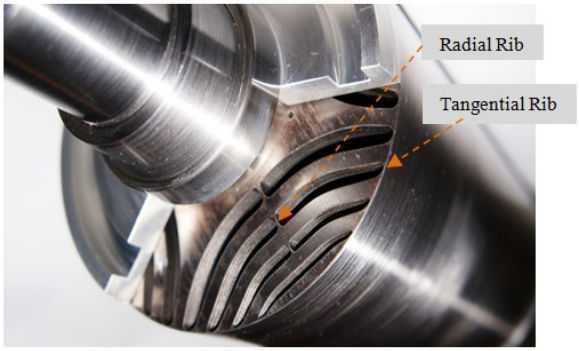

Figure 5.2. Structure of a 4-pole, TLA rotor of the SynRM, KSB curtesy.

In this structure the laminations are identical and can be cut in the traditional way. Some thin connections which are called "Ribs" connect the ends of the segments to each other axially and transversally. These connections maintain enough mechanical integrity in the rotor structure when rotational forces are applied in high speed operations. Therefore, from a mechanical robustness point of view the rib's width needs to be as thick as possible to withstand the maximum stress at the desired operating speed. However, as a drawback, they allow an increase in the flux in q-axis and a decrease in the saliency ratio. As a result, they reduce the machine's

output torque. The torque reduction caused by tangential ribs is dominant due to higher numbers and saturation effects. This can be expressed for a single lamination as in (2.35) [18].

5.3 Magnetic Circuit

A cascade substitution scheme of the SynRM equipped with a transverse laminated rotor is a convenient tool to analyze the machine internal magnetic characteristics. Since, the magnetic behavior of the core is analyzed in this section, it is appropriate to use the universal scheme for K_{th} layer of the rotor structure in d and q-axis that is shown in Figure 5.3a and b respectively. For an arbitrary machine, the corresponding d and q axis magnetic circuits are shown in Figure 5.4a, b, and c. f_k is magnetic motive force (MMF) applied to the core by machine ampere-turns (NI), r_k is the rotor magnetic reaction potential, F_q and F_d are the q and d-axis corresponding MMFs. R_g, R_y, R_t, R_{sk}, and R_{gk} are the air gap, yoke, teeth, the k_{th} segment, and k_{th} barrier reluctances respectively. To realize the magnetic behavior of the core, it is necessary to verify the mathematical expressions of these parameters that are shown in (5.1) and (5.2) in per-unit of the stack length [18];

$$R_g = \frac{g}{\mu_0 T_w} \quad , \quad R_y = \frac{\tau}{\mu_0 \mu_r y} \quad , \quad R_t = \frac{T_h}{\mu_0 \mu_r T_w} \tag{5.1}$$

$$R_{sk} = \frac{W_{sk}}{\mu_0 \mu_r S_k} \quad , \quad R_{gk} = \frac{W_k}{\mu_0 S_k} \quad , \qquad \mu_r \gg \mu_0 \tag{5.2}$$

g, τ, y, T_h, and T_w are the air gap length, pole pitch, yoke width, tooth height, and tooth width. μ_0 is the air permeability and μ_r is the core magnetic relative permeability. W_{sk}, S_k , and W_k are k_{th} segment width, segment length, and barrier width respectively.

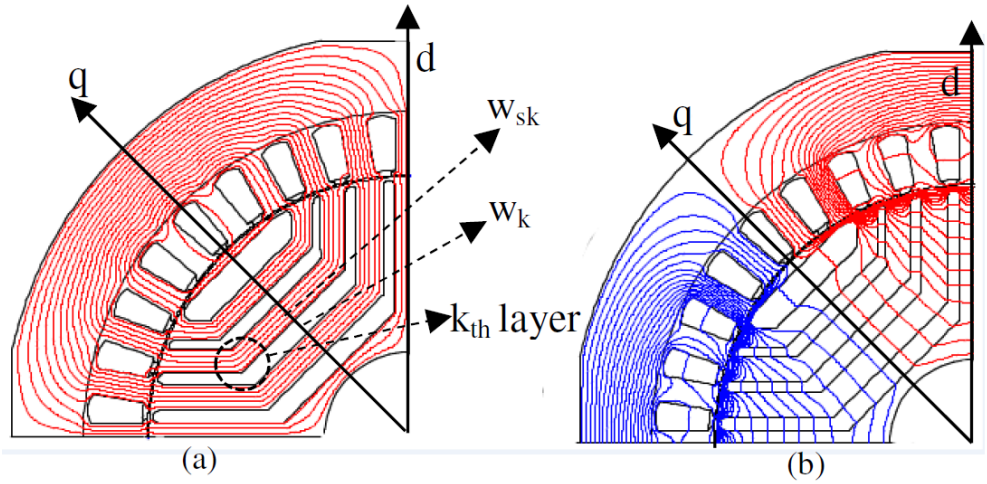

Figure 5.3. Typical d- axis (a) and q-axis (b) flux distributions.

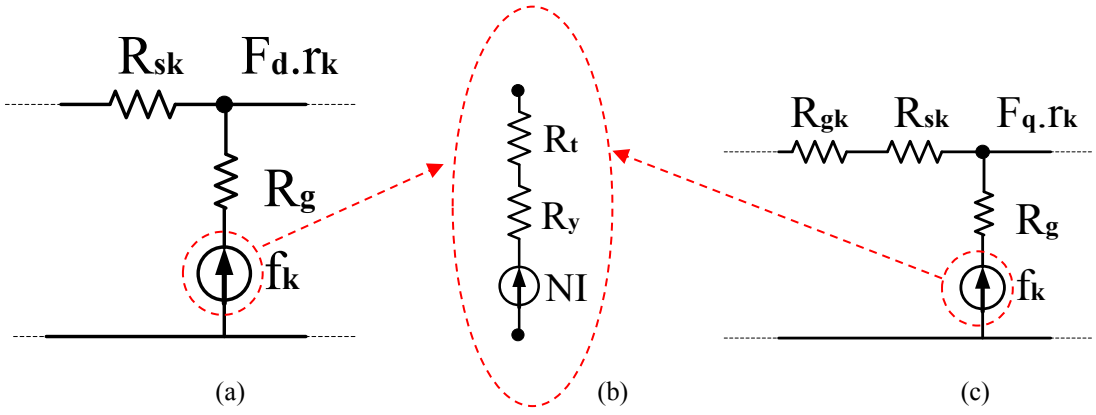

Figure 5.4. Rotor magnetic equivalent circuit of the K_{th} layer in d (a) and q (c) axis.

Referring to Figure 5.3a when a d-axis MMF is applied, no rotor reaction (r_k) is presented ($F_d.r_k = 0$) and magnetic motive force imposes a sinusoidal flux distribution to the rotor k_{th} segment through the air gap. Since $R_{sk} << R_g$ (Figure 5.4a), the flux density is highly sensitive to the air gap length. This is the reason why the SynRM is designed with small air gap for high performance applications such as traction. However, the rotor core magnetic characteristic affects R_{sk} and contributes to the machine's performance with d-axis excitation. On the other hand, to maximize the flux density in the d-axis, it is also required to minimize R_t and R_y (Figure 5.4b) that leads to use of higher quality material in the stator core. Furthermore, when a q-axis MMF is applied (Figure 5.4c), the flux density is dictated by the width of the barrier because $R_{gk} >> (R_{sk}, R_t, R_y,$ and $R_g)$. Hence, to reduce the q-axis flux as an important goal in SynRM design criteria, a proper insulation ratio is required.

5.4 Magnetic Performance Analysis of Proposed Machine

The performance of a 45kW, 4-pole, 4-layer TLA type rotor, and 300Nm SynRM has been analyzed while a maximum speed of 8000 rpm was desired. This machine has been designed to operate for traction and cooled by water-glycol coolant through the vehicle's cooling system. Previously, the geometry of the machine was identified, tested, and analyzed in [35, 51] to obtain the maximum possible saliency ratio and output torque. In this study the proposed machine with proper rotor geometry has been examined by FEA to identify its performance when different core types and sizes of the tangential and radial ribs were used. Table I shows the machine's specifications.

Table 5.1 Proposed Machine Specifications

Symbol	Parameter	Quantity
P_{mo}	Continuous output power	45kW
T_{em}	Peak torque at intermediate mode	300 Nm
T_{ep}	Peak torque at continuous mode	170 Nm
ω_b	Base speed	1800 rpm
ω_{max}	Maximum speed, mechanical limit	8000 rpm
P_o	Number of poles	4
N_s	Number of stator slots	48
I_{ph}	Rated current	120 A
V_o	DC-bus voltage	600 V

5.4.1 Effects of Core Type

The simulations have been carried out using current source operation and lumped parameters; due to the symmetrical nature of the rotor and stator geometries, the machine was operated for 45 degrees mechanical to realize its performance at different loads. As opposed to voltage source operation, this eliminates the effects of current harmonics on the output torque, results in a torque ripple caused by the non-uniformed air gap that is only dictated by the rotor geometry. The circuit diagram of the simulation is shown in Figure 5.5 in which I_1, I_2, and I_3 are the current source inverter supplies, R_1, R_2, and R_3 are the end winding resistors, L_1, L_2, and L_3 are the end winding inductances, B_1, B_2, and B_3 are the magnetizing coils including resistance and inductance.

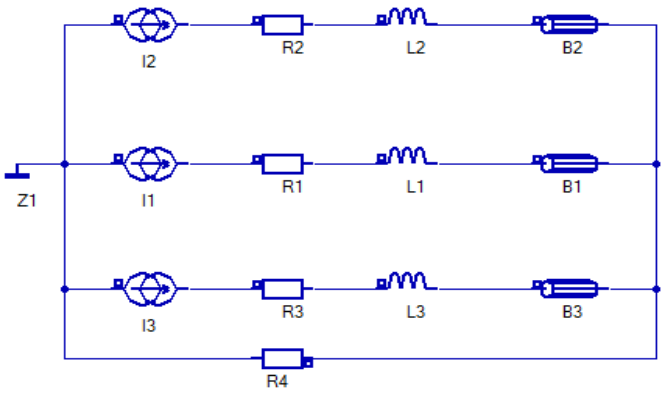

Figure 5.5. Circuit diagram of the current source simulation.

Figure 5.6 shows the characteristics of the saliency ratio versus rotor mechanical position for different loads of the proposed SynRM when rotor and stator core types are M13 and all rib widths are adjusted to 1mm.

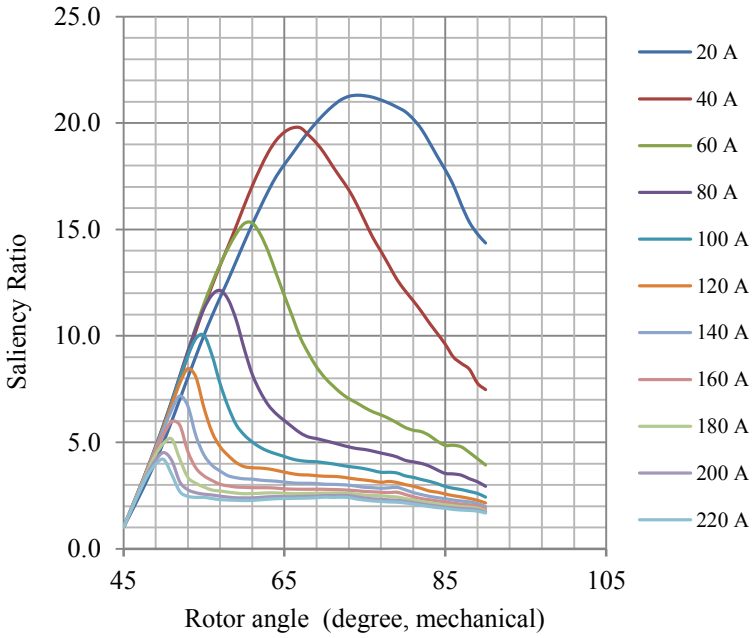

Figure 5.6. Saliency ratio versus rotor position in different loads.

As is illustrated, a proper saliency ratio can be achieved at rated current that refers to the continuous mode of operation. This yields maximum power at maximum speed in continuous mode which is compatible with vehicle highway driving scheme (cruising). Furthermore, to develop maximum torque at start-up (300 Nm); the phase current would be magnified to 220A for a short period of time (10-30 second) to accelerate high inertia in start-up. However the saliency ratio becomes poor due to the core saturation. FEA has been used to characterize the proposed machine performance in maximum torque operation (300 Nm) when different core types were considered. Rotor and stator geometrical parameters were kept the same for different alternatives (a, b, c, d, and e) except the stator and rotor core types. The machine operated under direct current control at 220A (current angle θ=68°) and all rib widths adjusted to 1mm as a reference. Figure 5.7 shows the simulation of the d-axis flux density and distribution in full load operation. Table 5.2 and Figure 5.8 show a performance comparison of the machines with different core characteristics.

Referring to machine (e), it should be pointed out that the CRGOs are silicon steel which have a special quality of grain surface. As discussed in 4.5, the grain's easy magnetization direction is aligned to the rolling direction. Therefore, this product features excellent magnetic properties in the rolling direction. Hence, cutting the rotor core laminations aligned with the rolling direction (machine-e) may be a technique to improve the SynRM's output torque that leads to higher torque density, lower losses, and smaller size. These features are attractive for today's automotive industry. However, torque ripple is maximized. As are illustrated in the Table 5.2 and Figure 5.8, a comparison between machine-a and c shows that, in spite of using a lower quality steel in the rotor core in machine-c compared to its stator (M45 versus M13), the average torque reduced only by 3.5% while the torque ripple improved and reduced by 31%.

This is due to lower magnetic reaction potential of the rotor using the steel with lower magnetic quality.

Table 5.2 Torque Characteristics of Different Core Types

		Alternatives of core types				
Unit	Core	a	b	c	d	e
	Stator	M13	M13	M13	M45	M13
	Rotor	M13	M19	M45	M45	M5
Nm	Average torque	302.7	299.2	292.2	288.6	316.4
%	Torque ripple	10.7	7.4	7.4	5.9	10.9
A	Phase current	220	220	220	220	220
Nm/A	Torque/Current	1.38	1.33	1.33	1.02	1.43

Whereas, by using steel M45 in the stator core in machine-d, the machine's performance has been degraded more than 5% compared to machine-a that results in an increase in phase current for maximum torque and may require a higher rated converter. As a major requirement, in order to enhance the performance of a SynRM for automotive applications, it is desirable to minimize torque ripple, which may cause undesirable effects, such as noise or undulated machining patterns. Although different solutions have been proposed to reduce torque ripple, several magnetic, mechanical, and electrical limitations still remain as obstacles to achieve a SynRM with minimized torque ripple. These results confirm that designing a SynRM with different core types in the rotor and stator suggests an improvement in torque ripple, although the converter rating limit needs to be met.

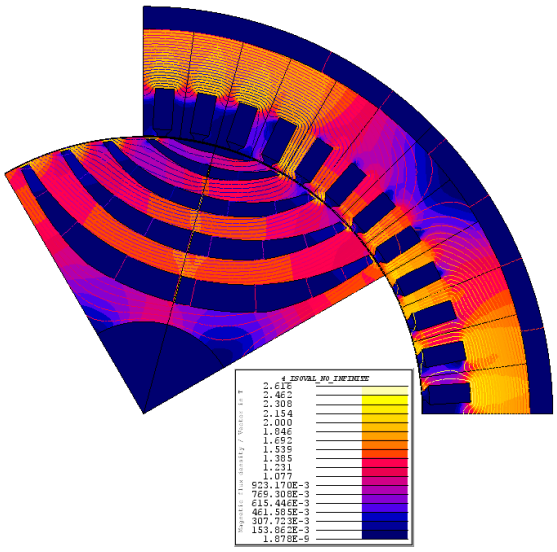

Figure 5.7. D-axis flux distribution at full load, θ = 68°.

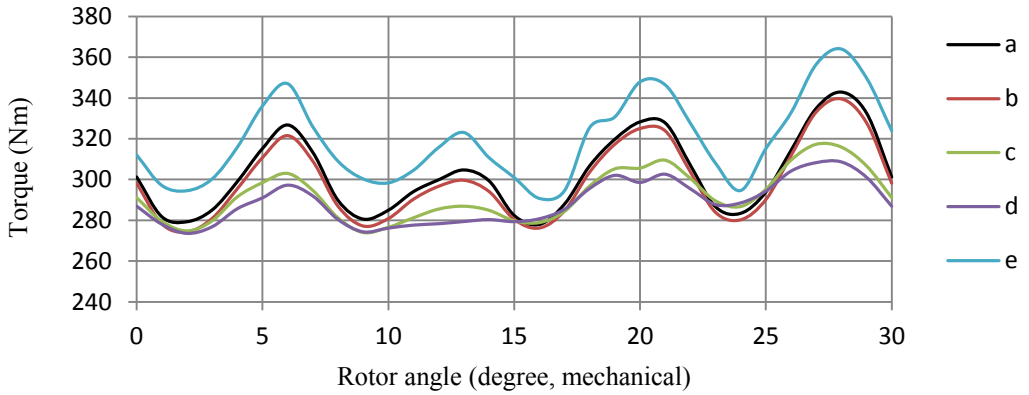

Figure 5.8. Torque- angle characteristics with different core types.

5.4.2 Effects of the Tangential and Radial Ribs

To analyze the effect of ribs on the machine performance, machine (a) from section 5.4.1 was selected as a reference. All the machine's electrical and geometrical parameters were kept the same in different alternatives (a, b, c, d, e, and f) except the width of "RR" and "TR". The

machine operated for 30 degrees mechanical under direct current control at 220A to develop the maximum torque. Figure 5.9 shows a general perspective representation of the rotor's single pole structure.

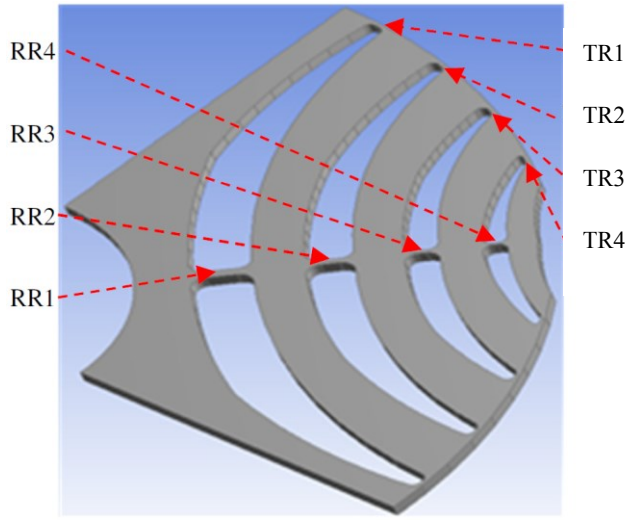

Figure 5.9. Single pole perspective of a 4-layer, 4-pole rotor lamination.

Table 5.3 and Figure 5.10 show a comparison of the machine's performance characteristics. As is illustrated, the average torque and torque/ampere of the SynRM depend on the width of tangential and radial ribs. They reach the minimum, (141.4Nm, 0.94Nm/A) when the rib widths are maximized (2mm). On the other hand, the torque characteristics correspond to the alternatives (c, e, and f) in Table 5.3 and Figure 5.10 confirm that the machine's magnetic performance is more sensitive to the width of tangential ribs than the radial ones (2.35). Furthermore, the FE results correspond to the machine (d) with second high average torque show that, a combination of various rib's widths may be a proper solution to improve the machine's performance when the mechanical integrity at high speed operation is required. Therefore, it is crucial to identify the proper dimensions of the ribs which can be validated through the mechanical analysis. This is the subject of the next section.

Table 5.3 Magnetic Performances of the Proposed SynRMs

		Alternatives					
Unit	Ribs	a	b	c	d	e	f
Rib Width (mm)	TR1	1.0	1.5	2.0	1.0	2.0	1.0
	TR2	1.0	1.5	2.0	1.0	2.0	1.0
	TR3	1.0	1.5	2.0	1.0	2.0	1.0
	TR4	1.0	1.5	2.0	1.0	2.0	1.0
	RR1	1.0	1.5	2.0	2.0	1.0	2.0
	RR2	1.0	1.5	2.0	1.5	1.0	2.0
	RR3	1.0	1.5	2.0	1.0	1.0	2.0
	RR4	1.0	1.5	2.0	0.5	1.0	2.0
Nm	Average torque	302.7	295.7	288.6	300.1	293.7	297.4
%	Torque ripple	10.7	11.2	10.4	11	11.4	10.9
A	Phase current	220	220	220	220	220	220
Nm/A	Torque/current	1.38	1.34	1.31	1.36	1.33	1.35

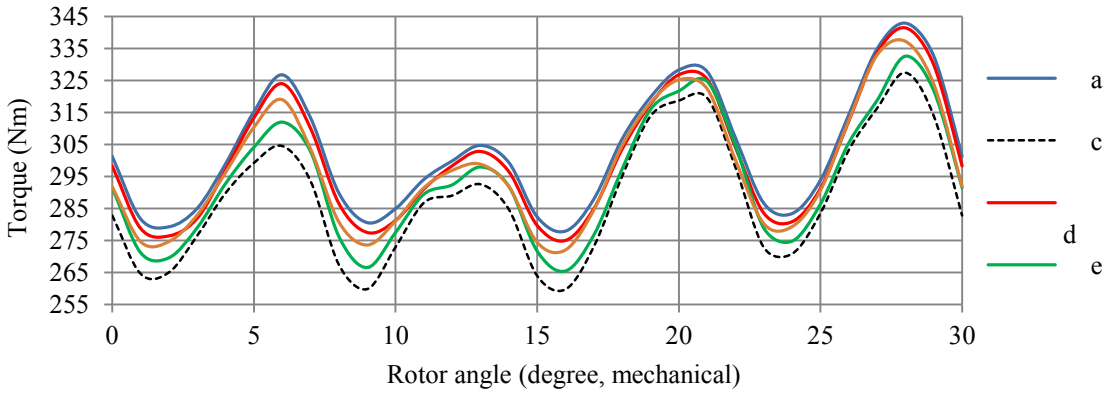

Figure 5.10. Torque- angle characteristics of the machines with different rib dimensions.

5.5 Mechanical Performance Analysis of Proposed Machine

Mechanical robustness of the rotor structure needs to be analyzed with regards to the effects of rotational forces that cause deformation in critical points such as tangential and radial ribs. These may occur at low and high speed in automotive applications. At low speed, the high current demand for maximum torque applies the magnetic force to the rotor while, at high speed

operations the rotational forces are dominant. Since the SynRM is regularly designed with small air gap, rotor structural deformation is a challenge. Hence, in this study the FEA is focused on two important characteristics that are recognized as “equivalent stress (Von-Misses stress)” and “deformation”.

Machine (a) and (d) from Table 5.3 show a better magnetic performances with regards to ribs widths. Amongst them, machine (d) has thicker RR1 and RR2. Thus, it is expected to exhibit a higher mechanical robustness in high speed operation. Hence, it is subject of the mechanical FEA in this section. The Von-Misses stress and deformation have been characterized for different speeds up to 8000rpm. Taking into account the total force, the magnetic forces applied to the flux carriers at 8000rpm which were calculated trough the magnetic FEA have been used as input force in mechanical FE calculations.

Table 5.4 and Figure 5.11 show the mechanical specifications of the core magnetic steel and the rotor total deformation at 8000 rpm respectively. As illustrated, the total deformation calculated by FEA is 0.228mm which is larger than the half of the machine’s air gap length (g = 0.5mm) as well as, its corresponding Von-Misses stress is 2500MPa which is much higher than the secure value rate.

Table 5.4 Mechanical Specifications of the Magnetic Steel (M250-35A)

Symbol	Parameter	Quantity	Unit
σ_y	Yield stress	465	MPa
σ_T	Tensile stress	575	MPa
E	Elasticity	$2.1e^{11}$	Pa
ν	Poisson’s ratio	0.29	---

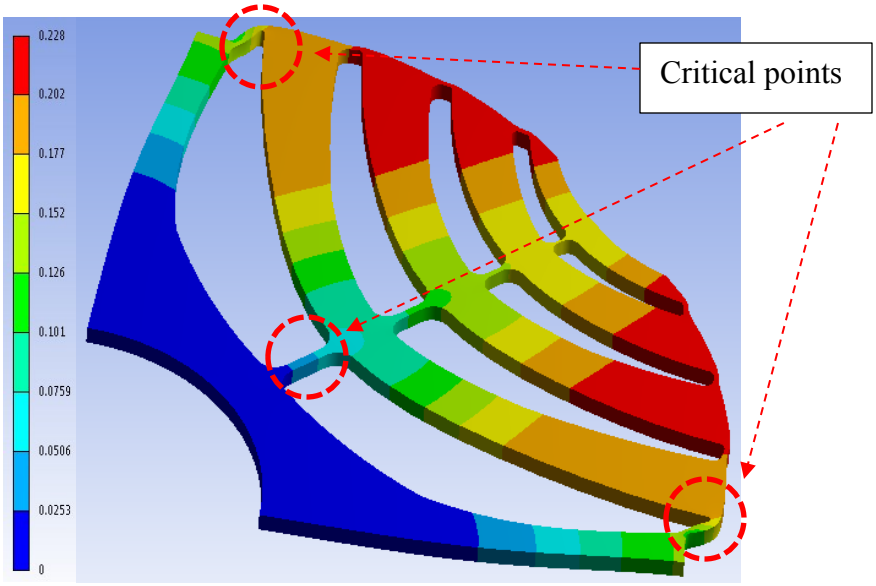

Figure 5.11. Rotor deformation of the machine (d) at 8000rpm.

Since the maximum stresses of the critical points at 8000rpm are exceeded beyond the yield and tensile stress, this causes deformation in plastic mode, resulting in a failure in the rotor structure. Therefore, the widths of the tangential and radial ribs of the proposed machine (Figure 5.9) need to be modified.

5.5.1 Rotor Geometry Modifications

Two different alternatives of the rotor structure, machine (d_1) and (d_2) are defined and examined in which the tangential and radial ribs widths are modified. The modifications are mostly focused on the critical point such as RR1, RR2, and TR1s as are shown in Figure 5.9 and Figure 5.11 and the results are summarized in Table 5.5. As is illustrated, in spite of having considerable change of the ribs widths in machine (d_1), the von-Misses stress and deformation are still at critical levels. Furthermore, as has been mentioned in section 5.4.2, the output torque and torque ripple are also degraded by -4.5% and +3% respectively.

Table 5.5 Comparison of the Machines Performance

		Alternatives		
Unit	Ribs	d	d1	d2
Rib Width (mm)	TR1	1.0	3.0	4.0
	TR2	1.0	1.5	2.0
	TR3	1.0	1.0	1.0
	TR4	1.0	1.0	1.0
	RR1	2.0	3.0	4.0
	RR2	1.5	1.5	3.0
	RR3	1.0	1.0	2.0
	RR4	0.5	1.0	1.0
Nm	Average torque	300.1	290	279.9
%	Torque ripple	11	14	15.7
A	Phase current	220	220	220
Nm/A	Torque/current	1.36	1.32	1.27
MPa	Von-Misses stress	2500	900	377
mm	Total deformation	0.28	0.126	0.072

The mechanical robustness of the new rotor in the machine (d2), Table 5.5, was examined by FEA up to 8000rpm. Figure 5.12 shows considerable reduction of the maximum stress at critical points (377MPa) that would be applied to the rotor within the elastic boundary. Moreover, the maximum deformation characterized in Figure 5.13 shows 72μ displacement of the rotor body in the air gap area that can be tolerable compared to the 500μ air gap length. In this machine the output torque and torque ripple are also degraded by -7% and +4.7% respectively.

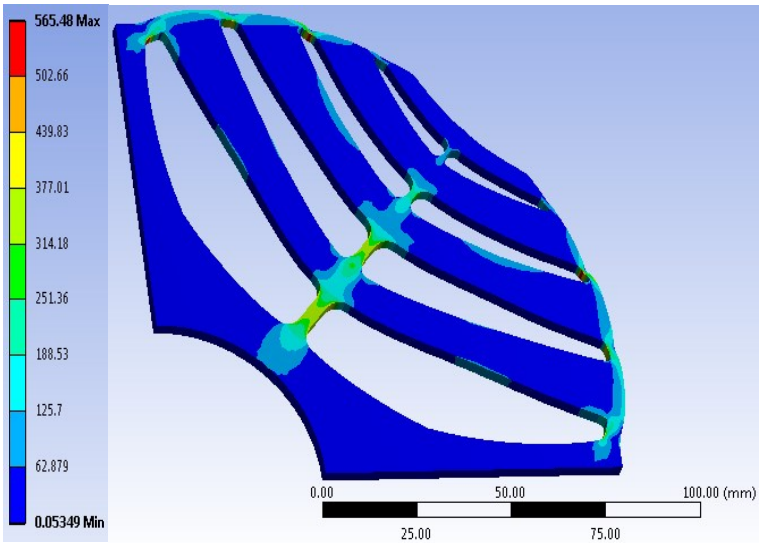

Figure 5.12. Von-Misses stress of machine (d2) at 8000rpm.

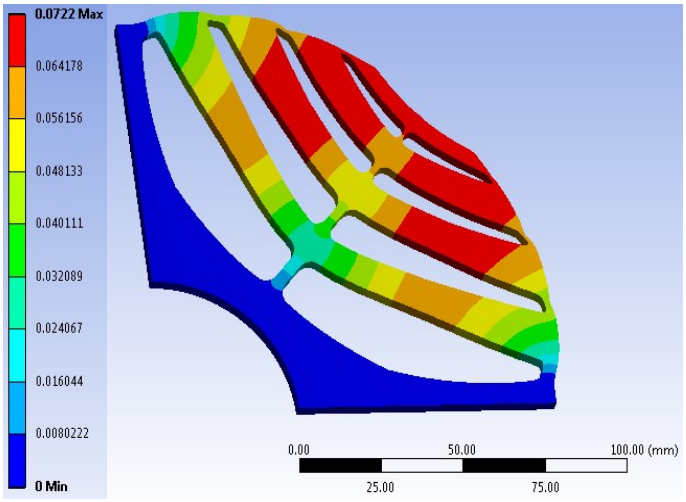

Figure 5.13. Rotor deformation of machine (d2) at 8000rpm.

An increase in the width of the targeted ribs are limited due to the fact that, this amplifies the q-axis flux and reduces the saliency ratio, as a result, it degrades the machine output torque (2.35) and torque ripple. This implies a higher phase current and converter rating when the maximum torque of 300Nm is desired.

5.5.2 Secure Operating Speed

Figure 5.12 shows the maximum stress of 377MPa at 8000rpm is localized at RR1 and RR2 that is close to the core yield stress in Table 5.4. Taking into account the total force that are applied to the rotor structure (rotational, magnetic), the machine safe operation speed may not be guaranteed at 8000rpm. The maximum secure speed of the rotor can be approximated by defining a safety factor as in (5.3) [58].

$$\omega_{op} = \omega_{FE}\sqrt{\frac{\sigma_y}{K\sigma_{FE}}} \tag{5.3}$$

Where; ω_{FE} is the calculated speed by FEA, σ_y is yield stress, σ_{FE} is the maximum stress calculated by FEA, and K is the safety factor. Using (5.3), Table 5.4, and safety factor of 1.5 yield the machine maximum secure operation speed ω_{op} (ω_{op}= 7254rpm).

In order to evaluate the performance of the proposed machine using the modified rotor (Table 5.5 and Figure 5.12), the output functions such as maximum torque and torque ripple that are characterized by FEA are compared to the machine (d) that is previously designed (Table 5.5 and Figure 5.11). The results are presented in Figure 5.14.

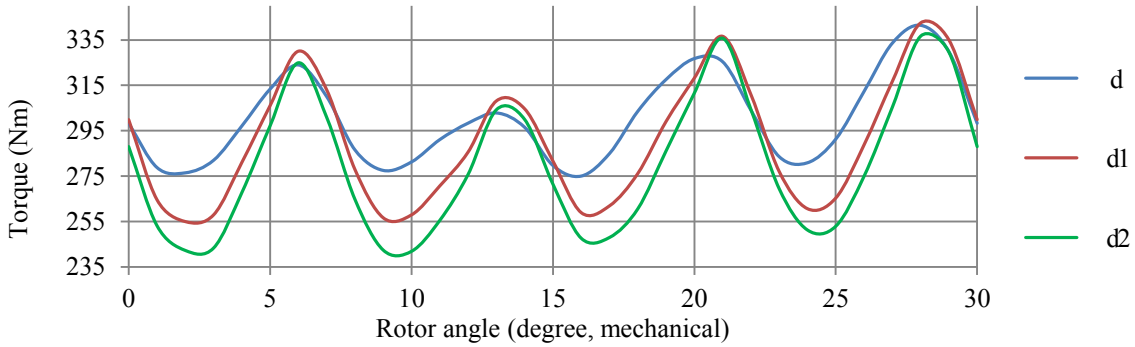

Figure 5.14. Torque- angle characteristics of the machines (d), (d1), and (d2).

Figure 5.14 shows a reduction of 7% in average torque and an increase of 4.7% in torque ripple when the modified rotor in machine (d2) is used. This confirms that; although the modification in rotor structure can improve its mechanical robustness, it degrades the machine magnetic performance. Since in automotive applications the cooling system controls the machine's thermal reaction properly, the reduction of the output torque may be compensated by phase current if the converter rating is met. On the other hand, the results show that; in order to reduce the mechanical robustness issues in high speed operation, it is necessary to design the SynRM with longer stack length and smaller rotor outer diameter if the length in powertrain's architecture is not a constrain.

According to the results, Magnetic and mechanical FEA confirmed that using different magnetic steel types in rotor and stator core leads to better performance. Moreover, the dimensions of the ribs would not be necessarily identical. A combination of various ribs widths may be a proper solution to improve the machine's performance when the mechanical integrity at high speed operation is also desired. Corresponding to the geometrical nature of this study, the results can be generalized to different designs with different rating and size when the machine is equipped with TLA rotor.

5.6 Effects of the Number of Poles

Design of a high performance SynRM is aimed at maximizing the saliency ratio (L_d/L_q). Thus, minimization of the q-axis inductance (L_q) is one way to achieve a higher saliency ratio when the same d-axis inductance (L_d) is maintained. The performance characteristics of the SynRM are affected by the number of poles. It is due to the fact that the saliency ratio and electromagnetic torque depend on this number. As is shown in Figure 2.7b, the q-axis flux is composed of circulating flux across the segments ends and the stator teeth (φ_{qc}) as well as the

flux that is flowing through the segments and barriers (φ_{qf}). These fluxes lead to their corresponding inductances (L_{qc}) and (L_{qf}) respectively. Equations (2.9), (2.27), (2.28), and (2.29) express the above-mentioned parameters relations.

In (2.29), a lower pole number refers to a lower value of L_{qf}. Consequently, it reduces L_{qm} in (2.27) which means a higher saliency ratio can be achieved with a lower number of poles. In theory the lowest number of pole (2-pole) is desirable for design, but this degrades either the average torque as it is shown in (2.9) or torque quality due to higher torque ripple that magnifies the phase current for the same output torque. This is a major challenge with regards to the thermal and converter rating limits in traction motor design. Furthermore, a larger pole pitch when the number of poles reduces causes additional manufacturing, magnetic, and thermal issues due to the longer end winding in the stator coils. Hence, in a practical high performance SynRM the pole numbers higher than 2 is preferable. On the other hand, multi-layer structure of the TLA rotor type limits the pole number when the rotor outer diameter is small. For that reason a pole number higher than 6 is not practically feasible when the pole pitch is short in a compact electric machine. In this study the proposed machines are designed based on two alternatives (4-pole, 6-pole). A comparison between two machines will be performed with respect to the design requirements such as maximum torque, torque ripple, size, converter rating, and maximum mechanical speed limit that lead to identify better design.

5.6.1 Comparison of the Magnetic Performance

The study presented hereafter refers to a 45hp SynRM equipped with 4-layer TLA type rotor that needs to develop the maximum torque of 150Nm at low speed. Two different alternatives including 4-pole and 6-pole machines are taken into consideration while a maximum speed of 9000rpm is desired. These machines have been designed to operate as traction and cooled by

water-glycol coolant through the vehicle's cooling system. Let's suppose the cooling system is capable of cooling the machines properly. The geometry of the machines have been identified using a sizing methodology [51] in order to meet the design limitations with regards to proper stack length for both machines and modified to obtain maximum possible saliency ratio and output torque using rotor high performance design scheme [25, 47, 50, 59]. Since, this study is focused on the effects of the number of poles on the performance of the SynRM, the geometry design criteria are not discussed in detail. Table 5.6 summarizes the main design specifications of the 4-pole (M4P) and 6-pole (M6P) machines.

Table 5.6 Design Specifications of the Proposed Machines

		Alternatives	
Parameter	Unit	M4P	M6P
Number of poles	-	4	6
Continuous output power	hp	45	45
Peak torque	Nm	150	150
Maximum speed	rpm	9000	9000
Number of stator slots	-	36	36
Air gap	mm	0.4	0.4
Stack length	mm	150	150
Insulation ratio	-	0.65	0.65
Rotor outer diameter	mm	150	160
Stator outer diameter	mm	231	240
Stack volume	dm^3	4.2	4.5
DC-bus voltage	V	400	400
Converter rating	A	350	350
Base speed	rpm	2400	2400

5.6.1.1 Effects on the Maximum Torque

The finite element analysis has been performed using current source operation; the M4P and M6P have been operated for 45 and 30 degrees mechanical respectively to realize their performances for maximum torque operation. As it has been previously mentioned, this eliminates the effects of the current harmonics on the output torque, results in a torque ripple caused by the no uniformed air gap that is only dictated by the rotor geometry. The circuit diagram of the FEA is shown in Figure 5.5.

As is illustrated in Table 5.6, the stack volume of the M6P is 7% larger than M4P ($4.5dm^3$ compared to $4.2dm^3$) while both machines are designed for the same power and torque rating. An increase in the number of poles reduces the saliency ratio, results in a slight larger machine for developing the same torque. This has been discussed previously in 5.6 and has been confirmed by (2.27), (2.28), and (2.29) as well. To compare the effects of the number of poles on the machines performance, the M6P has been selected as the reference machine and designed with insulation ratio of 0.65. A combination of various rib widths has been selected for M6P to improve the machine's performance for proper mechanical integrity at the desired maximum speed (9000 rpm) that is shown in Figure 5.15.

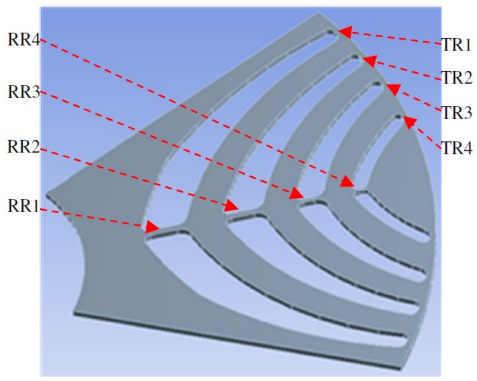

Figure 5.15. General perspective of the single pole, 4-layer, 6-pole rotor structure.

The same insulation ratio and ribs configurations have been applied to the M4P. Therefore, all the machines geometrical parameters have been kept the same for two alternatives except the number of poles. FEA has been carried out at full load operation. Figure 5.16 presents the flux distributions of the 6-pole (a) and 4-pole (b) and Table 5.7 shows comparison between the machines performance characteristics. As is illustrated, compared to the M6P, the maximum torque and torque per ampere of the M4P degrade considerably. This means the 4-pole machine needs much higher current (360.2 A compared to 244.2 A) to develop the same peak torque at full load operation. This can be also confirmed by its lower torque production capability (0.72 Nm/A compared to 1.07 Nm/A), although, the results could have been predicted through (2.9).

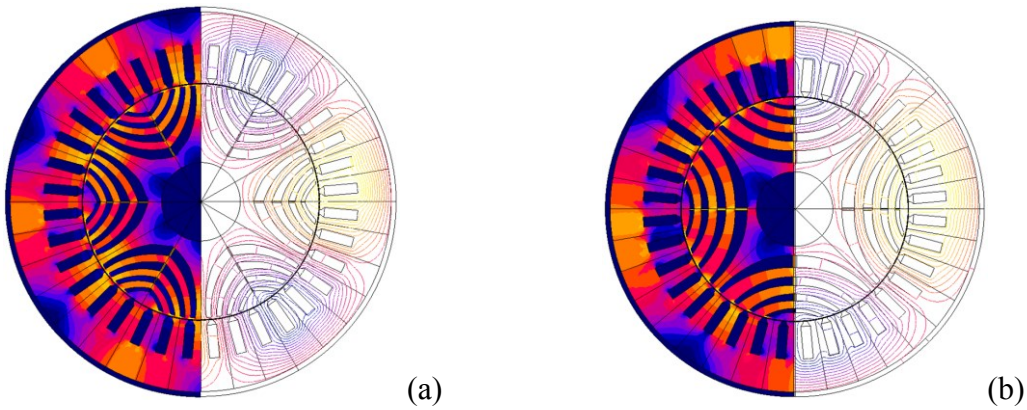

Figure 5.16. Flux distributions of the 6-pole (a) and 4-pole (b) machines at full load.

Table 5.7 Magnetic Performances of the 4-pole and 6-pole SynRM by FEA.

		Alternatives	
Unit	Ribs	M6P	M4P
Rib width (mm)	TR1	2.0	2.0
	TR2	1.5	1.5
	TR3	1.0	1.0
	TR4	1.0	1.0
	RR1	2.0	2.0
	RR2	1.5	1.5
	RR3	1.0	1.0
	RR4	1.0	1.0
Nm	Average torque	150.4	150.2
%	Torque ripple	7.5	11.1
A	Phase current	141.0	208.0
A	Current	244.2	360.2
Nm/A	Torque/current	1.07	0.72

The importance of these results may be highlighted in automotive applications where, the converter rating is considered as the design limitation. As are illustrated in Table 5.6 and Table 5.7, the current demand at peak torque exceeded beyond the converter rating in 4-pole machine. This implies an increase in the converter switches ratings. Furthermore, higher current demands for peak torque in M4P leads to an additional thermal issue that causes an increase in cooling system capacity and an extra cost in the entire drive system.

5.6.1.2 Effects on the Torque Ripple

Torque ripple causes mechanical vibration, acoustic noise, and additional iron losses. If torque harmonics of different rotor slot barriers in the air gap eliminate each other, the torque harmonics amplitudes are directly proportional to the flux harmonics when a pure sinusoidal current is applied to the stator winding.

In SynRM, the d-q axis inductances depend on the rotor position (δ). Hence, an additional term is added to the torque equation that represents torque pulsations. However, the average

value of this term is zero. Taking into account the dependency of inductances to rotor position, (2.35) can be rearranged as (5.4) below [36];

$$T_e(\delta) = (9Pq/4\pi)\, Sin(\pi/3q)\, (\, (L_d - L_q) i_d i_q + (\Delta L_d + \Delta L_q) i_d i_q$$

$$.Cos(3Pq\delta) - \Delta L_{dq}(i_d^2 - i_q^2) Sin(3Pq\delta)) \qquad (5.4)$$

Equation (5.4) shows that the torque ripple has two components; the first component is proportional to the average torque ($i_d i_q$) caused by oscillation of no uniformed air gap and circulating flux component (L_{cq}). These two oscillations create considerable variations of d-q inductances (ΔL_d, ΔL_q) respectively. However, they can be eliminated by distributed anisotropic structure of the TLA rotor. The second component is due to the stator slots effects which can introduce variations of d-q axis mutual inductance (ΔL_{dq}) and produces the total torque ripple. As is illustrated in (5.4), it depends on the number of poles (P) in Pq and Sin terms where, q is the number of stator slots per phase per pole. This has been already discussed in Chapter 4 in details.

Figure 5.17 and Table 5.7 show the torque-angle characteristics and magnetic performances of two machines respectively that are characterized by FEA. As is illustrated, a significant reduction in torque ripple (-68%) in M6P compared to the 4-pole machine is obtained. This improves the machine's performance when it is operated as traction.

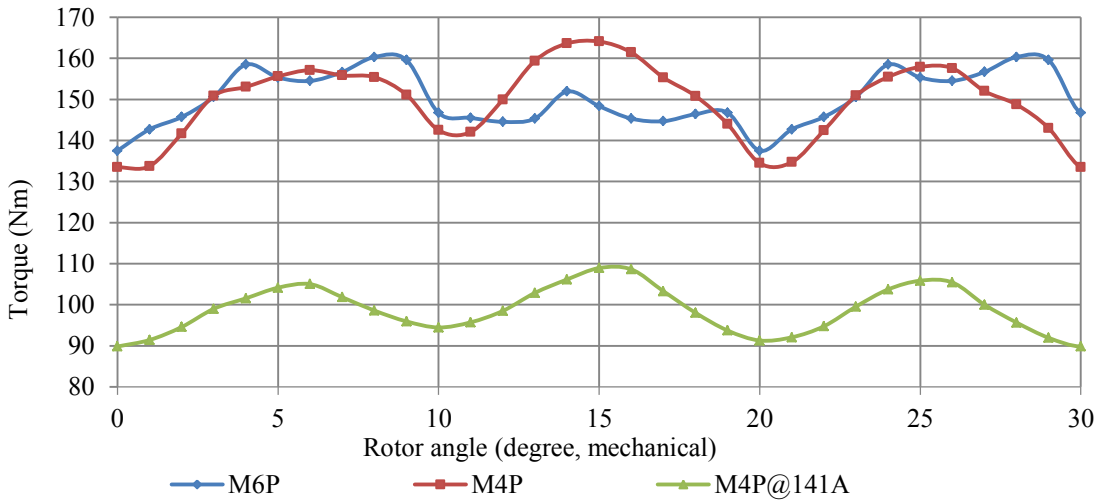

Figure 5.17. Torque- angle characteristics of the machines with different pole numbers.

5.6.1.3 Effects on the Core Losses

High performance of electric machines in high speed operations is desired for automotive applications. Since, the core losses are proportional to the supply frequency, the possibility of having a lower supply frequency in the machine with a lower pole number is a potential for having lower core losses compared to a higher pole machine at the same shaft speed. This may change the design strategy for traction motors. Hence, the M4P is expected to operate more efficiently than the M6P with respect to the core losses at high speed. However, higher current demand at the same torque causes higher copper losses in M4P and degrades the efficiency. The total core losses have been estimated by FEA using Bertotti model and the core lamination specifications in Table 5.8 that includes hysteresis, Eddy, and excess losses. Figure 5.18 shows the total core losses versus rotor speed of the design alternatives. As is illustrated, this confirms that a lower core losses of the M4P compared to the M6P at high speed operation can be achieved.

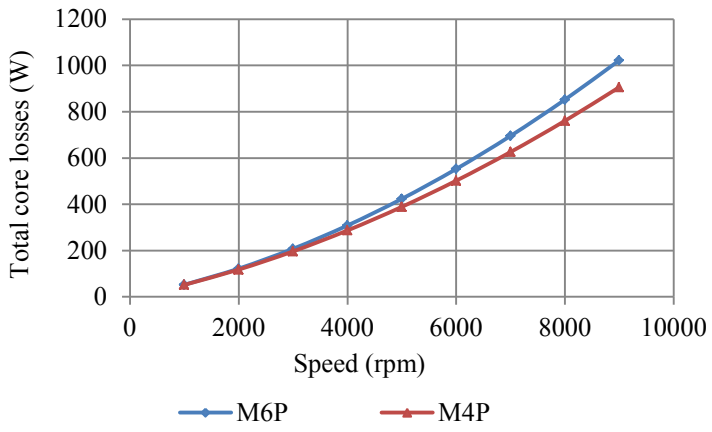

Figure 5.18. Total core losses of the machines at different speeds.

Table 5.8 Specifications of the Core Magnetic Steel (M250-35A)

Symbol	Parameter	Quantity	Unit
σ_y	Yield stress	465	MPa
σ_T	Tensile stress	575	MPa
E	Elasticity	$2.1e^{11}$	MPa
ν	Poisson's ratio	0.29	---
---	Hysthersis coefficient	104	$WS/T^2/m^3$
---	Electrical conductivity	1.96e+6	S/m
---	Excess losses coefficient	0.891	$W/(T/S)^{1.5}/m^3$
---	Thickness	3.5e-4	m

5.6.2 Comparison of the Mechanical Performance

Mechanical robustness of the rotor structure is analyzed with regards to the effects of the rotational forces that cause deformation in tangential and radial ribs and may occur at high and low speed. At low speed, high current demand for maximum torque applies the magnetic force to the rotor and at high speed, the rotational forces are dominant. Since, the SynRM is regularly designed with small air gap, the rotor structural deformation is an important challenge.

Two different alternatives of the rotor structure, M6P and M4P, are examined in which the tangential and radial ribs widths are kept the same (Table 5.7). Since, M6P is considered as the reference machine, its geometry has been modified for proper structural integrity and robustness at desired maximum speed (9000rpm). Figure 5.19 and Figure 5.20 show the mechanical performances of the M6P at 9000rpm which characterized by FEA. Table 5.8 summarizes the mechanical specifications of the core steel that leads to identify the rotor maximum secure speed.

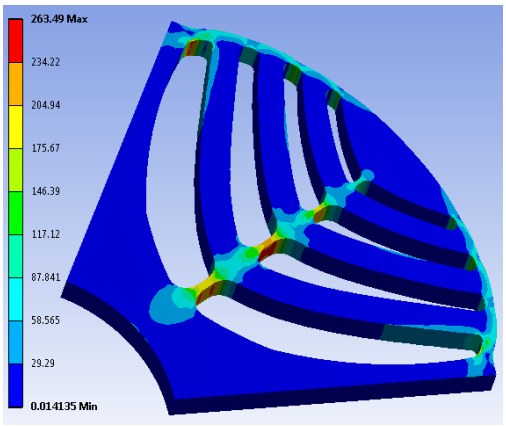

Figure 5.19. Von-Misses stress of the 6-Pole machine at 9000rpm.

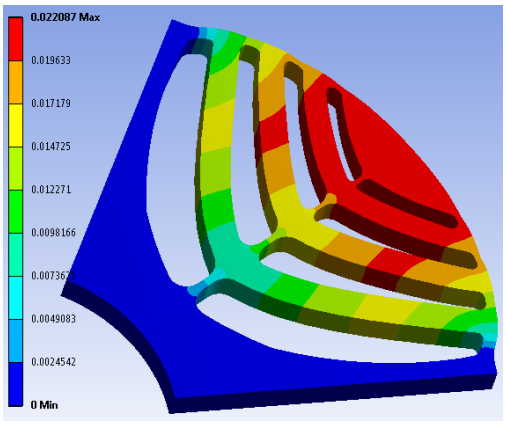

Figure 5.20. Rotor deformation of the 6-Pole machine at 9000rpm.

As is illustrated in Figure 5.19, the maximum stress of 263.5 MPa at 9000rpm is localized at the RR1s. Taking into consideration the total force that are applied to the rotor structure (rotational, magnetic), The rotor maximum secure operating speed (ω_{op}) can be approximated by defining a safety factor in (5.3) [58].

Using (5.3), Table 5.8, and safety factor of 1.5 yield the machine's maximum secure speed ω_{op} (ω_{op}= 9761.9rpm) that satisfies the desired maximum speed (9000rpm). Figure 5.20 shows 22 µ displacement of the rotor structure at TR1s through the air gap area that can be tolerable compared to the 400µ air gap. This confirms that, the maximum deformation in the rotor structure is not a concern for both machines at maximum desired speed. Figure 5.21 describes the mechanical performance of the M4P with regards to the rotor structural integrity at 9000rpm where, the maximum stress of 329 MPa is localized at critical points (RR1s). Using the same approach as M6P and (5.3) lead to the maximum secure operating speed of the machine that is ω_{op}= 8735.3rpm. This shows that, although the maximum stress at desired speed is below the rotor core material's yield stress (329 MPa compared to 465 MPa), it cannot guarantee the rotor structural robustness at the desired secure operation speed (9000rpm).

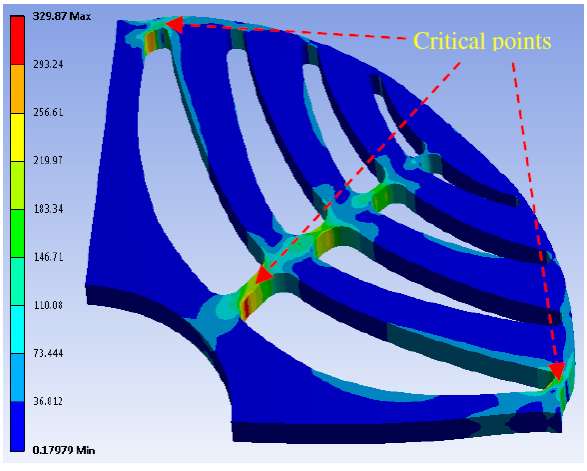

Figure 5.21. Von-Misses stress of the 4-Pole machine at 9000rpm.

To reduce the maximum stress in the critical areas, the width of RR1 has been modified by an increase of 1 mm. As previously mentioned, an increase in the width of the targeted ribs are limited due to the fact that, this amplifies the q-axis flux and reduces the saliency ratio, as a result degrading the machine's output torque. Table 5.9 and Figure 5.22 show the performances and torque-angle characteristics of the M4P and its modified version respectively.

Table 5.9 Magnetic Performances of the 4-Pole SynRM's by FEA

		Alternatives	
Unit	Ribs*	M4P	M4P(modified)
Rib width (mm)	TR1	2.0	2.0
	TR2	1.5	1.5
	TR3	1.0	1.0
	TR4	1.0	1.0
	RR1	2.0	3.0
	RR2	1.5	1.5
	RR3	1.0	1.0
	RR4	1.0	1.0
Nm	Average torque	150.4	145.9
%	Torque ripple	11.1	7.4
A	Phase current	208.0	208.0
A	Line current	360.2	360.2
Nm/A	Torque/current	0.72	0.70

* TR: Tangential Rib, RR: Radial Rib

These above-mentioned results show that the modification of the rotor structure at RR1could improve the rotor mechanical robustness and torque ripple. However, it degrades the machine output torque. Since, in automotive applications the cooling system is expected to control the machine's thermal performance, the reduction of the output torque may be compensated by an increase in the phase current if the converter rating is met.

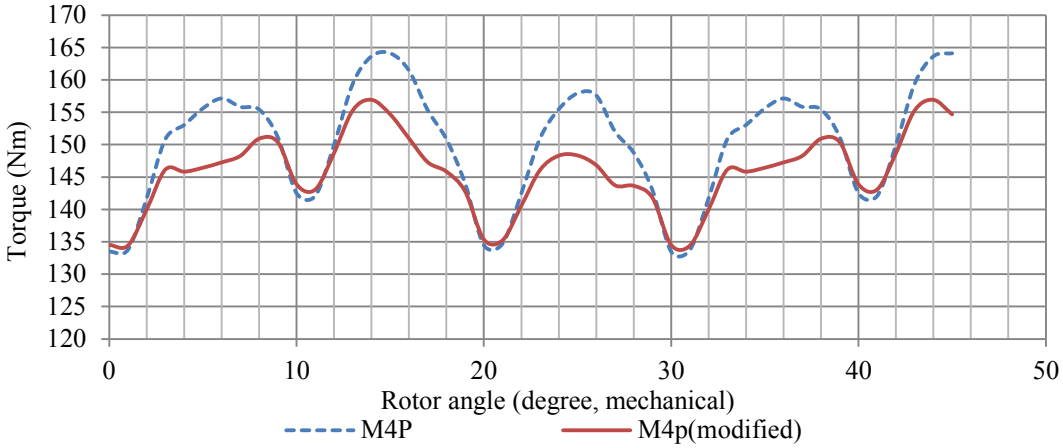

Figure 5.22. Torque- angle characteristics of the M4Ps.

In general the computer aided examinations confirmed that a higher number of poles in the rotor and stator core structures lead to better performance; this exhibits a higher T/A ratio, lower torque ripple, capability of developing desired peak torque at lower current that implies a lower converter rating and temperature rise at full load, and a higher mechanical robustness of the rotor structure in high speed operations that are all desired for automotive applications. However, increase in pole numbers in SynRM is limited due to mechanical and manufacturing issues in rotor structure.

5.7 Effects of the Number of Turns

Low speed range reduces the constant power capability of the SynRM beyond the base speed. This drawback is harmful when the machine is proposed to run as powertrain in automotive applications. In general, differing from the industrial applications, traction motors used in electric and hybrid electric vehicles usually require a wide flux weakening range within which the desired performance characteristic of the powertrain is to deliver a constant output power over the full extended speed range from base to maximum speed [1, 4, 8]. The SynRM may present enough flux weakening capability in industrial applications [48], where the electric

machines mostly operate at low or medium speed, but at high speed as traction, this machine cannot extend the speed in a constant power operations [60]. There have been intensive efforts to improve the performance of the SynRM over the past decade using magnet assisted topology. However, lower flux weakening range compared to IM, PMSM, and switch reluctance (SRM) has been remained as a major obstacle of SynRM for being properly adopted in automotive applications. This section presents a new design methodology for SynRM using variable ampere-turns (VAT-SynRM) concept to extend the machine's speed range when a mechanically robust rotor is used as well. This novel method is compatible with the conventional flux weakening methods in which the maximum torque per ampere (MTPA) or flux weakening control (FWC) techniques can also be applied. Hence, this significantly improves the speed range in high speed applications such as automotive.

5.7.1 Variable Ampere-Turns Method Criteria

Design limitations of the traction motors such as torque envelope, size, and converter rating contribute to the machine specifications strongly. Desired torque envelope for traction applications requires high torque at low speed characteristic for vehicle start-up as well as medium torque and high power at high speed for cruising or highway driving capability [51]. At low speed, high torque demand requires high current which is limited by converter rating. The electromagnetic torque of SynRM can be expressed as (5.5).

$$T_e = 1.5P\lambda_m i_m \tag{5.5}$$

Where, T_e is the electromagnetic torque, P is the number of pole pairs, λ_m in the air gap flux linkage, and i_m is the magnetizing current.

In one hand, achieving the maximum torque at low speed with taking into consideration the current limitation caused by converter rating leads to high air gap flux linkage (λ_m) which needs to be created by high number of turns. Therefore, compared to PMSM and IM, with the absence of any source of excitation in the rotor structure such as permanent magnet or cage, SynRM is normally designed with higher number of turns per slot. On the other hand, at high speed, extra ampere-turns reduce the base speed, degrade the flux weakening capability, and decrease the speed range. Equation (5.6) expresses the speed dependency of the air gap magnetic motive force in steady state and Figure 5.23 show the single phase equivalent circuit of the SynRM as follows;

$$E_m = \omega \lambda_m \tag{5.6}$$

E_m is the air gap magnetic motive force (MMF) and ω is the shaft electrical speed.

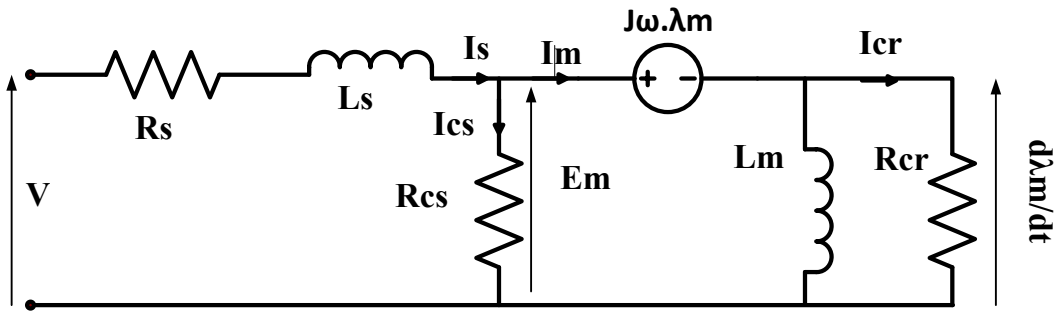

Figure 5.23. Single phase equivalent circuit of the SynRM.

As is illustrated, a large magnetic motive force (MMF) can limit the magnetizing current significantly. This reduces the maximum speed and speed range within which FWC or MTPA may be applied for a constant power operation. Therefore, conventional flux weakening method

based on d-q axis current regulation is not an adequate approach to obtain extended constant power operation. Equation (5.7) shows; the magnitude of E_m depends on parameters i.e., number of turns per slot (n_s), frequency (f), air gap length (g), magnetic loading (B_{1gm}), stack length (L) [40]. Thus, a variable n_s is another possibility for regulating the magnetizing current and the air gap flux linkage in the flux weakening. By reducing N_s at maximum speed, either air gap flux linkage or MMF will be decreased. As a result, the phase current is maintained around the rated, and a wider band for flux weakening may be obtained.

$$|E_m| = \sqrt{2}\, n_s q \pi L g f B_{1gm} \tag{5.7}$$

In practical, discrete step down and step up variation of n_s is feasible. This may be applied to the stator winding in one or more steps. Δn_s for achieving the desired speed range are limited by the rated current, voltage, and no load air gap flux linkage.

Figure 5.24 and Table 5.10 show a general configuration of the variable ampere-turns winding for delta connection and switching sequences of the proposed method respectively. As is illustrated, only one switch per phase per step is required. The switches operate at ON or OFF condition which are controlled by the speed signal receiving from the drive's controller. At the first glance, an additional switch per phase implies more switching loss, but possibility of having lower number of turns per slot in flux weakening for high speed operation results in a lower stator resistance which in turns reduces cupper losses and improves the efficiency. Online change of the winding scheme from full turns to other steps causes significant reduction in MMF, results in a high transient current at the same torque. Therefore, FWC is necessary during each change to limit the current prior to the MTPA.

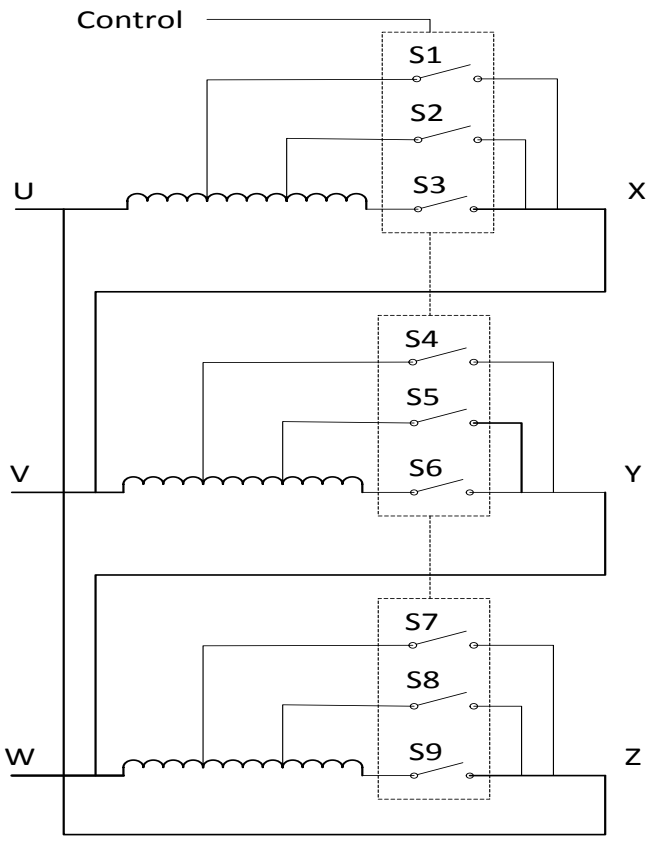

Figure 5.24. Delta connections of the variable ampere-turns windings.

Table 5.10 Switching Sequences for the Variable Ampere-turns Method

Switches	Steps		
	1	**2**	**3**
S1	0	0	1
S2	0	1	0
S3	1	0	0
S4	0	0	1
S5	0	1	0
S6	1	0	0
S7	0	0	1
S8	0	1	0
S9	1	0	0

5.7.2 Computer Aided Analysis and Results

Finite element analysis has been carried out using voltage source mode of operation and lumped parameters. Due to the symmetrical nature of the rotor and stator geometries, the machine operated for 45 degrees mechanical for each speed to verify output function such as average toque and power for different winding connections. As opposed to current source operation, this method takes in to consideration the effects of the rotor speed on the machine's output torque, torque ripple, and output power. The torque quality with respect to the torque ripple is affected by both no uniformed air gap and low order MMF space harmonic that is dictated by the rotor geometry and the stator current. The circuit diagram of the simulation is shown in Figure 5.25 in which V_1, V_2, and V_3 are the voltage source inverter supplies, R_1, R_2, and R_3 are the end winding resistors, L_1, L_2, and L_3 are the end winding inductances, B_1, B_2, and B_3 are the magnetizing coils including resistance and inductance. The geometry of the reference machine has been coded in the software. The software is modified to obtain full control of the rotor and stator geometries. All parameters are kept the same for different alternatives except the number of turns per slot.

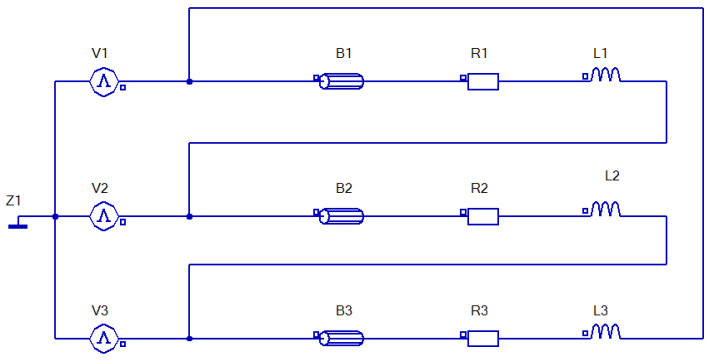

Figure 5.25. The circuit diagram of the voltage source supply simulation.

5.7.2.1 Performance of the Reference SynRM

To evaluate the method, a 7.5hp SynRM with a stator including 36 slots and a rotor with 4 internal flux barriers has been designed and selected as the reference. Table 5.11 shows the reference machine's specifications.

Table 5.11 Reference Machine Specifications

Parameters	Quantity
Rated power	7.5hp
Peak torque at low speed (transient)	60 Nm
Peak torque at max. speed (continuous)	35 Nm
Rated voltage	230 Δ
Air gap	0.4 mm
Magnetic load	0.8 T
Stator outer diameter (frame IEC132)	208 mm
Rotor outer diameter	134 mm
Stack length	200 mm
Number of pole	4
Number of stator slots	36
Number of turns per slot	25
Number of rotor internal layers	4
Rated current	20 A
Stator slot opening	3 mm
Shaft diameter	43 mm
Winding type	distributed
Skew	no
Coil pitch	full
Core steel type	M19
Max. speed	1450rpm
Base speed	850rpm

Since the goal of the current study in this section is to verify the speed range, the rotor geometrical parameters such as flux carriers and barriers widths, shapes, and the radial and tangential ribs widths have been designed such that to obtain the maximum possible saliency

ratio, output torque, and mechanical robustness [47, 50, 51, 61] which is not described in detail in this section. The speed limitation of the existed laboratory load (DC machine, 3400 rpm) has been taken into consideration to prevent over speed issues during the experimental test. Therefore, low base speed is expected. The reference machine with proper rotor geometry has been examined by FEA to identify the torque-speed characteristic during the flux weakening without variable n_s method.

Figure 5.26 shows the torque speed characteristic of the reference machine with 25 turns per slot. As is illustrated, the full number of turns contributes to develop the desired torque up to the base speed significantly, but it degrades the speed range. The speed range of 1.7 (1430/850) is characterized for constant power operation which is not enough for high speed operation.

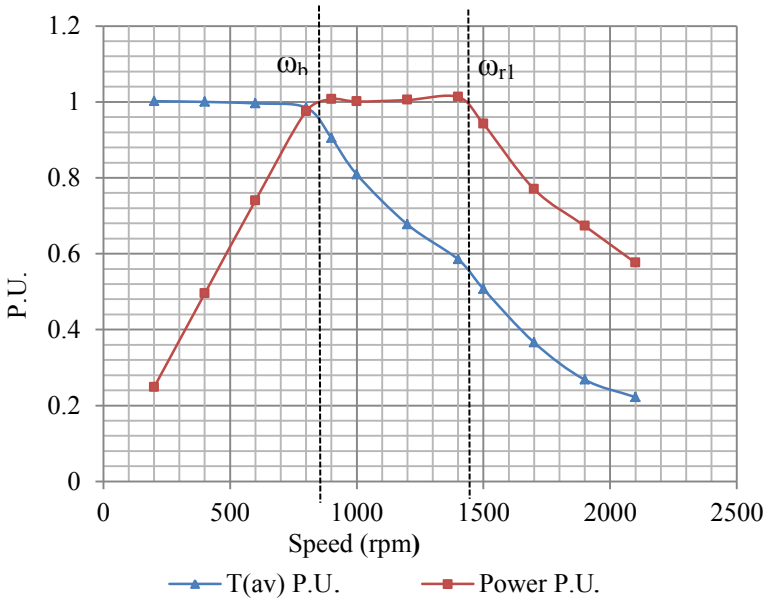

Figure 5.26. Torque and power characteristics of the reference motor.

5.7.2.2 Performance of the Variable Ampere-Turns SynRM

Referring to Figure 5.24, the stator winding of the reference machine has been design in three layers by three separated coils with 13, 7, 5 turns per slot. Therefore, by changing the positions of the switches, three alternatives of n_s including 25, 20, and 13 turns can be obtain respectively. The finite element analysis has been carried out for each step based on the sequences shown in Table 5.10. As is illustrated in Figure 5.27, compared to the reference machine (Figure 5.26) at the maximum speed (ω_{r1}= 1450rpm), n_s was reduced by 20% to 20 turns under FWC. The constant power operation has been extended to 1900rpm and the speed range increased by 31% to 2.24 (ω_{r2} = 1900rpm). In each step, it is necessary to apply the switching pulses at the corresponding maximum speed point to prevent any disturbance in the machine's output power. The effect of delay in switching time is evident at point A. In the third step, n_s was reduced by 35% to 13 turns and the result shows more extension of the constant power operation up to 3000rpm. This confirms an increase of 208% of speed range up to 3.53. Thus, by using the proposed method during the flux weakening and in conjunction with the FWC or MTPA, a significant boost of speed range can be obtained which may satisfy the high speed operation requirements.

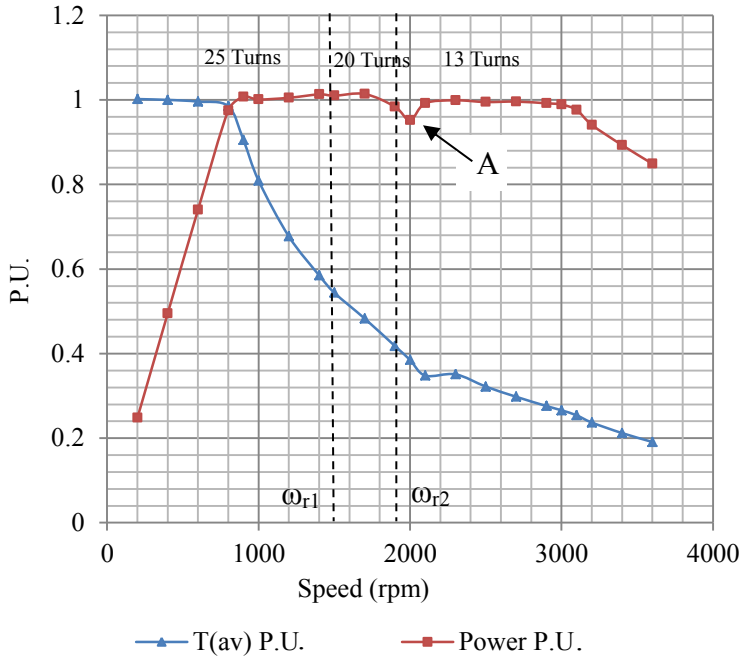

Figure 5.27. Torque and power characteristics of the VAT-SynRM.

Figure 5.28 shows the torque versus time at 1450rpm when the number of turns per slot has been changed from 25 to 20 turns in the second step of the operating sequences. As is illustrated, the machine experienced a short transient under current control scheme and reached to the steady state after 4 electric cycles by developing the average torque of 33.6Nm. As well as, this is confirmed by Figure 5.27 in which the output torque was regulated at 0.56p.u. (33.6Nm) when the number of turns was reduced from 25 to 20 turns. Accordingly, the output power of 5100W is deliverable on the shaft which is around the rated. This validates the constant power operation of the proposed machine after reducing the number of turns while the current remained at the rated level under a current control scheme.

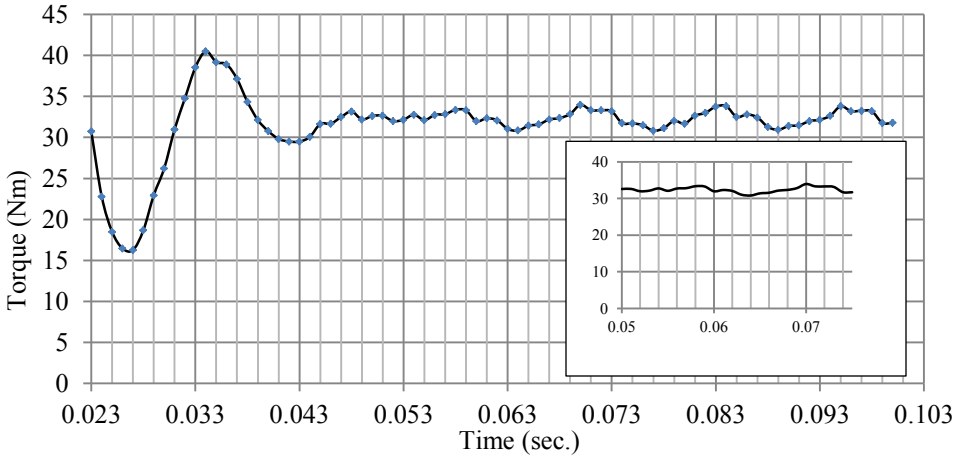

Figure 5.28. Torque- time characteristic of the VAT-SynRM at 1450rpm.

5.7.3 Experimental Test and Results

In order to evaluate the method, a 7.5hp SynRM has been designed and manufactured. Previously, the prototype has been described in 3.9.1 and 3.9.2. The design specifications were summarized in Table 3.5. As was discussed in Chapter 3, a DC machine rated at 3400rpm, 50A, and 250V was considered as the load and connected back to back with the prototype mechanically, and to the grid electrically. The VAT-SynRM operates as the prime mover and designed for low base speed (850rpm) to avoid over speed issues in DC machine during the test. The rotor was design by four poles and four internal layers which is shown in Figure 3.15. The rotor geometry has been modified according to the design criteria discussed in 5.5 to improve the mechanical robustness. In order to increase the rotor's mechanical integrity and rigidness, all flux barriers have been filled by Epoxy adhesive and machined to obtained 0.4mm air gap which is shown in Figure 5.29. The stator winding is design by two layers, 18 and 7 turns per slot, to simplify test into two steps of switching by contactors. In industrial type switching can be

performed by IGBTs which leads to faster and more efficient transition. This gives the possibility of operating in 25 and 18 turns per slot which is shown in Figure 3.16.

Figure 5.29. The prototype's rotor after injection of the Epoxy adhesive.

The proposed machine was examined under the load test for different speed. To prevent over current issues due to the low speed operation of the DC machine, the test has been performed at 40% of the nominal load. Figure 5.30 shows the measured torque-speed and power-speed characteristics of the prototype which have been measured in the steady state condition.

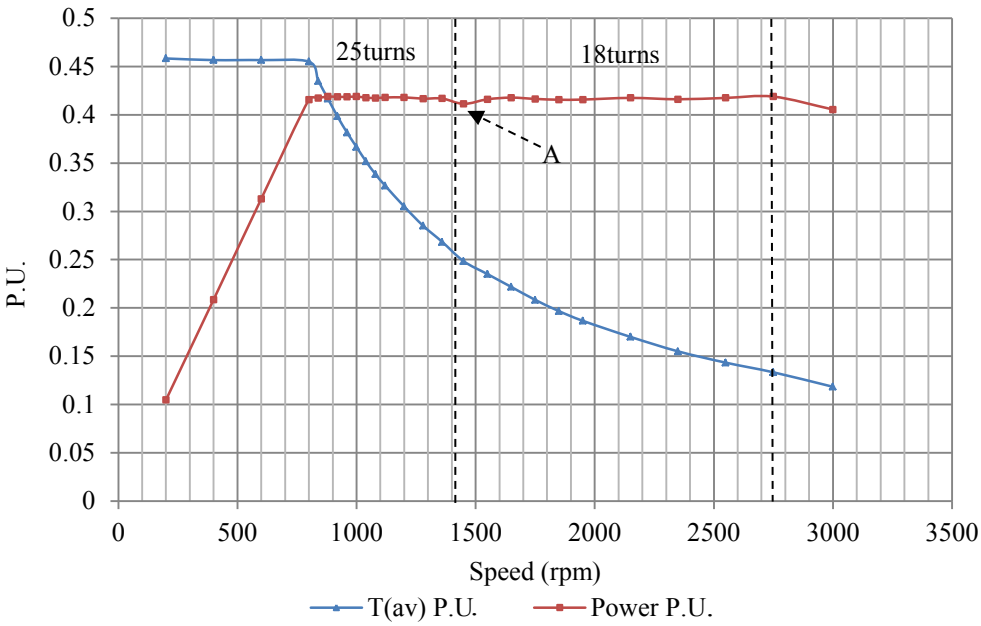

Figure 5.30. Measured power and torque-speed characteristics in the steady state.

As is illustrated in Figure 5.30, the machine operated at constant torque regime up to based speed (810rpm) and developed constant power up to maximum speed (1450rpm). The number of turns was reduced at this point from 25 to 18 under current control scheme when, the output power was tending to drop (point A). A considerable extension of the speed range (207%) from 1.18 to 3.75 is evident in which the machine's maximum speed increases up to 3000rpm. This confirms; the variable ampere-turns method can be used as a simple and reliable method to extend the speed range of the SynRM during the flux weakening operations in conjunction with the other conventional methods such as FWC or MTPA for automotive applications.

5.8 Summary of Chapter 5

This chapter discussed a computer aided analysis with respect to different core characteristics to improve the core magnetic and mechanical performances of the synchronous reluctance machine equipped with TLA rotor for automotive applications. The proposed machine's geometry with different tangential and radial ribs widths were investigated through a comparative study. It has been shown that; the average torque and torque ripple are more sensitive to the tangential ribs widths than the radial ones. The mechanical robustness of the rotor structure at desired speed were studied, it has been described that; improvements to the rotor mechanical robustness may degrade the machine magnetic performance. Thus, in order to design high performance SynRM for automotive applications, the mutual effects of the magnetic and mechanical parameters need to be taken into consideration simultaneously. Accordingly, the performances of the proposed machine with different number of poles were investigated. It has been shown that; higher number of poles is necessary to design high performance SynRM for traction application. This reduces the phase current, torque ripple, and the copper losses. Also, a novel method based on the variable ampere-turns concept was proposed to extend the speed range of the SynRM. In this method the number of turns per slot is changed in different steps when the machine reaches to the corresponding maximum speed, results in a wider constant power operation without increasing the drive's current limit which is desirable for traction motors.

Chapter 6 Conclusions and Future work

6.1 Conclusions

Worldwide demand for reducing fossil fuel consumption in different industrial sectors such as transportation infers to advancement of the vehicle technologies. The Electric Vehicle Technology Roadmap for Canada reported; by 2018, there will be at least 500,000 highway-capable plug-in electric vehicles on Canadian roads, as well as a larger number of hybrid electric vehicles. Recent advantages of high quality magnetic materials and power electronics have contributed to new energy efficient and high performance electric drives that use new electric motor technologies. Amongst them permanent magnet and induction machines are the most demanded in auto-industries owing to their higher efficiency.

In one hand, the prices of the permanent magnets are fluctuating and on the other hand, flexibility in the market suggests diversity of the products in the electric and hybrid auto-industries. Successful penetration of EVs into the electrified transportation market requires consumer's acceptance, infrastructure changes, and achieving competitive cost. Consumer reaction to the cost, charging time, and driving range will help to point the way forward for manufacturers. Advanced electric motors with high efficiency and reasonable cost in EV's powertrain systems have magnificent impact on the vehicle's drive range, battery life time, inverter rating, cooling system capacity, total weight, and cost.

Recently, a cost reduction is the main objective in the most worldwide electric vehicle manufacturer's design strategy. Hence, new traction motor topologies such as synchronous reluctance machine in which the rotor anisotropic geometry can eliminate expensive magnet and aluminum or copper bar from the rotor structure, became more attractive for automotive

applications. Backgrounds and related investigations of the research work relative to the automotive applications have been verified in the first chapter. The research goals, objectives, potential problems of the synchronous reluctance machines, and the research contributions have been discussed.

Operation of the synchronous reluctance machines, proposed in this research work, has been presented in Chapter 2. The machine's mathematical model, vector diagram, and the main design characteristics were presented. Different rotor geometries with respect to the anisotropic structure were introduced and compared for proposing the rotor type for the research work. The rotor and stator electrical, mechanical, magnetic, and geometrical parameters and their influences on the machine's performance were discussed. Furthermore, the machine's key parameters which are dominant for the design procedure have been addressed for automotive applications.

In Chapter 3, a sizing methodology was proposed. The Proper size of the SynRM considering today's compact passenger vehicles in which the size and weight are the design limitations, is necessary to be identified. Taking into consideration the desired requirements of the traction motor drives such as high torque and power density, low torque ripple, wide speed range, and proper size, this machine is still under investigation to be developed for traction applications. In general, the choice of electrical machine for traction application is determined by manufacturers with respect to three dominant factors; cost, weight, and size. Hence, the machine proper size estimation is one of the most important steps of the design procedure before attempting to the rotor geometry design.

In this chapter analytical design process of the synchronous reluctance machines for traction applications through which the stator geometry, rotor outer diameter, machine's electrical and

magnetic parameters i.e., inductances, resistances, winding specifications as well as the output functions such as maximum torque, power factor, and efficiency have been identified.

The proposed approach uses the machine's mathematical model i.e., the equivalent circuit, vector diagram, and mathematical equations in conjunction with the initial data, desired torque envelope, and assigned parameters. Proposed sizing method was evaluated successfully by comparison between FE analyses and experimental test results of the 7.5hp and 50hp industrial prototypes. It has been shown that this method can be sufficiently used as a fast and reliable procedure to identify the most important parameters of the machine e.g., the rotor and stator dimensions, stator geometry, saliency ratio, peak torque, maximum current, speed range, and stator winding specifications based on the design requirements prior to the rotor geometry design and the machine final design process.

High torque pulsation is one of the most common problems of the SynRM that is caused by the interaction between the spatial harmonics of the electrical loading and the rotor anisotropic geometry. The torque ripple causes additional losses, reduces the efficiency when the machine needs to operate at constant power region, decreases average torque, produces audible noise, and imposes a mechanical pulsation on the shaft that all of which are intolerable in most applications particularly in traction. Conventional methods such as chording of the stator windings or skewing the rotor or stator slots are not a proper solution for the design in automotive applications which are the subjects of Chapter 4.

In Chapter 4 torque ripple principles of the synchronous reluctance machines have been discussed. Furthermore, a geometrical method to identify a proper rotor slot pitch angle and their final fine tuning for minimizing the torque ripple using a given core material has been proposed.

Different machines with various rotor slot pitch angles and rotor barrier ends widths have been examined by the FEA and experimental test to evaluate the method. It is shown that; in order to achieve such reduced torque ripple, the angular spacing between two neighboring barriers ends needs to be set to a value which is called rotor slot pitch angle. The rotor slot pitch angle adjustment can reduce torque ripple significantly without any considerable change in output power. Moreover, a novel rotor core design and assembly with cold rolled grain oriented magnetic material is proposed to investigate further improvement to the magnitude of the output torque for traction applications. It is shown that the machine equipped with the segmented rotor made by grain oriented magnetic steel exhibits higher induction in d-axis and lower induction in q-axis at given operating point compared to the non-oriented magnetic steel. As a result, use of the oriented material in the rotor core improves the machine saliency ratio and magnifies the output torque by 5-10 percent. Consequently, this reduces the machine size at the same operating load or torque envelope which is desirable for automotive applications.

Chapter 5 discussed a computer aided analysis with respect to different core characteristics to verify the core magnetic and mechanical performance of the SynRM equipped with TLA rotor for automotive applications. The proposed machine's geometry with different tangential and radial rib widths were investigated through a comparative study and shown that; the average torque and torque ripple is more sensitive to the tangential ribs widths than the radial ones.

The mechanical robustness of the rotor structure at the desired speed was studied, it has been shown; improvements to the rotor mechanical robustness can degrade the machine magnetic performance. Thus, in order to design the SynRM properly, the mutual effects of the magnetic and mechanical parameters need to be taken into consideration.

Accordingly, the performance of the proposed machine with different number of poles including 4-pole and 6-pole has been investigated. It has been shown that higher number of poles is necessary for proper design of the SynRM for traction application. This reduces the phase current, torque ripple and copper losses as well as increases the output torque and the rotor mechanical integrity.

Low flux weakening or speed range reduces capability of the SynRM to operate at constant power beyond the base speed for a wide speed range. This drawback is harmful when the machine is designed to run as a traction motor in EVs or HEVs. In general, differing from the industrial applications of the electric motors, the motors used in EVs and HEVs usually require a wide speed range in which one of the desired performance characteristics of the powertrain is to deliver constant output power over the full speed range. By using conventional flux weakening control technique (FWC), SynRM cannot sufficiently satisfy the traction requirement with a speed range of 3-6 that is due to the dependency of the saliency ratio on the stator current.

A novel method based on variable ampere-turns concept has been proposed to extend the speed range of the machine. In this method, the number of turns per slot may be changed in different steps when the machine needs an increase or a decrease of the flux over the flux weakening. As a result, wider speed range (more than three times) with constant power operation can be obtained using FWC which is desirable for the traction motors. Computer aided analysis in conjunction with the experimental test have supported the proposed method.

6.2 Future Work

In this section, some suggestions are made for future studies of this research work.

6.2.1 Investigation of the thermal performance of synchronous reluctance machines for automotive applications

Frequent start-up, acceleration, and cruising of the SynRM under specific drive cycles in automotive applications contribute to temperature rise in the machine's windings and core. This may change the stator electrical parameters and core magnetic characteristics, as a result, affects the motor and drive's control system performances. Also, high temperature can destroy the stator insolation and windings. It is assumed in this work, the cooling system is capable of controlling operating temperature. Therefore, verifying the thermal behavior of the machine in transient mode of operation and critical points such as start-up or acceleration within which high current demand for peak torque causes temperature rise as well as thermal behavior of the machine in the other modes of operation i.e., intermediate and continues modes is an attractive area for investigation.

6.2.2 Investigation of the power factor improvements of synchronous reluctance machines for automotive applications

Low power factor (0.55-0.70) is one of the drawbacks of the magnet free SynRM. In automotive applications, in one hand, this increases the phase current which implies higher copper loss, higher wire gage, and larger size. On the other hand, reduces the battery state of charge, decreases the drive range, and increases the battery size and drive train's total weight and cost. Therefore, study on methods to improve the power factor of the SynRM for automotive application is an interesting research work.

6.2.3 Improvement to the speed range extension method of synchronous reluctance machines for automotive applications

As discussed in Chapter 5, Low flux weakening or speed range degrades capability of the SynRM to operate at constant power beyond the base speed for a wide speed range. A new method based on the variable ampere-turns concept has been proposed to extend the speed range. Improvement to the method using switches which are integrated in the motor drives and study on the transient response of the machine during the switching process as well as losses verification would be quite advantageous.

6.2.4 Efficiency estimation of the SynRM for traction applications

Investigation on the efficiency of the SynRM for automotive applications would be advantageous to build an efficiency estimation tool and application. This may be based on the automotive drive cycle in a real industrial environment and the application will lead to modify the limitations of the design methods.

6.2.5 Investigation of the vibration and acoustic noise of the SynRM for automotive applications

Torque ripple of the SynRM causes vibration and acoustic noise which are not desirable for automotive applications. Different conventional torque ripple minimization methods have been discussed as well as a novel geometrical method has been proposed and examined in this thesis to reduce the machine torque ripple. Although, it is still advantageous and interesting to verify the vibration and acoustic noise of the reduced torque ripple SynRM for automotive applications.

References

[1] M. Ehsani, Y. Gao, S. E. Gay, A. Emadi, and *Modern Electric, Hybrid Electric, and Fuel Cell Vehicles* vol. 1. United States: CRC Press, 2005.

[2] T. Fukami, M. Momiyama, K. Shima, R. Hanaoka, and S. Takata, "Steady-State Analysis of a Dual-Winding Reluctance Generator With a Multiple-Barrier Rotor," *Energy Conversion, IEEE Transactions on,* vol. 23, pp. 492-498, 2008.

[3] G. o. Canada, "Electric Vehicle Technology Roadmap for Canada," Technical Report2011 2011.

[4] M. E. z. Rahman, and KL.Butler, "An investigation of electric motor drive characteristics for ev and hev propulsion systems," *SAE Technical Paper Series,* vol. Paper # 2000-01-3062, 2000.

[5] G. Pellegrino, A. Vagati, P. Guglielmi, and B. Boazzo, "Performance Comparison Between Surface-Mounted and Interior PM Motor Drives for Electric Vehicle Application," *Industrial Electronics, IEEE Transactions on,* vol. 59, pp. 803-811, 2012.

[6] G. Pellegrino, A. Vagati, B. Boazzo, and P. Guglielmi, "Comparison of Induction and PM Synchronous Motor Drives for EV Application Including Design Examples," *Industry Applications, IEEE Transactions on,* vol. 48, pp. 2322-2332, 2012.

[7] K. Kiyota, H. Sugimoto, and A. Chiba, "Comparing Electric Motors: An Analysis Using Four Standard Driving Schedules," *Industry Applications Magazine, IEEE,* vol. 20, pp. 12-20, 2014.

[8] C. C. Chan, "The state of the art of electric and hybrid vehicles," *Proceedings of the IEEE,* vol. 90, pp. 247-275, 2002.

[9] M. Zeraoulia, M. E. H. Benbouzid, and D. Diallo, "Electric Motor Drive Selection Issues for HEV Propulsion Systems: A Comparative Study," *IEEE Trans. on Veh. Technology, ,* vol. 55, pp. 1756-1764, 2006.

[10] J. G. W. West, "DC, induction, reluctance and PM motors for electric vehicles," in *IEE Colloquium on Motors and Drives for Battery Powered Propulsion*, 1993, pp. 1/1-111.

[11] P. Pillay and V. Levin, "Mathematical models for induction machines," in *Industry Applications Conference, 1995. Thirtieth IAS Annual Meeting, IAS '95., Conference Record of the 1995 IEEE*, 1995, pp. 606-616 vol.1.

[12] P. Pillay and R. Krishnan, "Application characteristics of permanent magnet synchronous and brushless DC motors for servo drives," *IEEE Trans. on Ind. Applicat.,* vol. 27, pp. 986-996, 1991.

[13] S. Smaka, S. Masic, M. Cosovic, and I. Salihbegovic, "Switched reluctance machines for hybrid electric vehicles," in *Electrical Machines (ICEM), 2010 XIX International Conference on*, 2010, pp. 1-6.

[14] T. Zhangjun, P. Pillay, C. Yicheng, and A. M. Omekanda, "Prediction of electromagnetic forces and vibrations in SRMs operating at steady state and transient speeds," in *Industry Applications Conference, 2004. 39th IAS Annual Meeting. Conference Record of the 2004 IEEE*, 2004, p. 400 Vol.1.

[15] J. K. Kastko, "Poly phase reaction synchronous motors," *Jornal Amer. Inst. Elect.,* vol. 42, pp. 1162-1168, 1923.

[16] A. Vagati, "The synchronous reluctance solution: a new alternative in AC drives," in *Industrial Electronics, Control and Instrumentation, 1994. IECON '94., 20th International Conference on*, 1994, pp. 1-13 vol.1.

[17] A. Vagati, A. Fratta, G. Franceschini, and P. M. Rosso, "AC motors for high-performance drives: a design-based comparison," in *Industry Applications Conference, 1995. Thirtieth IAS Annual Meeting, IAS '95., Conference Record of the 1995 IEEE*, 1995, pp. 725-733 vol.1.

[18] A. Vagati, G. Franceschini, I. Marongiu, and G. P. Troglia, "Design criteria of high performance synchronous reluctance motors," in *Industry Applications Society Annual Meeting, 1992., Conference Record of the 1992 IEEE*, 1992, pp. 66-73 vol.1.

[19] A. Vagati, M. Pastorelli, G. Francheschini, and S. C. Petrache, "Design of low-torque-ripple synchronous reluctance motors," *Industry Applications, IEEE Transactions on,* vol. 34, pp. 758-765, 1998.

[20] R. R. Moghaddam, F. Magnussen, and C. Sadarangani, "Theoretical and Experimental Reevaluation of Synchronous Reluctance Machine," *Industrial Electronics, IEEE Transactions on,* vol. 57, pp. 6-13, 2010.

[21] T. Matsuo and T. A. Lipo, "Rotor design optimization of synchronous reluctance machine," *IEEE Trans. on Energy Conv. ,* vol. 9, pp. 359-365, 1994.

[22] J. Malan, M. J. Kamper, and P. N. T. Williams, "Reluctance synchronous machine drive for hybrid electric vehicle," in *Industrial Electronics, 1998. Proceedings. ISIE '98. IEEE International Symposium on*, 1998, pp. 367-372 vol.2.

[23] T. J. E. Miller, A. Hutton, C. Cossar, and D. A. Staton, "Design of a synchronous reluctance motor drive," *IEEE Trans. on Ind. Applicat.,* vol. 27, pp. 741-749, 1991.

[24] P. Jung-Min, K. Sung-Il, H. Jung-Pyo, and L. Jung-Ho, "Rotor Design on Torque Ripple Reduction for a Synchronous Reluctance Motor With Concentrated Winding Using Response Surface Methodology," *Magnetics, IEEE Transactions on,* vol. 42, pp. 3479-3481, 2006.

[25] N. Bianchi, S. Bolognani, D. Bon, Pre, x, and M. D., "Rotor Flux-Barrier Design for Torque Ripple Reduction in Synchronous Reluctance and PM-Assisted Synchronous Reluctance Motors," *IEEE Trans. on Energy Conv.,* vol. 45, pp. 921-928, 2009.

[26] G. Pellegrino, E. Armando, P. Guglielmi, and A. Vagati, "A 250kW transverse-laminated Synchronous Reluctance motor," in *Power Electronics and Applications, 2009. EPE '09. 13th European Conference on*, 2009, pp. 1-10.

[27] T. Matsuo and T. A. Lipo, "Rotor position detection scheme for synchronous reluctance motor based on current measurements," *Industry Applications, IEEE Transactions on,* vol. 31, pp. 860-868, 1995.

[28] T. Matsuo, A. El-Antably, and T. A. Lipo, "A new control strategy for optimum efficiency operation of a synchronous reluctance motor," in *Industry Applications Conference, 1996. Thirty-First IAS Annual Meeting, IAS '96., Conference Record of the 1996 IEEE*, 1996, pp. 109-116 vol.1.

[29] M. J. Kamper, F. S. Van der Merwe, and S. Williamson, "Direct finite element design optimisation of the cageless reluctance synchronous machine," *Energy Conversion, IEEE Transactions on,* vol. 11, pp. 547-555, 1996.

[30] K. Sungmin, S. Seung-Ki, K. Ide, and S. Morimoto, "Maximum efficiency operation of Synchronous Reluctance Machine using signal injection," in *Power Electronics Conference (IPEC), 2010 International*, 2010, pp. 2000-2004.

[31] T. Matsuo and T. A. Lipo, "Field oriented control of synchronous reluctance machine," in *Power Electronics Specialists Conference, 1993. PESC '93 Record., 24th Annual IEEE*, 1993, pp. 425-431.

[32] Y. Inoue, S. Morimoto, and M. Sanada, "A novel control scheme for maximum power operation of synchronous reluctance motors including maximum torque per flux control," in *Electrical Machines and Systems, 2009. ICEMS 2009. International Conference on*, 2009, pp. 1-6.

[33] F. Fernandez-Bernal, A. Garcia-Cerrada, and R. Faure, "Efficient control of reluctance synchronous machines," in *Industrial Electronics Society, 1998. IECON '98. Proceedings of the 24th Annual Conference of the IEEE*, 1998, pp. 923-928 vol.2.

[34] J. J. Germishuizen, F. S. Van der Merwe, K. Van der Westhuizen, and M. J. Kamper, "Performance comparison of reluctance synchronous and induction traction drives for electrical multiple units," in *Industry Applications Conference, 2000. Conference Record of the 2000 IEEE*, 2000, pp. 316-323 vol.1.

[35] X. B. Bomela and M. J. Kamper, "Effect of machine design on performance of reluctance synchronous machine," in *IEEE Ind. Applicat. Conference Record of* 2000, pp. 515-522

[36] A. Fratta, G. P. Troglia, A. Vagati, and F. Villata, "Evaluation of torque ripple in high performance synchronous reluctance machines," in *Industry Applications Society Annual Meeting, 1993., Conference Record of the 1993 IEEE*, 1993, pp. 163-170 vol.1.

[37] N. Bianchi, S. Bolognani, D. Bon, and M. Dai Pre, "Torque Harmonic Compensation in a Synchronous Reluctance Motor," *IEEE Trans. on Energy Conv.,* vol. 23, pp. 466-473, 2008.

[38] G. Lusu and L. Parsa, "Torque improvement of synchronous reluctance machines by utilizing orthogonal experimental design methodology," in *Industrial Electronics, 2008. IECON 2008. 34th Annual Conference of IEEE*, 2008, pp. 1427-1432.

[39] J. Malan and M. J. Kamper, "Performance of a hybrid electric vehicle using reluctance synchronous machine technology," *IEEE Trans. on Ind. Applicat.,* vol. 37, pp. 1319-1324, 2001.

[40] T. A. Lipo, T. J. Miller, A. Vagati, I. Boldea, L. Malesani, and T. Fukao, "Synchronous reluctance drives," *Totorial Presented at IEEE IAS Annual Meeting, Denver, Co,* Oct. 1994.

[41] M. J. Kamper and A. F. Volsdhenk, "Effect of rotor dimensions and cross magnetization on Ld and Lq inductances of reluctance synchronous machine with cageless flux barrier rotor," *Electric Power Applications, IEE Proceedings -,* vol. 141, pp. 213-220, 1994.

[42] D. A. Staton, T. J. E. Miller, and S. E. Wood, "Maximising the saliency ratio of the synchronous reluctance motor," *Electric Power Applications, IEE Proceedings B,* vol. 140, pp. 249-259, 1993.

[43] I. Boldea, *Reluctance Synchronous Machines and Drives*, 1st ed. vol. 1. new York: Oxford, 1996.

[44] I. Boldea, Z. X. Fu, and S. A. Nasar, "Performance evaluation of axially-laminated anisotropic (ALA) rotor reluctance synchronous motors," in *IEEE Ind. Applicat. Society, Annual Meeting, Conference Record of* 1992, pp. 212-218 vol.1.

[45] D. Platt, "Reluctance motor with strong rotor anisotropy," *Industry Applications, IEEE Transactions on,* vol. 28, pp. 652-658, 1992.

[46] I. Boldea and S. A. Nasar, *The Induction machine Design Handbook*, 2st ed. New York: CRC Press, 2009.

[47] R. R. Moghaddam, F. Magnussen, and C. Sadarangani, "Novel rotor design optimization of synchronous reluctance machine for high torque density," in *Power Electronics, Machines and Drives (PEMD 2012), 6th IET International Conference on*, 2012, pp. 1-4.

[48] ABB, "Technical journal of ABB, "ABB Review 1/11, innovation", 2011," Switzerland 1/11, 2011 2011.
[49] N. Bianchi, M. Degano, and E. Fornasiero, "Sensitivity analysis of torque ripple reduction of synchronous reluctance and interior PM motors," in *Energy Conversion Congress and Exposition (ECCE), 2013 IEEE*, 2013, pp. 1842-1849.
[50] R. R. Moghaddam and F. Gyllensten, "Novel High-Performance SynRM Design Method: An Easy Approach for A Complicated Rotor Topology," *Industrial Electronics, IEEE Transactions on,* vol. 61, pp. 5058-5065, 2014.
[51] S. Taghavi and P. Pillay, "A Sizing Methodology of the Synchronous Reluctance Motor for Traction Applications," *Emerging and Selected Topics in Power Electronics, IEEE Journal of,* vol. 2, pp. 329-340, 2014.
[52] T. Finken, M. Felden, and K. Hameyer, "Comparison and design of different electrical machine types regarding their applicability in hybrid electrical vehicles," in *Electrical Machines, 2008. ICEM 2008. 18th International Conference on*, 2008, pp. 1-5.
[53] W. T. Villet, M. J. Kamper, P. Landsmann, and R. Kennel, "Hybrid position sensorless vector control of a reluctance synchronous machine through the entire speed range," in *Power Electronics and Motion Control Conference (EPE/PEMC), 2012 15th International*, 2012, pp. LS4b-1.1-1-LS4b-1.1-7.
[54] W. Ming-Yen and L. Tian-Hua, "Design and Implementation of an Online Tuning Adaptive Controller for Synchronous Reluctance Motor Drives," *Industrial Electronics, IEEE Transactions on,* vol. 60, pp. 3644-3657, 2013.
[55] J. Ikaheimo, J. Kolehmainen, T. Kansakangas, V. Kivela, and R. R. Moghaddam, "Synchronous High-Speed Reluctance Machine With Novel Rotor Construction," *Industrial Electronics, IEEE Transactions on,* vol. 61, pp. 2969-2975, 2014.
[56] M. El Hadi Zaim, "High-Speed Solid Rotor Synchronous Reluctance Machine Design and Optimization," *IEEE Trans. on Magnetic,* vol. 45, pp. 1796-1799, 2009.
[57] H. Hofmann and S. R. Sanders, "High-speed synchronous reluctance machine with minimized rotor losses," *Industry Applications, IEEE Transactions on,* vol. 36, pp. 531-539, 2000.
[58] J. Kolehmainen, "Synchronous Reluctance Motor With Form Blocked Rotor," *IEEE Transactions on Energy Conversion* vol. 25, pp. 450-456, 2010.
[59] W. T. Villet and M. J. Kamper, "Variable-Gear EV Reluctance Synchronous Motor Drives, 2014; An Evaluation of Rotor Structures for Position-Sensorless Control," *Industrial Electronics, IEEE Transactions on,* vol. 61, pp. 5732-5740, 2014.
[60] M. Barcaro, N. Bianchi, and F. Magnussen, "Permanent-Magnet Optimization in Permanent-Magnet-Assisted Synchronous Reluctance Motor for a Wide Constant-Power Speed Range," *Industrial Electronics, IEEE Transactions on,* vol. 59, pp. 2495-2502, 2012.
[61] S. Taghavi and P. Pillay, "A mechanically robust rotor with transverse-laminations for a synchronous reluctance machine for traction applications," in *Energy Conversion Congress and Exposition (ECCE), 2014 IEEE*, 2014, pp. 5131-5137.